INTERFACIAL ENGINEERING OF HYBRID HETEROJUNCTION PV DEVICES FOR THE NEXT GENERATION LIGHTWEIGHT, FLEXIBLE, AND LOW-COST SOLAR MODULES

by
David Alejandro Angel Trujillo

A dissertation submitted to the Faculty of the University of Delaware in partial fulfillment of the requirements for the degree of Doctor of Philosophy in Materials Science and Engineering

Spring 2024

INTERFACIAL ENGINEERING OF HYBRID HETEROJUNCTION PV DEVICES FOR THE NEXT GENERATION LIGHTWEIGHT, FLEXIBLE, AND LOW-COST SOLAR MODULES

by
David Alejandro Angel Trujillo

Approved: _____
Joshua Zide, Ph.D.
Chair of the Department of Materials Science and Engineering

Approved: _____
Levi Thompson, Ph.D.
Dean of the College of Engineering

Approved: _____
Louis F. Rossi, Ph.D.
Dean of the Graduate College and Vice Provost for Graduate and Professional Education

I certify that I have read this dissertation and that in my opinion it meets the academic and professional standard required by the University as a dissertation for the degree of Doctor of Philosophy.

Signed: _____

Robert L Opila, Ph.D.
Professor in charge of dissertation

I certify that I have read this dissertation and that in my opinion it meets the academic and professional standard required by the University as a dissertation for the degree of Doctor of Philosophy.

Signed: _____

Joshua Zide, Ph.D.
Member of dissertation committee

I certify that I have read this dissertation and that in my opinion it meets the academic and professional standard required by the University as a dissertation for the degree of Doctor of Philosophy.

Signed: _____

David Martin, Ph.D.
Member of dissertation committee

I certify that I have read this dissertation and that in my opinion it meets the academic and professional standard required by the University as a dissertation for the degree of Doctor of Philosophy.

Signed: _____

Cecil Dybowski, Ph.D.
Member of dissertation committe

ACKNOWLEDGMENTS

First and foremost, I would like to thank God, as through this process I have grown in faith and without him none of this would have been possible. Second, I would like to thank my loving mother for supporting me and believing in me at every stage. Professor Opila for believing in my vision from the first day. Prior and current Opila group members for teaching me so much. The other countless Professors and Staff at the University of Delaware for being so helpful and teaching me so much. The staff at Horn entrepreneurial center and the broader entrepreneurial community at UD for giving me so many opportunities to develop as a businessman and entrepreneur. The staff at the Delaware Department of Natural Resources and Environmental Control (DNREC) for believing in my vision and contributing to the funding used for some of the work in this dissertation through the Green Energy Fund program. The staff at the Partnerships for Innovation (PFI) program at the National Science Foundation (NSF) for challenging me to develop a plan worthy of federal funding. Conan Weiland and all the staff at Brookhaven National Laboratory (BNL) for all the help in taking Hard X-ray Photoelectron Spectroscopy (HAXPES) measurements. Our collaborators at Rowan University and the University of Pennsylvania for all the help and support. Huge thanks to all those who believed in me. I am sincerely committed to combating climate change through entrepreneurship and hope this will be the first chapter of a much longer story.

TABLE OF CONTENTS

LIST OF TABLES

LIST OF FIGURES

ABSTRACT

This dissertation aims to develop a more complete framework for understanding the behavior of silicon-organic hybrid electronics, focusing on the development of high-performance hybrid heterojunction photovoltaic (hybrid HJT PV) devices based on thin silicon substrates and PEDOT:PSS as a hole-selective contact. Despite recent advancements in the field of organic and hybrid electronics, the behavior of these devices and their rapid degradation under ambient conditions remains poorly understood. Nevertheless, this technology remains highly promising for the next generation of flexible and hybrid electronics, due to the additional mechanical resilience provided to the thin substrates by the polymer films. Many aspects of this hybrid system have been investigated previously, which is why the scope of this dissertation is limited to: (1) Developing a more comprehensive theoretical framework of understanding the behavior and rapid degradation of hybrid PV devices under ambient conditions. (2) Developing strategies for empirically optimizing the performance of these devices and identifying the major shortcomings of the current processing techniques. (3) Understanding the role of the buried hybrid interface and the development of interfacial oxide between the silicon substrate and the organic film in the performance and degradation of the devices. (4) Identifying and testing alternative processing techniques to address the major challenges identified

The broader impact/commercial potential of the work presented in this dissertation is to enable photovoltaic deployment on water rather than just on land. The growth of solar photovoltaic energy has highlighted the increasing problem of competing land use, scarcity, and cost. Floating photovoltaics have emerged as a solution to this problem; deploying solar modules on existing bodies of water lessens the need for land-based installations. However, the high cost has inhibited growth of this renewable energy source. This project advances a new system that is lighter and cheaper. Furthermore, the modules are fabricated with non-toxic and environmentally friendly materials, mitigating the risk posed by other novel photovoltaic technologies of contaminating the bodies of water.

The work presented here advances the development of lower cost lightweight alternatives for solar photovoltaic generation. This hybrid photovoltaic technology combines innovative polymer science with silicon, the most abundant and significant photovoltaic material in use today, to provide cheaper, lighter, and more efficient flexible modules. Recent computer model simulations indicate that the use an alternative polymer deposition method (oxidative chemical vapor deposition) coupled with an optimized surface treatment of silicon will enable the power efficiencies to exceed 20%. Furthermore, this hybrid approach allows the polymer to mechanically support the brittle silicon substrate, enabling the fabrication of flexible modules (to address wind load) encapsulated by plastic films rather than glass panels.

Chapter 1 . INTRODUCTION AND MOTIVATION

1.1. Motivation

The development and adoption of sustainable and renewable energy sources is increasingly becoming the most important challenge of our time. The recent geopolitical conflict between Russia and Ukraine has reminded us that the urgency in this matter goes beyond ameliorating the alarming rate and effects of global warming but is also critical for national-security, economic, and ethical reasons. In the words of former secretary-general of the United Nations, Bank Ki-Moon: "We are the first generation that can put an end to poverty, and we are the last generation that can put an end to climate change. Future generations will judge us harshly if we fail to uphold our moral and historical responsibilities." [1] One of the most pressing issues in the US is the almost complete reliance on Chinese manufacturing for PV panels and components. The US employs about 250,000 workers in the solar industry, with only 34,423 in manufacturing, a ten-gigawatt increase in production is projected to result in 62,500 direct and 75,000 total new manufacturing jobs. The effort needed to re-build the American PV manufacturing industry over the coming years will be significant, and its difficulty compounded by the high upfront capital investment required to establish the manufacturing infrastructure that has been lost to China. Solar energy has been the fastest growing source electrical power in the United States for several years, with solar photovoltaic (PV) having the biggest impact on this growth totaling 43% of new generating capacity in 2020.

Despite the decreasing costs of PV, declining by 82% between 2010 and 2019, and accounting for 3% of total electricity generation, there are several challenges that must be addressed in order to meet the ambitious goals of the "Terawatt Challenge" and make solar PV a true alternative to fossil fuels. Namely:

1. High cost of high-vacuum and high-temperature equipment. Furthermore, manufacturing these solar modules is still a very carbon intensive process, due to the high temperatures needed in the manufacturing process, which makes them much less renewable.
2. Low flexibility of manufacturing process and difficulty for continuous innovation.
3. Use of scarce and expensive materials.
4. Lack of a clear strategy for recycling end-of-life modules.
5. The constituent materials of some novel PV technologies pose a significant health and safety risk. Some of the materials such as cadmium and gallium are carcinogen and toxic while heavy metals such as copper can cause long-term exposure disease.

Hybrid heterojunction technology (hybrid HJT) has emerged as a promising approach to address these concerns. This hybrid HJT PV technology combines traditional semiconductors with electrically conductive organic materials that act as carrier selective contacts and induce the formation of a photoactive junction in a manner analogous to the operation of the conventional hydrogenated amorphous silicon heterojunction technology (a-Si:H HJT). This Hybrid PV technology has several key advantages over other PV

technologies and provides a unique opportunity to address these challenges to have a direct impact on the PV industry within the next five years. Namely these include:

1. By combining traditional semiconductors with electrically conducting organic materials, the energy requirements for processing the cells as well as the overall cost of production is greatly reduced.
2. Optimal for fabrication of flexible cells based on thin substrates due to low temperature processing and the enhanced mechanical resilience from the polymer films.
3. Lower weight and versatile form factors, which translate into lower transportation and installation costs and opportunities in specialized applications.
4. Low upfront capital investment requirements and inexpensive fabrication.
5. Versatile cell architecture and fabrication process, which provides opportunities for continuous innovation such as the development of a tandem architecture at a later stage of development.
6. Ease of recycling and repurposing component materials.
7. Use of non-toxic and environmentally friendly materials and processes, as many of the novel PV technologies under development are fabricated with materials that pose a significant health and safety risk such as cadmium and gallium being carcinogen and toxic.

Nevertheless, the field of hybrid electronics is still in its infancy and several technical R&D challenges must be addressed to realize the potential advantages for the PV industry. The main technical goal of this dissertation is to outline the framework used to

identify and address the main technical challenges in translating the hybrid HJT PV technology into a competitive solar energy solution. Broadly speaking the hope is that this framework along with the results of the R&D work performed thus far provides a comprehensive path for the development of commercially competitive next generation hybrid electronic devices, with a specific emphasis on emerging PV technologies.

Economic considerations are inexorably linked to R&D activities in all technical fields of science, however, the PV industry is particularly sensitive to this issue due to the high upfront capital investments that hinder the scope and speed of innovation. It is for this reason that the success of R&D activities requires an informed assessment of the techno-economic considerations at play. In addition to the R&D efforts we have also conducted extensive customer and market development work and founded SHIO LLC with the goal of bridging the gap between the fundamental research conducted at the university and the commercialization of our hybrid HJT technology. Keeping in line with the entrepreneurial and leadership education goals of the NSF-Partnership for Innovation (NSF-PFI) program as well as various other the proof-of-concept and customer development (I-Corps) grants that have been awarded to this project totaling upwards of $500,000 USD, this dissertation also aims to outline the major learnings of this entrepreneurial journey with the hopes it may inspire and guide future scientists to pursue innovative entrepreneurial projects.

1.2. Objectives

This dissertation aims to record the progress we have made in the understanding of hybrid photovoltaic technology, the hybrid material systems more broadly, and the buried hybrid interface. In addition to documenting our most recent progress in the development of our hybrid photovoltaic technology this dissertation aims to provide a clear path forward all the way to the commercialization of the technology. I believe this work will be a valuable case study for future entrepreneurial scientists wanting to start their own entrepreneurial projects. This dissertation also stands as publicly available educational material in line with the goals of entrepreneurial and leadership education of the Partnerships for Innovation (PFI) program of the National Science Foundation (NSF) that is sponsoring this project.

The technical R&D goals of this dissertation are:

1. Establish a comprehensive framework for understanding the behavior of silicon-PEDOT hybrid HJT PV devices and hybrid devices more broadly.
2. Develop a computer simulation model for hybrid HJT PV devices to investigate the source of degradation mechanisms and establish a theoretical maximum achievable performance.
3. Develop empirical optimization strategies for hybrid HJT PV devices and investigate the gap in performance to the expected simulated results.
4. Investigate the major challenges and opportunities in the field of hybrid HJT PV devices.

5. Develop a model for the degradation mechanisms in hybrid HJT PV devices by investigating the buried silicon-PEDOT interface to explain the source of the development of s-shaped JV characteristics.
6. Identify an organic silicon surface treatment compatible with hybrid HJT PV technology with high passivation quality and optimal interfacial characteristics for in-situ PEDOT deposition.
7. Identify and investigate alternative PEDOT deposition strategies to minimize oxide growth and film quality degradation.

1.3. Outline and Chapter Structure

The remainder of this chapter provides a brief introduction to the topics covered in this thesis. Chapter 2 outlines the theoretical understanding of hybrid HJT devices, and the details of the simulation modeling work we have performed. Chapter 3 documents our efforts to optimize empirically the hybrid HJT devices. Chapter 4 describes the major challenges and opportunities that were identified in the device structure under investigation. Chapter 5 elaborates further on our investigations of the degradation mechanisms of this hybrid PV technology and the source of s-shaped JV behavior. Chapter 6 outlines our efforts investigating the quality of the silicon surface passivation from small-molecule solution treatments. Chapter 7 describes the first principles assessment that motivated us to explore alternative PEDOT deposition strategies using electrodeposition as the technique of choice. Chapter 8 outlines our ongoing and future work, providing preliminary results and analysis to guide future R&D efforts. Chapter 9

is dedicated to the entrepreneurial efforts of our project and outlines the vision for a successful American PV manufacturer.

1.4. Introduction and First Principles Approach to Problem Solving

The research and development of hybrid electronic technologies is a highly interdisciplinary endeavor that necessitates the comprehensive understanding of independent scientific fields, including polymer science, solid state physics, electrical engineering, chemistry, and surface and interface science. R&D projects that have a broad interdisciplinary scope such as the development of a competitive solar PV solution based on hybrid HJT technology benefit greatly from a first principles approach to problem solving. Which is the approach that was chosen to structure this dissertation. The first principles approach to problem solving may seem overwhelming and an uncomfortable path to take, considering the age-old adage “don’t fix what is not broken” there is a strong desire to limit innovation to iterations of proven methods and techniques to avoid incurring the additional risk associated with the unknown. Nevertheless, historical, and anecdotal evidence have shown that it is the riskiest endeavors that result in the most significant technological developments. It is for this reason that a brief introduction to the first principles framework used in the structuring of this project is in order:

First principles thinking; how should we think?:

1. Consider the challenges and opportunities in the existing field

    a. The first step is to comprehensively consider the current state-of-the-art and ask, “which aspects of the technology provide value and which ones are pain points that are currently garnering interest.”
2. Ask the question “what is the goal.”
    a. What are the quantitative parameters that would constitute a success?
3. Consider the future and its needs.
    a. Sustainability particularly, and the current technical trends.
4. Define and explore a completely new path.
5. Create a new recipe from the fundamental truth.
6. Evaluate and analyze your findings to guide the iteration of this process from step 4.

Within this context the first step taken was to consider the opportunities in employing novel organic materials for the fabrication of electronic devices. This step is indistinguishable from the formation of an informed hypothesis after the consideration of the state-of-the-art and the trends that preceded it. The following section briefly recounts the progress in the field of organic electronics.

The beginning of the 20th century was marked by the rise in popularity of petrochemical products and the development of an entirely new field of chemistry that gave rise to plastics as we know them in 1907. This new material system which has been both a blessing and a curse was a convenient and economic alternative for just about any engineering material imaginable and gave rise to the democratization of many products that were cost prohibitive just a few years prior. Just as many historians chose to refer to

different periods of time by the prevailing materials used, such as the stone, bronze, or iron ages, this event marked the beginning of the age of plastics.

However, only a few decades later in 1947 the transistor would be developed at Bell Labs. The technology that has had perhaps the most profound impact on the course of human history. This event sparked the semiconductor revolution that would result in the rise of modern electronics, computing and the field of solar PV more broadly. The growth rate of the energy requirements to power the resulting modern infrastructure has been on an unsustainable upwards trend ever since.

These two material systems shaped the development of modern material science as a discipline distinct from metallurgy. Since then, the field has traditionally been split between experts in soft materials (plastics and polymers) and hard materials (semiconductors, insulators, and metals). However, in 1977 electrically conducting polymers were discovered by Professors Heeger, MacDiarmid, and Shirakawa [2]. This discovery would spark a paradigm shift in the material science field and the birth of the field of organic electronics, as the promises of a convenient and economic alternative to the traditional semiconductor materials in electronic devices were too good to ignore.

Despite initial excitement and promising results, the field of organic electronics would very rapidly stagnate despite considerable investment in R&D. The slow rate of progress towards high performing organic electronic materials and the unreliability of these materials would taint the public perception of the field for years to come.

Nevertheless, over recent years the development of novel chemistries with the help of advanced computing power and the promising results of hybrid approaches combining organic and traditional semiconductors have revitalized the field and fueled a new wave of scientific progress.

1.5. PEDOT:PSS and Organic Electronics

The field of organic and hybrid electronics is relatively new compared to the well-established field of traditional semiconductors and a comprehensive understanding of the structure-property relationships is still under development. In contrast to traditional semiconductors, the electronic properties of organic materials can be tuned easily and inexpensively by altering the chemistry, morphology, or composition of the polymer. This level of tunability is a great opportunity for the development of highly efficient hybrid electronics, however the interactions at the interface between the organic and inorganic materials are poorly understood which has hindered the development of hybrid technologies. Nevertheless, the field of organic electronics has seen exponential progress over the past decade with significant advances in the performance of semiconducting polymers, particularly in PV applications. Just last year, in Feb 2021, researchers from NREL achieved the organic photovoltaic (OPV) power conversion efficiency (PCE) record of 18% [3], a figure that places OPV as a competitive emerging PV technology.

The electronic properties of semiconducting polymers are a consequence of π-bond conjugation along the one-dimensional backbone of the polymer chains. This π-bond conjugation phenomenon arises when three or more *p*-orbitals join together to form

a system of delocalized charges in a manner analogous to the delocalization of charges in metals and inorganic semiconductors. However due to the conjugation happening only along the polymer backbone, the mobility of charge between polymer chains greatly compromises the electronic properties of the polymer films. Figure 1 shows a schematic of the π-bond conjugation mechanism by which semiconducting polymers develop energy bands.

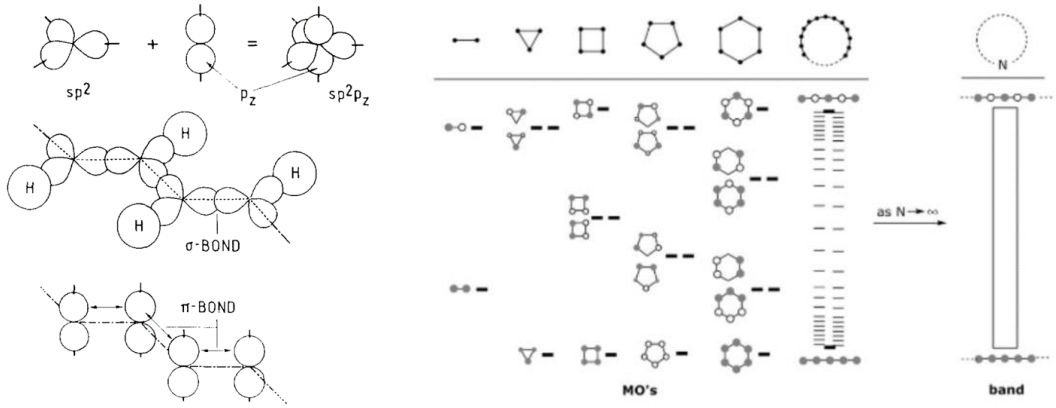

Figure 1. Schematic of the π-bond conjugation mechanism and band formation in one dimensional space.

As is the case with traditional semiconductors, the overall conductivity of the polymer film depends on the free carrier concentration in the material. This in turn necessitates the use of doping strategies to induce free charges along the conjugated polymer backbone to achieve high performance electronic systems. Furthermore, the chemical nature of these conjugated polymers results in high melting points and poor solubility which complicates the processing and fabrication of devices as well as limiting the range of viable chemistries.

Within this new wave of R&D efforts one material platform has risen to the pinnacle of organic electronic materials due to its superior conductivity, chemical stability, ease of processing, and relatively high transparency: Poly(3,4-ethylenedioxy thiophene):polystyrenesulfonate also known as PEDOT:PSS. In PV applications PEDOT:PSS has been investigated as an alternative to transparent conductive oxides (TCO) [4] as well as a Hole Transport Layer (HTL) in a variety of architectures [5]. However, despite garnering substantial attention and being researched abundantly, its behavior in solid state electronic devices is not yet completely understood. Understanding the behavior of this material platform and developing a comprehensive understanding of the relationships between its structure, processing techniques, and performance is key for the development of high performance organic and hybrid electronics.

PEDOT:PSS is an electronically active complex of the polythiophene family. In this form, the PSS acts as a p-type doping counter ion which allows hole mobility along the PEDOT conjugated backbone, promotes the dispersion of the complex in polar solvents such as water due to the micelle-like morphology that the complex develops, and allows for the transport of ionic charge through the material [6]. Figure 2 shows a schematic of the chemistry and morphology of PEDOT:PSS in aqueous dispersion. The conjugated polythiophene backbone provides a path of relatively high carrier mobility and is responsible for the remarkable chemical stability of the polymer.

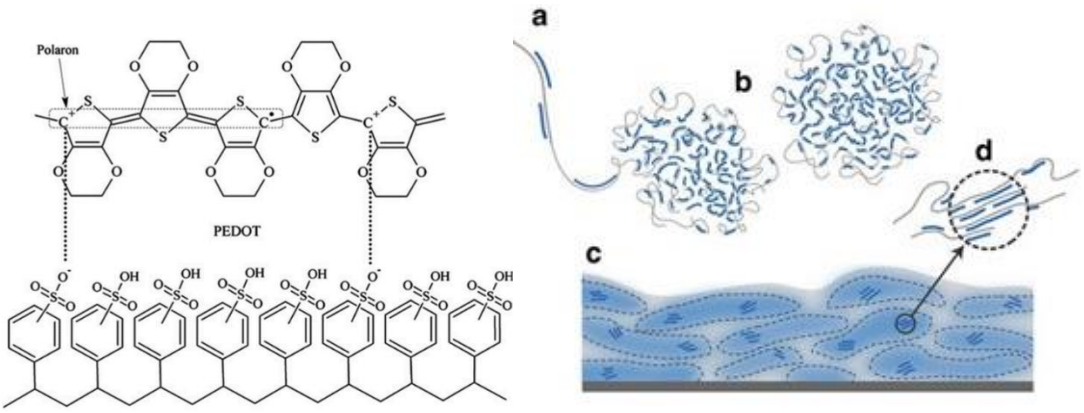

Figure 2. PEDOT:PSS chemical structure. (a) PEDOT oligomers (blue) polymerized onto a PSS template (gray). (b) Colloidal PEDOT:PSS micelle dispersion in water (c) Spin coated PEDOT:PSS film with PSS-rich outer shells (gray). (d) π-stacking in crystallites [7].

In these material systems the free charge carrier quasiparticles, known as polarons, are accompanied by a localized chain distortion as can be seen in Figure 2. Due to the localization of the chain distortion polarons exhibit much lower mobilities than free electrons and holes in inorganic materials. This phenomenon coupled with the low interchain mobility makes it challenging to develop high conductivity materials and necessitates the use of various strategies to improve the overall conductivity of the material. Nevertheless, due to the relative ease in tailoring the synthesis of these polymers, the doping concentration (and resulting free carrier concentration) can be maximized cost-effectively resulting in degenerate metal-like dispersions. In the case of PEDOT:PSS the free charge carriers are positively charged resulting in a degenerate p-type semiconductor material. By using geometric considerations, the maximum free carrier concentration in PEDOT:PSS has been estimated to be ~3×10^{20} cm^{-3} [6, p. 147].

Furthermore, morphological optimization of the PEDOT:PSS films may promote the development of crystalline stacking of the π-conjugated system such that the inter-chain mobility of carriers is enhanced.

The complex processing-structure-property relationships of this material, which are still under investigation, means the properties of a given PEDOT:PSS film are not easily predicted by theory. However, the measured and theoretical reported properties of the material provide a useful point of reference. PEDOT:PSS has reported conductivities as high as 1000 S/cm and a theoretical maximum carrier concentration of $3 * 10^{20} \text{cm}^{-3}$ which imply a hole mobility as high as the 20 $\text{cm}^2/(\text{V.s})$ typically reported for a-Si:H [6, Ch. 9]. However, the reported band alignments [8], [9] for PEDOT:PSS on Si are much more ideal than for a-Si:H, showing no valence band barrier for holes, a higher conduction band offset to block minority electrons, and reaching degenerate doping levels.

Chapter 2. THEORETICAL UNDERSTANDING OF HYBRID HJT TECHNOLOGY AND DEVICE SIMULATION

2.1. Solar Cell Basics

The current output of an ideal solar cell device can be expressed as:

$$J = J_0 \, exp\left[\frac{q}{nkT}(V - R_s J)\right] + R_{sh}V - J_L \quad (1)$$

where R_s is the series resistance, R_{sh} is the shunt resistance, n is the ideality factor, k is the Boltzmann constant, J_0 is the saturation current density and J_L is the light-induced current. J_0 is a measure of recombination in the device and can be expressed as:

$$J_0 = q\left(\frac{D_n n_i^2}{L_n N_A} + \frac{D_p n_i^2}{L_p N_D}\right) \quad (2)$$

where $D_{n/p}$ is the carrier diffusivity, n_i is the intrinsic carrier density, $L_{n/p}$ is the carrier diffusion length and $N_{A/D}$ is the doping density.

A solar cell may be described using an equivalent circuit as shown in Figure 3. The circuit consists of a current source I_{ph} connected in parallel to a diode (solar cell). An ideal solar cell is a current source in parallel with a diode, however in practice we must consider two sources of parasitic resistance: one in parallel known as the shunt resistance R_{sh} and one in series aptly named series resistance R_s.

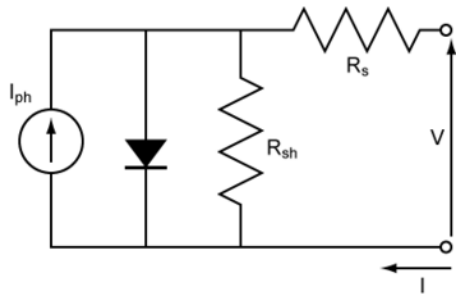

Figure 3. Solar cell equivalent circuit [10].

The resulting current-voltage (I-V) behavior of the solar cell equivalent circuit is often referred to as current-voltage (IV curves), or current density-voltage (JV curves). Figure 4 shows a typical solar cell JV curve. Most JV analysis includes both the performance under (known as the light curve) and without (known as the dark curve) illumination.

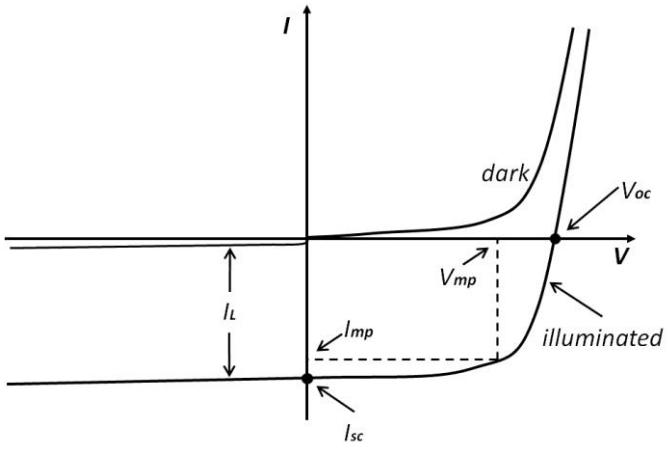

Figure 4. Typical JV plot for a solar cell in light and dark conditions [10].

Several important parameters used to characterize solar cell devices can be obtained from JV analysis as shown in Figure 4. These include the open circuit voltage (V_{oc}), short circuit current density (J_{sc}), fill factor (FF) and the power conversion

efficiency (N). The open circuit voltage represents the maximum voltage output of the solar cell device and can be identified visually from the x-intercept of the JV plot. From Eq 1 we have,

$$V_{oc} = \frac{nk_b T}{q} \ln\left(\frac{J+J_l}{J_0}\right) \quad (3)$$

Where J is the current density, J_0 is the dark saturation current, q is the elementary charge, k is the Boltzmann constant, T is the temperature, n is the ideality factor and J_l is the illuminated current density. J_0 provides a measure of carrier recombination in the device and can be expressed in terms of Eq 2.

Among the solar cell parameters V_{oc} is arguably the most important characteristic of a solar cell as it reflects the potential maximum performance of the device. From Eq 3 it can be seen that Voc, and consequently the maximum performance of the cell, depends on several factors including: the quality and band gap of the absorber, doping density, light generated current density, dark saturation current and temperature. These factors reflect the relevant carrier recombination mechanisms limiting the photoconversion efficiency of the device.

Minimizing the performance loss due to carrier recombination is a critical component of PV device design and engineering. There are three main mechanisms by which carriers recombine in the bulk (within the absorber substrate) of PV devices: (1) Radiative recombination. (2) Auger recombination. (3) And trap-assisted (TA) recombination. Equation 4 shows the relationship between the total bulk recombination

rate τ_b and the individual recombination rates of each of the three constituent mechanisms ($\tau_{radiative}, \tau_{auger}, \tau_{TA}$ respectively):

$$\frac{1}{\tau_b} = \frac{1}{\tau_{radiative}} + \frac{1}{\tau_{auger}} + \frac{1}{\tau_{TA}} \quad (4)$$

The recombination rates correspond to the average time an exciton exists before recombining through one of the three aforementioned mechanisms. Radiative recombination is most prevalent in direct-band gap semiconductors with very little effect on the overall carrier recombination rate of Si. In the radiative mechanism a photon is emitted upon the electron-hole recombination. In the Auger mechanism the excess energy released by the minority carrier is transferred to a secondary minority carrier which is then excited into a higher energy state. The trap assisted mechanism is the result of contaminants or defects of the substrate that act as mid-gap states, which can be either deep or shallow, that trap minority carriers such that recombination is both kinetically and thermodynamically favorable. The trap-assisted mechanism is perhaps the most significant challenge to address in designing and optimizing solar cell devices, as it is impossible to avoid it completely due to entropy considerations. Among the different trap-assisted mechanisms, the surface dangling bonds are among the most significant source of performance losses and is one of the main concerns addressed in this dissertation.

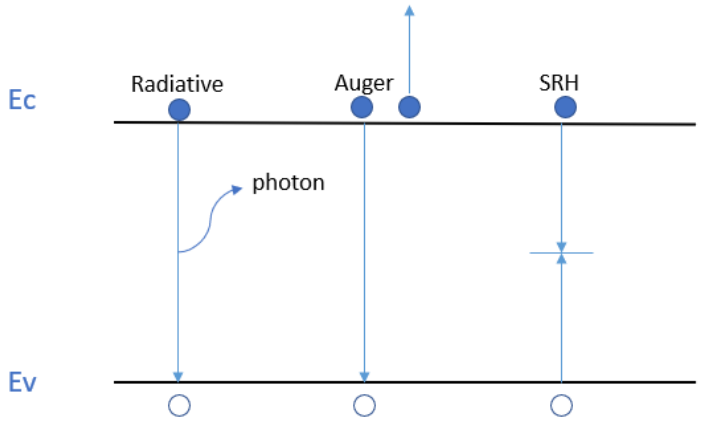

Figure 5. Illustration of carrier recombination mechanisms [10].

The second most important parameter that can be obtained from a JV plot is the short-circuit current density (J_{sc}). This parameter is equivalent to the reading taken when the external circuit attached to the cell is shorted, in the plot it is the intersection between the JV curve and the zero-voltage point. The optical performance of the cells primarily dictates the Jsc value, specifically:

1. Light trapping ability: The J_{sc} is a direct measure of the power of the incident light source and the ability of the solar cell to absorb it, this quality is commonly referred to as the light trapping ability of the cell. A common strategy used to improve the light trapping ability of silicon-based solar cells is the texturiring of the substrate. Bare silicon substrates may reflect up to 30% of incident light without any additional treatment. The most common light-trapping strategy is the texturing of the Si substrate into random pyramids via chemical etching [11]. These random pyramid structure allow the reflected light to collide with another silicon surface to be absorbed. The chemical etch is done via alkaline solutions

such as potassium hydroxide, sodium hydroxide or tetramethylammonium hydroxide (TMAH) and the resulting surface structure of the pyramids has been shown to be etched preferentially along the (111) crystal planes, which is the most thermodynamically stable of the Si crystal planes [12].

2. Anti-reflective coating (ARC): Silicon based solar cells also often make use of a surface treatment known as anti-reflective coating (ARC) on the front of the device. These coatings are usually composed of a thin layer of dielectric material with an index of refraction that allows for destructive interference upon internal reflection of the light. In order to take advantage of the anti-reflective properties of the coating, the thickness of the layer must be one quarter the wavelength of the incoming light wave. Silicon nitride is the most popular ARC coating material for silicon based solar cells, this material is optimized such that the reflected light from the device appears blue, maximizing photocollection efficiency in the desired spectral range.

3. Incident light spectrum: the spectrum of incident light from the sun that reaches the surface of the earth is known as terrestrial AM 1.5 G spectrum. This spectrum consists primarily of the visible spectrum (350-780nm), such that the absorber of the solar cell device must have a high quantum efficiency (QE) within the visible spectrum to achieve a high-performance device. Solar cell measurements are always done under AM 1.5 G. AM refers to air mass which is the path length sunlight takes in comparison to when the sun is perpendicular in the equator during noon. The term G refers to global radiation which includes both direct and

diffused radiation. The QE parameter is essential to understand the photocurrent of a solar cell. QE is the ratio of the photocurrent generated by the solar cell to the number of incident photons.

The third and final solar cell parameter that can be obtained from the JV plot is the fill factor (FF). Graphically, fill factor is a measure of the squareness of the light JV curve of the solar cell as seen in Figure 6. It is the ratio of the maximum power from the solar cell to the product of V_{oc} and Jsc as shown in Eq 5. The maximum power is obtained at maximum voltage and current density denoted by V_{mp} and J_{mp} respectively. The FF of a solar cell needs to be maximized and be as close as possible to 1.

$$FF = \frac{V_{mp} * J_{mp}}{V_{oc} * J_{sc}} \tag{5}$$

The efficiency of a solar cell is the ratio of output power to input power. The input for the irradiation power for efficiency calculations is 1 kW/m^2or 100 mW/cm^2. The output power is also known as the maximum power. The formula for calculating the solar cell efficiency is then:

$$\eta = \frac{P_{out}}{P_{in}} = \frac{P_{max}}{P_{in}} = \frac{J_{mp}V_{mp}}{P_{in}} = \frac{J_{sc}V_{oc}FF}{P_{in}} \tag{6}$$

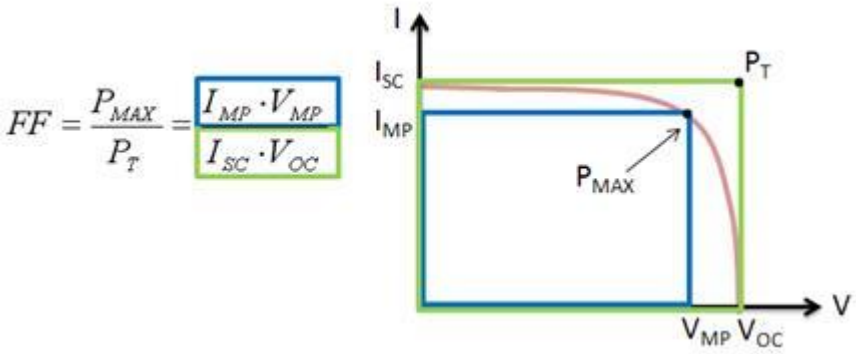

Figure 6. J-V curve parameters and their relationships [10].

2.2. Hybrid Heterojunction and PV Technology Overview

The photovoltaic effect, the process by which an electron is excited from its ground state to a higher energy level when interacting with photons, is the fundamental principle that allows for direct solar energy harvesting using solar cell devices. Solar cell devices utilize semiconductor materials, which exhibit a gap of electronic states between the valence and conduction bands (the energy difference between the two is referred to as the band gap or EG), as the absorber substrate. Upon excitation of an electron from the valence band to the conduction band through interaction with a photon of energy hv>EG an electron-hole pair quasiparticle known as an exciton is formed. Due to electrostatic considerations the two charge carriers, electron and hole, are bound to each other such that it is thermodynamically favorable for the electron to relax back to its original state by recombining with the hole. In order to effectively transform the solar energy into a useful electric current the charge carriers must be extracted from the device prior to recombining. In addition to maximizing the photo-collection efficiency, the strategies

employed to efficiently extract the photo-generated carriers are the most important challenges in designing solar cell devices.

The strategies for efficient carrier extraction involves four main components:

1. The induction of an electric field in the device, also known as junction formation.
2. Minimization of bulk recombination in the absorber substrate.
3. Minimization of surface recombination at the interfaces of the device.
4. Minimization of resistive losses across the device.

Traditionally the induction of the electric field in solar cell devices was accomplished by the formation of a p-n junction in an inorganic semiconductor substrate such as silicon. Solar cell devices are in essence the same as diodes in their operating principles. A p-n junction is formed when opposite charged dopants are introduced to a single-material substrate by drive-in diffusion, an energy intensive and costly process. A more recent approach to junction formation utilizes distinct materials to induce the electrostatic field in the device, this is known as heterojunction technology and has shown great promise in delivering high performance solar cell devices. The heterojunction approach utilizes carrier-selective materials as the contacts to the device. Carrier selective contacts work by having offset conduction and valence band energy levels relative to the absorber, with one of the offsets providing an energetically favorable transition path for carriers and the other one a large transition barrier; a hole-selective contact will have a higher valence band and much higher conduction band energy levels

than the absorber, a depiction of which can be seen in the right of Figure 7. Upon the contact of the two materials with offset bands charge equilibrium must be reached such that the Fermi level is spatially uniform, this results in the depletion of free carriers at the interface between the two materials such that any fixed dopant charges create an electrostatic field. This space is also known as the depletion or space-charge region. Upon the photo-generation of free carriers in the presence of a junction both the drift and diffusion of carriers result in a net current that can be harvested by an external circuit. Figure 7 shows a schematic of the formation of a typical p-n junction as well as the band diagram of a typical heterojunction device.

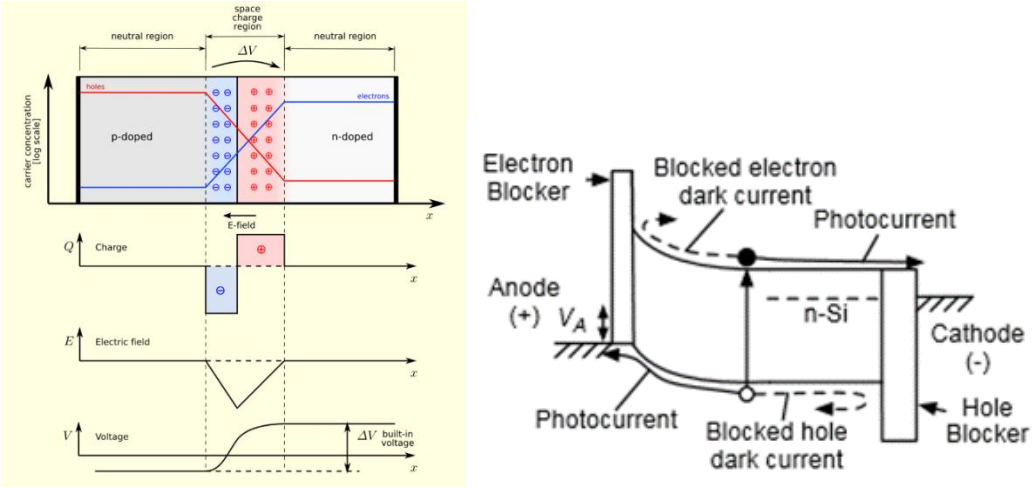

Figure 7. Schematic of the formation of a p-n junction [13] (left) and band diagram of a typical heterojunction device [14] (right).

Given the semiconducting behavior of conjugated polymers the same principles can be applied to fabricate solar cell devices incorporating a variety of organic materials. This provides the opportunity to realize the benefits relating to inexpensive and simple

fabrication techniques greatly reducing the fabrication cost of solar cell devices. Nevertheless, incorporating these materials into solar cell devices introduces additional complications relating to the performance and reliability of the devices. First, in the case of organic photovoltaic (OPV) technologies the use of semiconducting polymers as the absorber material greatly complicated the challenge of exciton dissociation and charge separation due to the high exciton binding energies resulting from limited conjugation and polaronic effects. Second, organic materials are prone to rapid degradation from UV-assisted oxidation under ambient conditions, necessitating the development of advanced packaging and encapsulation strategies.

Although the recent advancements in the field of OPV have demonstrated the potential of this technology platform, hybrid technologies that combine traditional and organic semiconductors have shown more promise of delivering high performance solar cell devices in the short term. By utilizing traditional semiconductors as the absorber and limiting the use of semiconducting polymers as carrier selective contacts the fabrication costs remain low while leveraging the well-established expertise for the optimization of the absorber base material. In the development of hybrid PV technologies the application of PEDOT:PSS as a hole transport layer (HTL) has been a growing area of interest in recent years due to the opportunity for simple low-temperature processing and its anti-reflective properties [15]–[18].

Although many Hybrid PV device architectures incorporating PEDOT:PSS have been investigated, the most popular approach utilizes n-type silicon substrate as the absorber with PEDOT:PSS as the front contact of the device as can be seen in Figure 8.

In this structure the PEDOT:PSS front contact of the device serves three main purposes: induce a photoactive junction with the silicon substrate, selectively collect holes, and act as an antireflective coating.

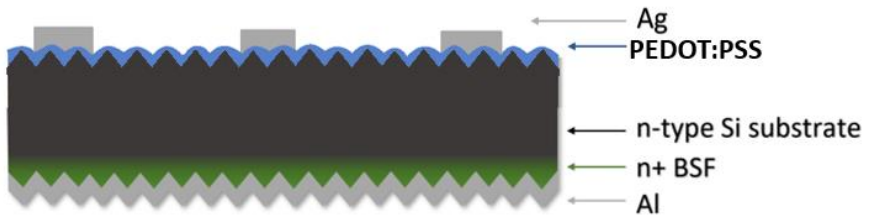

Figure 8. Schematic of PEDOT:PSS-front junction hybrid solar cell device.

Given the extensive records of investigations reported in the literature on both PEDOT:PSS and silicon, this simple hybrid solar cell architecture holds great promise as a commercially competitive PV solution as well as a research platform to advance the understanding and design paradigm of hybrid PV technology and hybrid solid state devices more broadly. This dissertation focuses on outlining the most recent learnings regarding these solar cell devices as well as recounting the experimental results of the projects focused on its design and optimization.

In the device architecture show in Figure 8, the PEDOT:PSS film behaves like a degenerate p-type semiconductor inducing a photoactive heterojunction by causing the development of an inversion layer, or a region where the minority and majority carrier concentrations are switched, within the n-type silicon substrate. It is thought that due to the high doping level of the PEDOT:PSS all the band bending occurs in the silicon such that the junction is one-sided as is the case with a metal-semiconductor Schottky junction,

the band diagram for which can be seen in Figure 9. The resulting band alignment due to this inversion is such that the PEDOT:PSS effectively acts as an HTL by repelling electrons, promoting charge separation and extraction, and minimizing recombination losses at the interface. This aspect of hybrid heterojunctions, however, remains poorly understood, particularly regarding the potential for defect-induced Fermi level pinning common in metal-semiconductor Schottky junctions or other factors responsible for the measured energy level alignment. It is well known that the reproducibility of these energy level alignment measurements is inconsistent across the literature, showing significant differences that have been attributed to differences in the quality of the PEDOT:PSS stock dispersions used [8], [9], [19].

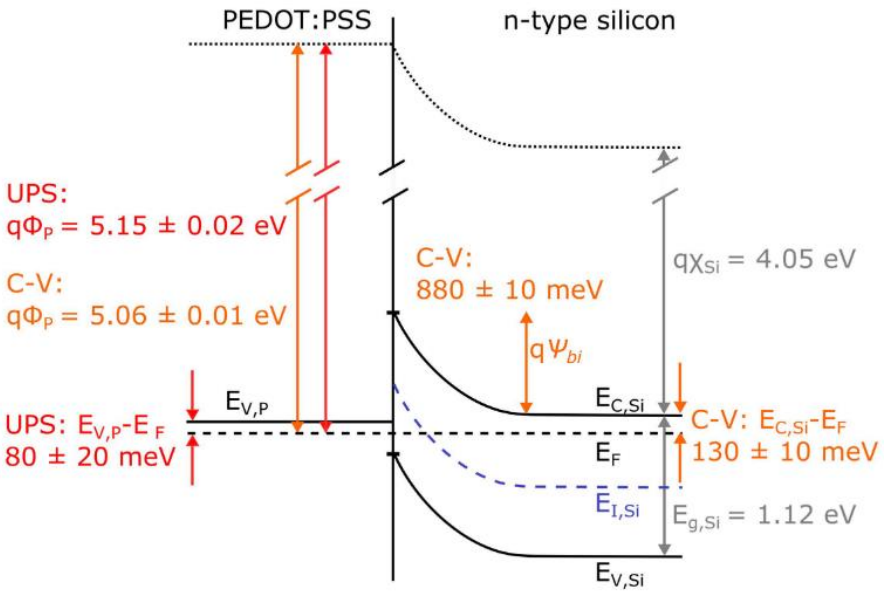

Figure 9. Band diagram of PEDOT:PSS-Silicon heterojunction energy level alignment [8].

Other properties of the PEDOT:PSS film are also important to the overall efficiency of the resulting device and have been studied and optimized thoroughly to achieve the champion efficiencies. Most notably, despite having such a high carrier concentration, the conductivity of PEDOT:PSS is limited by the hole mobility and results in a much lower conductivity than traditional metals and semiconductors. This is because holes exist in the PEDOT chain as polarons which occupy a significant portion of the chain and their movement involve a significant chain distortion. This lower conductivity has prompted numerous studies on improving it by different methods. One such method is the addition of co-solvents to the PEDOT:PSS dispersion which modifies its structural morphology, promoting the closer packing of the micelles which in turn increases the conductivity of the films. Solutions of ethylene glycol (EG) and dimethyl sulfoxide (DMSO) have emerged as the most effective co-solvents for this purpose [20]–[22]. Carrier collection is a major concern in designing solar cells, and transport losses due to the resistance of the materials are highly detrimental. The conductivity of the topmost layer of the device is clearly a significant factor in the performance of the devices and can potentially be an impasse if this layer hinders carrier transport significantly.

Finally, the optical properties of the PEDOT:PSS film are also of important significance. PEDOT:PSS has a high reported transparency in the visible spectrum, with 80nm films exhibiting an almost flat transmission curve hovering around 90% with a slight tilt to higher absorption in the red [6, p. 141]. In order to understand the behavior of this polymer film on hybrid devices, particularly how the absorption of light and the antireflective effects affect device performance we must consider the complex index of

refraction, which has previously been reported by Hoppe et al. [23]. We utilized this dataset to optimize the antireflective performance of the PEDOT:PSS films utilizing the OPAL 2 online optical simulation tool [24] and found the optimal thickness to be around 65-70nm. In this thickness range we further determined that the PEDOT:PSS films parasitically absorbs between 1.9-6.5% of incident light.

In this work we investigate the principles that dictate the behavior of these hybrid devices in order to understand the source of the technology's shortcomings and formulate a path for the development of reliable, high efficiency (PCE>20%) hybrid cells that can be processed at room temperature and have a reduced production cost. Many aspects of these devices have been thoroughly studied and optimized previously, especially in the case of the cell architecture seen in Figure 8. Therefore, we will limit the scope of the research to three particularly important areas that are still less understood:

- First, we will attempt to identify the mechanisms of the degradation of hybrid solar cells fabricated by spin coating, focusing on the role of the interface between the silicon base and the conjugated polymer and the junction that develops as a result.
- Second, we will try to understand the fundamental shortcomings of using spin coated PEDOT:PSS in hybrid devices and explain the gap between the champion cells that have achieved maximum efficiency and the more commonly achieved efficiencies.
- Third, we will explore in-situ deposition as an alternative processing method for the deposition of PEDOT films paired with alternative doping materials

and surface treatment of the silicon surface to overcome the shortcomings of the devices fabricated by spin coating PEDOT:PSS.

2.3. Hybrid HJT PV Device Simulation

A model of PEDOT:PSS-Silicon solar cell was constructed in the numerical simulation tool AFORS-HET (Automat FOR Simulation of HETero structures) [25]. A 65 nm thick PEDOT:PSS layer was modeled on top of a 150-micron n-type silicon substrate. The silicon had a shallow dopant density of $5*10^{15}$ cm^{-3} and was modeled with a mid-gap trap density of 10^{9} cm^{-3}, giving a high bulk minority carrier lifetime of 10 ms. Dangling bonds at the front c-Si interface were modeled using a 1 nm thick layer with a trap density of $1*10^{20}$ cm^{-3}. These traps are modeled as two Gaussian distributions of acceptor and donor states centered at 0.635eV and 0.485eV, with widths 0.18eV.

PEDOT:PSS was modeled as a p-type semiconductor with variable acceptor doping concentration (maximum value of $3*10^{20}$ cm^{-3}), representing the effective doping level of mobile positive charge in the material. Hole mobility was set to 10 cm^2/Vs. This gives a hole conductivity of 480 S/cm, in line with experimentally measured sheet resistance values [21]. Modeled material properties were selected to match with the band energy positions reported by Jäckle et al. [8], [9]. The PEDOT:PSS bandgap was given an electron affinity of 3.6 eV and a bandgap of 1.3eV[11]. The PEDOT:PSS was modeled as degenerately doped, with the Fermi level 80 meV below the valence band [8]. In order to achieve the appropriate Fermi level position, the effective density of states (DOS) of the conduction and valence bands were each adjusted to $1.35*10^{19}$ cm^{-3}. It is assumed that

photon absorption in the PEDOT:PSS layer is parasitic, modeled by adding a midgap trap state with a density of $1*10^{16}$ cm^{-3} to reduce the carrier lifetime in the PEDOT:PSS layer to 1 ns. The low frequency permittivity of PEDOT:PSS has not been well established and is known to be sensitive to free carrier concentration. An approximate relative permittivity of 10 is used for this simulation, in accordance with typical values from the Drude-Smith model shown by Reynolds et al. for localization parameter values $c_1 < -0.5$ [26]. Data from Hoppe et al. was used for modeling the refractive index at optical frequencies [23].

The oxide layer was modeled using an interfacial tunneling layer with an electron affinity of 0.9 eV, bandgap of 8.9 eV, and dielectric constant of 3.9. For the rear contact, a back surface field was modeled with shallow n-type dopant density increasing linearly from the bulk density to 10^{19} cm^{-3} over 10 nm. Flatband metal contacts were assumed for the front and rear.

Based on the best-known properties of the system (PEDOT conductivity of 7500S/cm [27], silicon surface recombination velocity of 1.6cm/s [28], and no oxide formation) we found our cell architecture to have an upper photoconversion efficiency (PCE) limit of 21%, a figure comparable with the performance of a-Si:H HIT technology, see Figure 10.

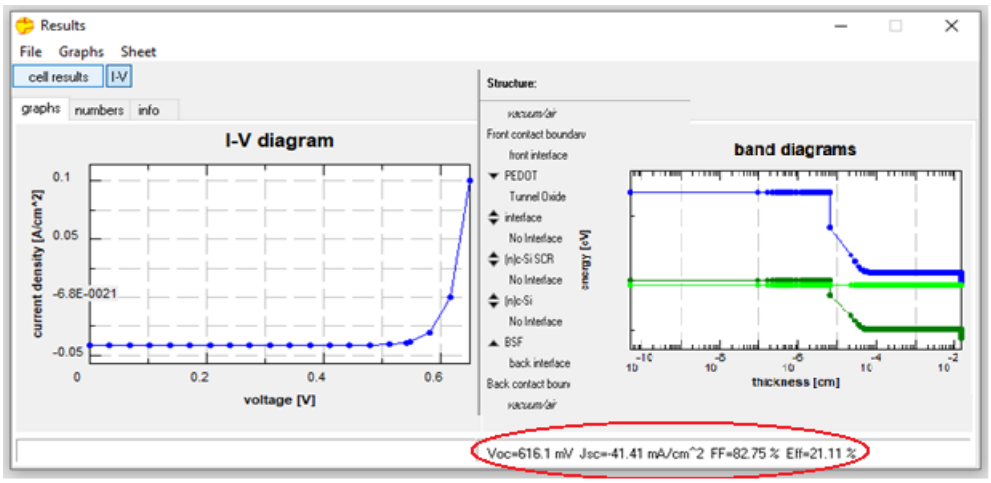

Figure 10. Simulation results of upper theoretical limit of hybrid silicon-PEDOT solar cell with an efficiency of 21.11%, V_{oc}=*616.1mV*, J_{sc}=*41.41mA/cm*^{2}, *FF=82.75%*.

The results of the simulated model reveal the high potential of the hybrid HJT PV device architecture. Throughout the remaining chapters of this dissertation, it will be clear that the main factors hindering the performance of prototype devices are:

1. The lack of an appropriate organic silicon surface passivation strategy.
2. The rapid growth of an interfacial oxide layer that degrades the quality of the junction and promotes the development of s-shaped JV characteristics.
3. The degradation of the electrical properties of the PEDOT film under ambient conditions.

Chapter 3. EMPIRICAL OPTIMIZATION OF SPIN-COATED HYBRID HJT DEVICES[1]

3.1.Introduction

Many materials and cell architectures are currently being investigated in the field of hybrid PV devices in order to achieve competitive cell performances. The most popular approach being currently investigated for these hybrid devices is to use a traditional semiconductor base and an appropriate conjugated polymer as a carrier selective contact to induce a photoactive junction and act as an emitter. Conjugated polymers have significant advantages compared to small molecules primarily due to their increased stability and processability. One of the most promising hybrid PV cell architectures currently under study can be seen in Figure 11. This cell employs the conjugated polymer Poly(3,4-ethylenedioxy thiophene):polystyrenesulfonate (PEDOT:PSS) as a hole carrier selective contact on n-type silicon. One of the main advantages of this architecture is that PEDOT:PSS, besides having a relatively low-cost and being easy to process, acts as an anti-reflective coating improving the photo collection efficiency of the device [15], [20], [22], [29]–[31].

[1] This chapter draws heavily from A. Iyer, J. Hack, D. A. A. Trujillo, B. Tew, J. Zide, and R. Opila, "Effects of co-solvents on the performance of PEDOT: PSS Films and hybrid photovoltaic devices," *Applied Sciences (Switzerland)*, vol. 8, no. 11, pp. 1–12, 2018, doi: 10.3390/app8112052. Reproduced with permission.

Furthermore this cell employs a passivating layer between the silicon and the PEDOT:PSS layer, in this case a small organic molecule known as Benzoquinone (BQ) has been employed for this purpose [32].

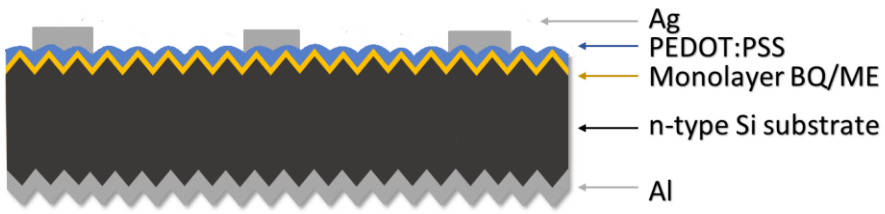

Figure 11. schematic of the hybrid photovoltaic device architecture [21].

Heterojunction with intrinsic layer (HIT) cells based on amorphous silicon have achieved exceptionally high efficiencies and the physical principles that dictate their performance are applicable to the hybrid solar cells being developed in this work. Understanding the behavior of these heterostructure cells is important because use of hybrid technology would overcome the high cost of production and high processing temperatures traditionally required.

There are two key features of the amorphous silicon heterostructure cell that allows them to reach such high efficiencies are: first, optimal passivation of the silicon surface which minimizes carrier recombination. Second, the carrier selective contacts on both ends of the cell maximize carrier separation and minimizes current loss to recombination or carrier extraction [33]. In these cells, the crystalline silicon base is first

contacted with an intrinsic layer of amorphous Si:H which has exceptional passivation qualities. Following the intrinsic layer, heavily doped amorphous silicon is deposited on each side. This essentially induces a photoactive junction in the silicon base. In a similar manner, PEDOT:PSS acts as a heavily doped p-type semiconductor that acts as a hole carrier selective contact which induces a photoactive junction on the n-silicon base. The most obvious advantage of replacing amorphous silicon with organic materials is the decrease in processing cost due to the much lower temperatures required. Due to apparent similarities between these two systems, it should be possible to reach efficiencies comparable to the already demonstrated a-Si HIT cell performance. The gap between this maximum potential efficiency and the current state of the technology has to be bridged by identifying and correcting the main design challenges.

Theoretically, considering the electrical behavior of the organic materials and their interaction with traditional semiconductors, these hybrid devices should have a competitive performance compared to traditional PV cells. However, due to the relative newness of the technology, and of the field of electrically conducting organic materials in general, poor efficiency and fast degradation remain the most notable shortcomings of this technology. The market space for PV energy is highly competitive and due to the high efficiencies achieved by the current technologies, emerging technologies have a challenging bar to overcome.

We have investigated iterations of the cell structure shown in Figure 11 and have achieved a maximum PCE of 12.6% on a cell with amorphous silicon back contact and a textured front silicon surface. The textured silicon paired with the antireflective

properties of the PEDOT:PSS layer optimizes the photo collection efficiency of the device. Furthermore, we have employed an organic treatment of the front surface with BQ to passivate the silicon surface prior to the PEDOT:PSS deposition. In the case of this champion cell, its comparatively high performance emphasizes the need for proper passivation of both silicon surfaces. We have been able to achieve reliable cell performance with an Aluminum-BSF back contact scheme, but their efficiency though consistent are lower than 12%. Using these back-contact schemes defeats the main goal of this research: fabricating the cells at low temperatures and reduced cost. However, they are an important tool to isolate the lesser-known behavior of the front contact.

Alternative cell structures have been investigated by other groups achieving better performances which demonstrate the potential of this cell architecture to achieve commercially competitive performance. Notably, the record performance for this cell architecture on a planar silicon substrate using PEDOT:PSS as the front contact has been of 17.3% [34] and the use of PEDOT:PSS as a back contact with an alternative front contact has led to a cell with 20.6% efficiency [35]. These back-PEDOT cells utilize a phosphorous diffused front emitter and silicon nitride passivation. Understanding the underlying principles that dictate the behavior of these devices and the reasons behind the performance gap between the champion devices and other samples will allow for this technology to become a real competitive commercial alternative.

Carrier collection is a major concern in designing solar cells. For our devices, we employ a silver fingers-bus bar scheme as a front contact deposited by electron beam physical vapor deposition with the use of a shadow mask. In designing the shadow mask

for the contact, the primary goal is to minimize the shading caused by the metal while maintaining an optimal carrier collection. The efficiency of carrier collection is limited by transport losses through each of the materials and at the interfaces between them. For ohmic contacts, the transport losses at the interface are inversely proportional to the total contact area, such that there is a tradeoff between losses due to shading and those due to transport. In order to design the shadow mask, losses due to the metal contact resistance and shading, the contact resistance at the interface, and the resistance of the PEDOT:PSS must be quantitatively determined and optimized. This optimization was performed using the open access PV Lighthouse calculator [36]. In this case, silver was used as the front metal contact due to its high bulk conductivity and its reported compatibility with PEDOT:PSS, the specifics of which have not been adequately investigated previously. In this work, we quantitatively characterize the electrical properties of the Ag/PEDOT:PSS interface and used these results for our mask design. We demonstrate this interface develops ohmic characteristics with an even lower resistance than previously reported.

It is not surprising that the performance of these hybrid solar cells is highly dependent on the properties of the PEDOT:PSS film, particularly its optical and electrical properties, and the behavior of the interfaces between the materials. PEDOT:PSS behaves like a degenerate p-type semiconductor which is why it induces a photoactive junction with n-type silicon, with the depletion region located exclusively in the active silicon layer. By using geometric considerations, the theoretical maximum doping concentration of PEDOT:PSS can be estimated to be 3×10^{20} cm^{-3} [6]. Despite such an allegedly high carrier concentration, the conductivity of PEDOT:PSS is limited by the carrier mobility

and results in a much lower conductivity than traditional metals and semiconductors, which has prompted numerous studies on improving it by different methods [18], [37], [38]. One such method is the addition of co-solvents to the PEDOT:PSS dispersion, which modifies its structural morphology, promoting the closer packing of the micelle, which in turn results in better conductivity of the deposited films [22]. Solutions of ethylene glycol (EG) and dimethyl sulfoxide (DMSO) have emerged as the most effective co-solvents for this purpose [7], [15].

The final purpose of the PEDOT:PSS layer is to acts as an antireflective coating which can be combined with texturing of the front silicon surface to increases the photo collection efficiency of the device. Achieving this effect, however, poses several unique design challenges. First, the antireflective effect that can be achieved by PEDOT:PSS must be balanced against the parasitic absorption of the film and the resistive losses owing to the lateral conductivity of the film. A thinner film will exhibit less parasitic absorption but its lateral conductivity will be compromised increasing the series resistance of the device. Like other antireflective treatments the antireflective effects of the PEDOT:PSS film occur at a specific film thickness dictated by its optical properties and the spectrum of incident light. The researchers of the high performing back-PEDOT cell architecture blame parasitic absorption as the sole reason behind the much higher performance of their cell compared to the traditional front PEDOT architecture. [35], [39], [40] This is a bold assumption due to the fundamental potential for PEDOT to act as an effective antireflective coating.

Within this context it is clear that accurately controlling the deposition conditions of PEDOT:PSS is critical to ensure films of proper thickness and homogeneity in order to maximize the photovoltaic performance of the devices. Spin coating is a highly reliable solution-based deposition technique that produces highly homogeneous films, however this technique is most suitable for planar substrates such that considerable care had to be taken in adapting this process to the textured substrates used in this work. In spin coating, the rheological properties of the fluid, its interfacial interactions with the substrate, as well as the spin speed and time ultimately determine the thickness and homogeneity of the resulting film. Non-uniformity of the PEDOT:PSS coating will translate into an increase of parasitic absorption and ineffectiveness of the desired antireflective effect.

In this chapter, we aim to understand the implications of using the two co-solvents mentioned previously, EG and DMSO, in the design and fabrication of hybrid solar cells which employ a benzoquinone solution-based surface passivation treatment, a pyramidal textured silicon active layer, and a silver bus bar-finger front metal contact [28].

- First, we validate the spin coating procedure for the PEDOT:PSS dispersions on textured substrates by analyzing the homogeneity and uniformity of the films.
- Second, we test the effects of these co-solvents on the electrical properties of PEDOT:PSS films.
- Third, we characterize the effects of the co-solvents on the photo collection efficiency of our device architecture.

- Fourth, we quantitatively characterize the electrical interfacial behavior between PEDOT:PSS and silver.
- Fifth, we fabricate and characterize the hybrid solar cells, following the design described previously, using these co-solvents, and explore their effects on device performance.

3.2. Materials and Methods

N-type silicon (100) textured substrates (doped with phosphorous, CZ) with a back surface field (BSF) were fabricated at Arizona State University (Solar Power Lab, ASU, Tempe, AZ, USA). These wafers are 145 microns thick with 1–5 ohm-cm resistivity. Random texturization was performed on both sides using potassium hydroxide (2% KOH yielding pyramid sizes of about a 3–5μm base size) alkaline etching. To create BSF n+ layer on the N-type wafers, phosphorous oxychloride diffusion was performed at 820^{o}C for 15 min with a $POCl_3$ carrier gas flow rate of 1500 sccm (standard cubic centimeters per min). This step is for the phosphosilicate glass (PSG) growth and drive-in. Finally, the wafers were then exposed to a 10 min buffered oxide etch to remove the PSG. The sheet resistance value of the BSF side is 55 ohm/square. Double-side polished intrinsic silicon substrates were purchased from Virginia Semiconductors (Fredericksburg, Virginia, USA). These polished wafers are 300 microns thick and have a resistivity >5000 ohm-cm.

PEDOT:PSS PH1000 (Heraeus Clevios, Vandalia, OH, USA) was used as the stock polymer dispersion. The solvents ethylene glycol (EG), dimethyl sulfoxide

(DMSO), and surfactant Triton X-100 (non-ionic surfactant) were purchased from Fischer Chemical (Waltham, MA, USA) (>95%) and used as purchased.

The substrates were cleaned using a Piranha etch (H2SO4:H2O2 = 4:1) for 5 min, followed by a 5-min DI water rise and a 2-min immersion in hydrofluoric acid (HF, 2 wt%). After cleaning, the substrates were quickly dried by blowing nitrogen and immediately placed in the passivation solution of benzoquinone (BQ) and methanol (MeOH). The wafers are allowed to stay in the sealed bag containing a passivation solution for 2 hours in ambient light conditions. Passivation studies performed in the group previously have suggested that benzoquinone (BQ) does an effective job of passivating the surface. Post-2-hour immersion in BQ, the wafers were removed and given a quick rinse with methanol. The wafers were dried and put on a spinner chuck for spin coating.

PEDOT:PSS dispersions were prepared in advance of the spin coating procedure by adding the appropriate co-solvent amounts as well as 0.25 wt% Triton X-100 as a surfactant. The dispersions were then deposited by spin coating on the appropriate wafers at different spin conditions in a Headway Research (Garland, TX, USA) spin coater. All spin-coated samples were baked on a hot plate at 135^{o}C for 15 min immediately following the PEDOT:PSS deposition.

Textured silicon wafers of 1 cm x 1 cm were used as substrates for the validation study of the spin coating procedure. An X-ray energy dispersive spectroscopy (XEDS) analysis was conducted on a JEOL JSM-7400F (Peabody, MA, USA) scanning electron

microscope (SEM). X-ray photoelectron spectroscopy (XPS) measurements were conducted on a Physical Electronics (PHI) model 5600 X-ray photoelectron spectrometer (Chanhassen, MN, USA) using an Al 7 mm filament monochromated source with an X-ray energy of 1486.6 eV.

Double-side polished intrinsic silicon wafers were used as substrates for the PEDOT:PSS conductivity measurements. Conductivity measurements were carried out by the van der Pauw technique on a custom-built room temperature resistivity and Hall Effect system. The resistivity of the films was measured twice (bi-directional by switching the four contacts between voltage and current probes) and the resulting values were averaged.

Device reflectivity measurements were carried out on 2 cm x 2 cm textured silicon substrates with different PEDOT:PSS spin-coated recipes. A Perkin-Elmer Lambda 750 UV/Vis/NIR spectrophotometer (Hopkinton, MA, USA) was used to conduct ultraviolet-visible spectrophotometry (UV-VIS).

Textured silicon wafers of 1 cm x 1 cm were used as substrates for the transmission line measurements (TLM). Ag contact pads that are 500 nm thick were deposited via electron beam physical vapor deposition with length L = 0.5 mm and widthW= 10 mm at spacings of d = 0.1 mm, 0.2 mm, 0.4 mm, 0.8 mm, 1.6 mm, and 3.2 mm. The resistance was measured between adjacent sets of contact pads with a Keithley 2400 sourcemeter (Beaverton, OR, USA).

Completed 1 cm x 1 cm solar cell devices were fabricated on textured silicon wafers prepared using the described cleaning procedure. After approximately 10 min, appropriate PEDOT:PSS dispersions were then spin-coated on the front of the wafers (face without BSF) through a 0.22-micron filter. Metal contacts were then deposited on the samples via electron beam physical vapor deposition on a dual electron-beam evaporator (Wilmington, MA, USA). Aluminum was used as the back contact and deposited on the BSF-treated side of the wafer, while silver was used as the front contact and was deposited with the help of a shadow mask directly on the PEDOT:PSS films. The shadow mask which was designed following the guidelines described previously had a total power loss of 19%, 10.4% due to shading, 6% estimated due to contact resistance, and the remaining estimated due to resistive losses in the PEDOT film and Ag fingers. The shading losses in particular are comparatively higher than in commercial crystalline silicon panels which have been reported to be around 4-7% [41].

The performance of these devices was evaluated using illuminated current density-voltage measurements (JV). The JV response was measured by means of a DC source meter (Keithley 2400 sourcemeter (Beaverton, OR, USA)) both in dark and light, under an air mass 1.5 G standard illumination.

3.3. PEDOT:PSS Coating Uniformity on Textured Substrates

Due to the texturing of the substrate and the addition of co-solvents, the quality of the spin-coated PEDOT:PSS films had to be validated in order to confirm proper homogeneity and uniformity. Furthermore, the performance of an anti-reflective coating

is dependent on the thickness of the film and the wavelength of light such that there is an optimal thickness for the solar spectrum that optimizes photo-collection and device performance. In the case of PEDOT:PSS, previous simulations performed using the online optical simulator OPAL 2 suggested an optimal thickness of 65-70 nm on a planar silicon substrate for the optimization of the anti-reflective properties of the coating at AM1.5g direct illumination conditions. Previous ellipsometry studies on PEDOT:PSS with both EG and DMSO spin-coated on planar silicon substrates have confirmed the reproducible film thickness results for different spin conditions: 4000 rpm for 300 s having a thickness of 50 nm and 2250 rpm for 300 s for a thickness of 65 nm [32].

Testing the thickness of PEDOT:PSS films spin-coated on textured surfaces poses a technical challenge as it is obvious that the texturing of the substrate induces additional roughness and inhomogeneity to the films. In fact, preliminary ellipsometry studies of films deposited on textured substrates confirm significant thickness variations throughout the deposition area, such that we are not confident in reporting the thickness of these films quantitatively. Due to the additional roughness and inhomogeneity introduced, it was important to confirm the complete coverage of the substrates as it is not immediately obvious that the spin coating procedure on these substrates guarantees complete coverage. It is also important to, at least qualitatively, understand the magnitude of the thickness variation of the film throughout the deposition area.

PEDOT:PSS dispersions containing 7 wt% EG or DMSO were spin-coated on textured silicon wafers at 2250 rpm for 300 s. X-ray Energy Dispersive Spectroscopy (XEDS) and X-ray Photoelectron Spectroscopy (XPS) were conducted on the samples in

order to confirm the complete coverage of the substrates and study the homogeneity of the films. Figure 12 shows the elemental mapping results of the XEDS analysis. The image reveals a greater concentration of C and S near the base of the pyramids of the substrate, indicating that during the spin coating, the PEDOT:PSS accumulates in the valleys of the texturing. It is difficult to establish complete PEDOT:PSS coverage of the silicon substrate based on the XEDS data alone due to the probing depth of the electron beam being thicker than the PEDOT:PSS films. XPS is a more surface sensitive technique and is capable of probing the first few nanometers of the sample. XPS analysis shown in Figure 13 revealed that no measurable concentration of silicon was present at the surface of the samples, confirming complete coverage of PEDOT:PSS and indicating a lack of significant shunt through-holes in the PEDOT:PSS layer. Based on these results we can say that the reliability of the spin coating procedure translates well to the textured substrates and the use of co-solvents, but the accumulation phenomenon towards the valleys of the texturing is pervasive and its implications must be considered carefully. This accumulation phenomenon occurred in all the samples tested, however, from these techniques alone it is not possible to quantitatively characterize the irregularity of the film.

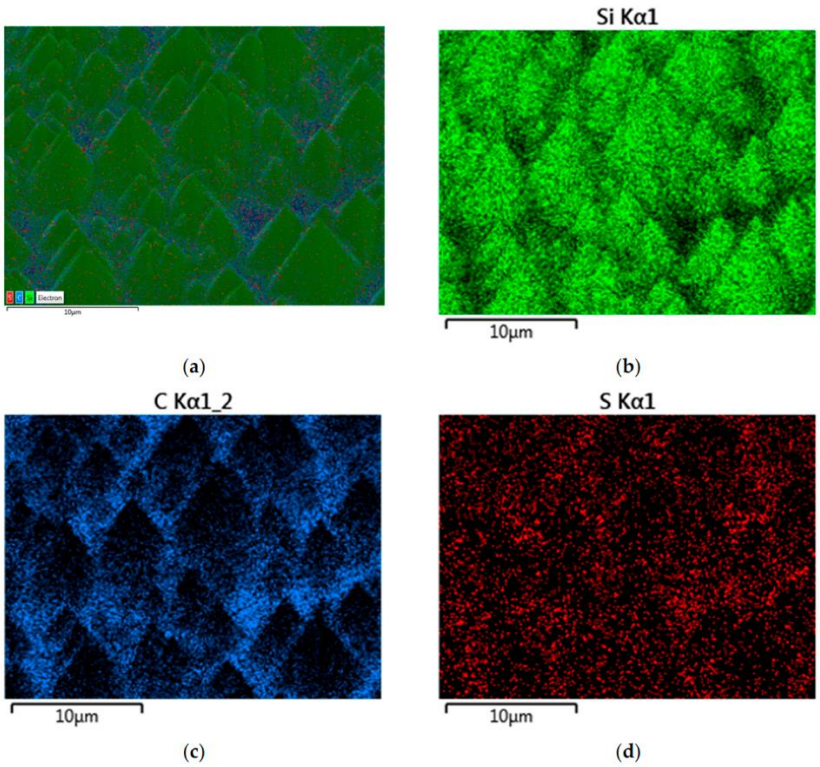

Figure 12. (a) The composite XEDS image of PEDOT:PSS solution spun on textured Si wafers (b) Si $K\alpha_1$ component peaks (c) C $K\alpha_{1\_2}$ component peaks, showing an accumulation of carbon in the valleys between the pyramids (d) S $K\alpha_1$ peaks show a similar accumulation in the valleys, but a lower image contrast is visible [21].

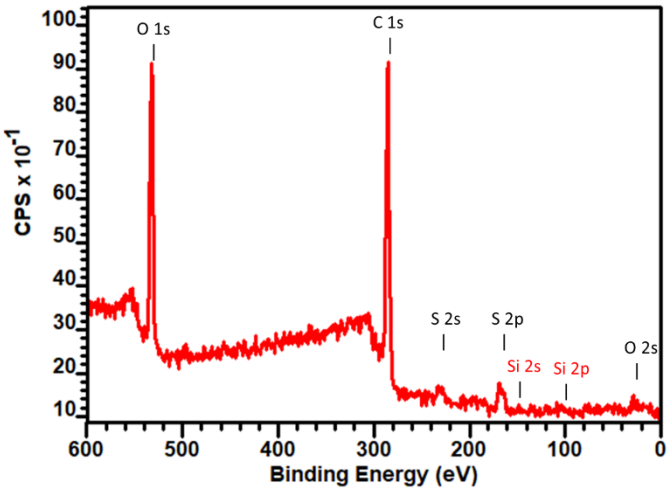

Figure 13. The XPS survey data, with locations of relevant 1s, 2s, and 2p (triplet) peaks indicated. The peaks for oxygen, carbon, and sulfur, prominent in PEDOT:PSS, are indicated in black. No silicon peaks are discernable, indicating the complete or near-complete coverage of the surface by the PEDOT:PSS layer [21].

3.4. Electrical Conductivity of PEDOT:PSS

PEDOT:PSS dispersions with different co-solvent compositions were spin-coated on planar silicon substrates, as opposed to the textured substrates used for devices, at different spin conditions and their electrical properties were tested by the van der Pauw technique. The additional roughness introduced by the substrate texturing would cause a large error that would make the results not comparable among themselves. Table 1 shows the electrical properties of the various films tested.

Table 1. The electrical properties of the PEDOT:PSS films spin-coated for 300 s on planar substrates [21].

Recipe	Sheet Resistance (Ohm/□)
7 wt% DMSO 2250 rpm	167.2
7 wt% DMSO 4000 rpm	296.4
7 wt% EG 2250 rpm	137.3
7 wt% EG 4000 rpm	324.1
Neat PEDOT:PSS 2250 rpm	335.3
Neat PEDOT:PSS 4000 rpm	530.7

It is no surprise that lower spin speeds and correspondingly thicker films, produce films with lower sheet resistance. Although these results are not directly translatable to the films spin-coated on textured substrates, as these films are considerably less homogeneous, we confirm the significant enhancement of conductivity by using co-solvents. Furthermore, we can confirm that at the target thickness, for anti-reflective optimization, of 65 nm (2250 rpm), 7 wt% EG produces the lowest sheet resistance of all samples tested. Therefore at this spin condition, the anti-reflective properties of PEDOT:PSS and the sheet resistance of the film are optimized for a planar substrate; thicker films will have lower sheet resistance but will compromise the anti-reflective properties. However, as will be discussed in more detail in later sections, optimizing the anti-reflective properties, which are directly related to the thickness of the films, and the conductivity of films deposited on textured substrates is not as straightforward and

requires a more empirical approach. It is also important to note that for irregular films the effective sheet resistance of the film will be limited by the thinner regions of the film. In other words, if the dispersion is more prone to accumulation in the valleys of the texturing, then the thinner regions in the peaks of the pyramids will limit the lateral conductivity of the film.

Previous work has explored the mechanisms by which co-solvents affect the conductivity of PEDOT:PSS dispersions. In this case, the co-solvents modify the micelle-like morphology of the PEDOT:PSS complex, in which the flexible PSS molecules encapsulate the rigid PEDOT chains forming a voluminous shell (this structure is commonly referred to as a gel) [6]. In this structure, the doped conjugated PEDOT backbone is the only pathway for charge transport, as PSS is not electronically active and only contributes to doping the PEDOT and inducing its solubility. The addition of co-solvents decreases the thickness of the PSS shell and induces a rearrangement of the PEDOT chains, from the coil-like benzoid structure that may be present along the grain boundaries to a more linear or extended quinoid structure resembling stacked pancakes[6], [20], [22]. Combined, these structural modifications promote the closer packing of the PEDOT chains which in turn facilitates cross-chain charge transfer and increases ionic conductivity [22]. This, in turn, results in a higher bulk conductivity and lower sheet resistance.

3.5. Antireflective Properties and Photo Collection Efficiency

One of the main advantages of using PEDOT:PSS, besides its relatively low-cost and simple processing, is its potential to increase the photo collection efficiency of photovoltaic devices by acting as an anti-reflective coating. Texturing the active substrate is another common method used to improve the photo collection. In this work, we aim to take advantage of both of these techniques by using textured silicon substrates as our base in order to maximize the photo collection of the device. Achieving this effect, however, poses several unique design challenges. Just like any other anti-reflective treatment, the anti-reflective properties of PEDOT:PSS are optimized at a specific film thickness. Furthermore, the homogeneity of the film is crucial not only for the anti-reflective effect but also for proper device performance, as incomplete or otherwise faulty coatings will cause shunts that will drastically hinder the efficiency of the device.

Therefore, for the fabrication of efficient hybrid devices, it is critical to accurately control the deposition procedure to achieve homogeneity and a proper thickness of the film. Spin coating has been the preferred casting method for PEDOT:PSS as it allows for very thin homogeneous films to be produced. In spin coating, the rheological properties of the fluid being cast, its interfacial interaction with the substrate, as well as the spin speed and time, ultimately determine the thickness and homogeneity of the resulting film. Spin coating parameters tend to produce highly reproducible results; however, this has only been validated for planar smooth substrates. Irregular or textured substrates, such as those used in this study, have not been studied as thoroughly in the context of spin

coating thus additional rigor is required to validate the spin coating procedure in order to confirm the homogeneity and coverage of the films.

Although quantitatively characterizing the thickness and irregularity of the PEDOT:PSS films on textured substrates is challenging, measuring the anti-reflective properties of the devices allows us to directly assess the impact of the spin conditions on the photo collection efficiency of the device and empirically deduce the resulting irregularity of the films. Figure 14 shows the UV-VIS reflection spectrum collected for the PEDOT:PSS films spin-coated on textured silicon wafers with different co-solvent compositions. It can be readily seen that the PEDOT:PSS films significantly reduce the reflectivity of the devices, confirming its anti-reflective properties. We can also observe that the addition of co-solvents does not affect the anti-reflective properties of the resulting films significantly. PEDOT:PSS has a transmission of more than 90% throughout the solar spectrum.

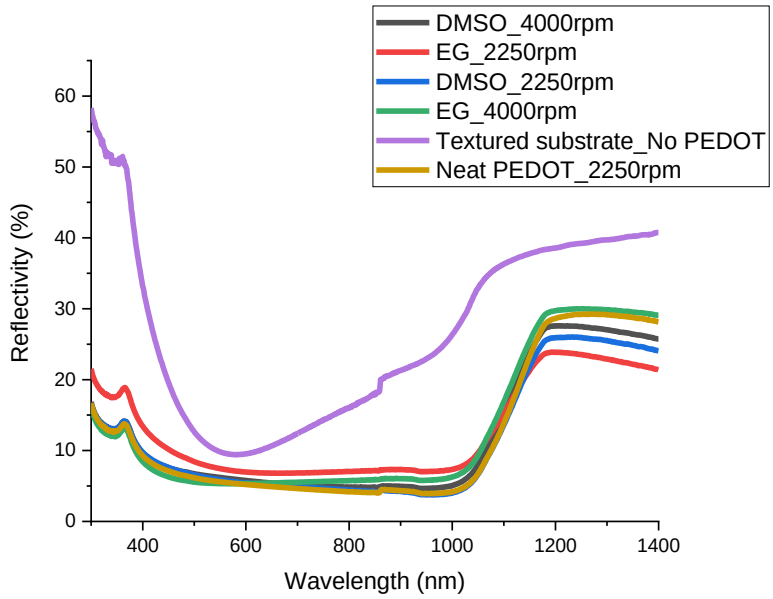

Figure 14. Reflectivity of PEDOT:PSS films on textured Si substrates [21].

Nevertheless, there are some slight differences between spin recipes that are important to point out. Particularly, PEDOT:PSS with 7 wt% EG has a better anti-reflective performance in the visible spectrum when spin-coated at 4000 rpm than 2250 rpm. DMSO, on the other hand, seems to perform just as well at either spin speed. The difference in anti-reflective performance seen for EG may be due to the rheological properties of the dispersion and their implications in spin-coating on a textured substrate. Although it is difficult to confirm the specific impacts of the rheological properties on the thickness distribution of the films obtained in these cases, the anti-reflective performance suggests that, at least for EG, 4000 rpm produces films with a thickness closer to 50 nm throughout the silicon substrate [32]. In other words, dispersions with EG are more sensitive to pooling which can be overcome by spinning at higher speeds. DMSO, on the

other hand, produces films which are more resistant to pooling and thus are more homogeneous. The implications of the difference in homogeneity of the films coated on textured substrates are important to consider in order to optimize their electrical performance. The more inhomogeneous films produced with EG at 2250 rpm will not only have a lower anti-reflective performance but may also have higher sheet resistance, as this property is limited by the thinnest regions of the film.

3.6. Metal/PEDOT:PSS Interface

As mentioned earlier, the contact resistivity between Ag and PEDOT:PSS is a critical parameter in designing the front contact and it is not well understood or reported. In the case of the devices presented in this work, the major limiting loss factor was initially assumed to be the resistance of the Ag/PEDOT:PSS interface. Mahato et al. performed a contact resistivity measurement for Ag thermally deposited on PEDOT:PSS films (Clevious PH 1000, with a 5 wt% DMSO cosolvent and 0.1% Capstone FS-31 fluoro-surfactant) on planar glass substrates and found contact resistivities of 0.79 Ohm·cm^2 [42]. Such large contact resistivities would make this interfacial resistance the largest source of power loss in the design of a front contact shadow mask. Furthermore, measurements from initial devices indicated that the total series resistance, as measured from the JV slope plateau beyond Voc, can reach down to 1 Ohm·cm^2. By analyzing the specific contact grid design in the PV Lighthouse Grid calculator, an upper bound of 0.064 Ohm·cm^2 can be deduced for the Ag contact resistivity in such devices. Clearly, the existing literature value for Ag contact resistivity was not applicable to the performance observed for most PEDOT:PSS devices on Si substrates. We used the transmission line

measurement (TLM) to quantitatively characterize the electrical properties of this interface for the PEDOT:PSS films with co-solvents and use these results directly in our device design. Figure 15 shows the results obtained from the TLM measurements of PEDOT:PSS films on textured silicon substrates.

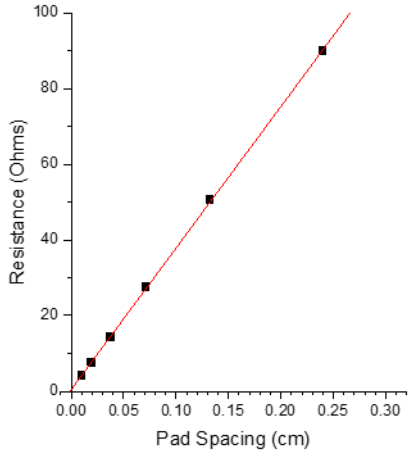

Figure 15. The measured resistance vs. the pad spacing to determine the sheet resistance and contact resistivity [21].

Table 2 shows the results obtained from the TLM data by the general analytical approach described by Schroder, including a correction factor to account for the edge effects of the contact pads [43]. Any nonlinearities in the fit can propagate into large errors in the estimation of the x- and y-intercepts used to calculate the contact resistance and transfer length. Here the effect of fitting errors was minimized by forcing the fit slope to pass through the first measured resistance data point. Using this approach, a low contact resistivity of 0.000133 Ohm·cm^2 was found. The range of the possible values using the 95% confidence interval for the slope and y-intercept are also reported in Table

2. The contact resistivity obtained for this specific device design is drastically lower than the previously reported values, indicating that Ag/PEDOT:PSS contact resistivity is not the series resistance bottleneck and can be largely neglected in future shadow mask design. These results indicate much lower shading ratios than can be achieved with the 10.4% mask used in this paper. Future devices could utilize masks with 4.8% shading ratios where front grid power losses are limited primarily by the sheet resistance of the PEDOT:PSS layer itself. The extent to which the choice of co-solvents modifies the contact resistivity for this interface has yet to be studied.

In addition to measuring contact resistivity, TLM can provide a reliable measurement of sheet resistance, since errors in the fit slope are typically small. For the case of a film with 7% DMSO spin-coated at 4000 rpm for 300 s, the measured sheet resistance was 374 Ohm/□. This sheet resistance measurement is in good agreement with the 296 Ohm/□ measured via the van der Pauw technique. The TLM measurements were performed on textured partially conductive (1–5 Ohm-cm) samples, which give a sheet resistance more relevant to the actual device conditions, but do not allow for the full isolation of the PEDOT:PSS conductivity. Additional variations can be expected as the Van der Pauw method measures the sheet resistance of the full sample, including any edge irregularities in spin-coating thickness, while the TLM method is more isolated to the central region of the sample.

Table 2. The summary of values extracted from the TLM analysis of Ag contacts on PEDOT:PSS films. A 95% confidence range from the linear fit is shown in parenthesis [21].

Spin Recipe	Sheet Resistance (Ohm/□)	Contact Resistance (Ohm)	Transfer Length (cm)	Contact Resistivity (Ohm·cm²)
7 wt% DMSO 4000 rpm 300 s	374 (369–380)	0.224 (0.0185–0.686)	0.000598 (4.87×10^{-5}–0.00186)	0.000133 (9.02×10^{-7}–0.00128)

3.7. Hybrid Device Fabrication and Characterization

Table 3 shows the performance of the solar cells, as measured by illuminated JV, fabricated with different PEDOT:PSS recipes. The devices were fabricated using the process described previously. Multiple devices were fabricated for each recipe, in order to understand the variations in device performances.

Table 3. Performance of photovoltaic devices fabricated with different PEDOT:PSS recipes [21].

Spin Recipe	V_{oc}(mV)	J_{sc}(ma/cm^2)	FF (%)	Efficiency (%)
Neat PEDOT:PSS@2250 rpm	517	18.0	44.5	4.17
Neat PEDOT:PSS@4000 rpm	507	19.6	42.9	4.29
7 wt% DMSO@2250 rpm	547	29.3	51.1	8.22
	567	29.8	52.1	8.84
	587	31.1	62.0	11.3
	577	30.2	60.0	10.5
7 wt% DMSO@4000 rpm	567	32.2	57.4	10.5
	577	31.2	58.7	10.8
	567	29.7	63.7	10.8
	557	30.3	62.5	10.6
7 wt% EG@2250 rpm	497	29.8	58.9	8.50
	547	29.5	64.5	10.5
	577	30.0	64.1	11.1
	587	31.2	57.1	10.5
7 wt% EG@4000 rpm	557	30.9	59.8	10.3
	577	31.3	57.4	10.4
	567	31.6	58.7	10.6
	578	31.2	59.7	10.7

Devices with neat PEDOT:PSS have very poor device performances especially lower short-circuit current. This is primarily a reflection of the lower conductivity of PEDOT:PSS, as the anti-reflective properties remain largely unchanged with the addition of co-solvents. It is unlikely that the neat PEDOT:PSS films coated on textured substrates were incomplete as the coating properties of the dispersions without co-solvents should not be significantly different, however, we cannot rule out this as a possible reason for the decreased performance. It is also possible that the contact resistivity of the Ag/PEDOT:PSS interface for neat PEDOT:PSS is larger than the value demonstrated for the films with co-solvents which would result in a non-optimal carrier collection and

increased series resistance. Upon the addition of co-solvents, the J_{sc} values increase to as high as 30 mA/cm^2. Devices with either co-solvent show similar devices performances but the champion cell was with 7 wt% DMSO recipe at lower spin speed. The DMSO sample at 4000 rpm also has the highest J_{sc}, a reflection of the low reflectance throughout the solar spectrum as seen from UV-VIS plot. Devices fabricated at 4000 rpm were consistent and had higher J_{sc} values which can be related to a lower reflectance. However, the highest performing cells for both EG and DMSO were obtained at lower speeds. In this work, considerable attention was given to investigate and optimize the individual properties of the materials being used, as well as the cell architecture as a whole, considering the a priori assumption that the addition of co-solvents would yield a better performing solar cell such that the same rigor was not given to neat PEDOT:PSS.

The devices fabricated with DMSO and EG show similar performances with the biggest variation coming in the fill factor. An analysis of the fill factor showed that shunting (R_{sh}) affected these cells the most. Series resistance losses cannot be dismissed but all cells faced similar losses. The origin of the shunt resistance is not known. Devices with EG co-solvents had more reproducible results, as can be seen in Figure 16.

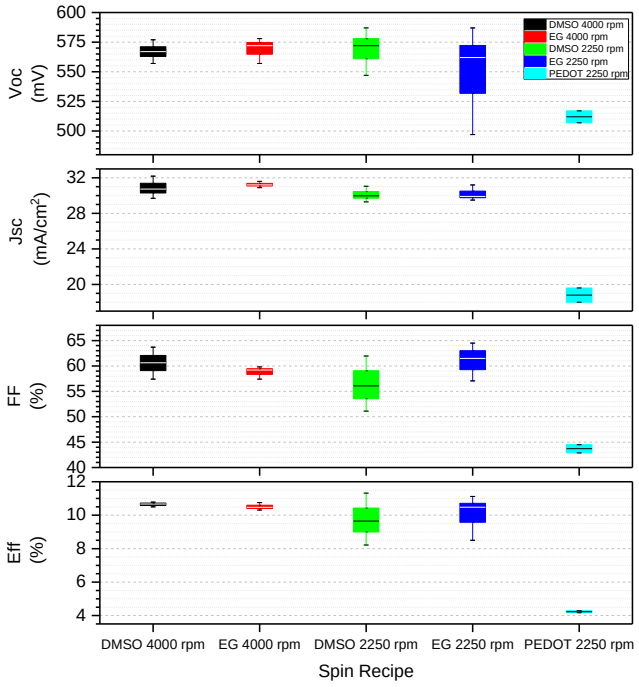

Figure 16. Reproducibility of device performance for different PEDOT:PSS recipes [21].

3.8. Conclusions

Spin coating was demonstrated for the deposition of PEDOT:PSS films with co-solvents on textured silicon substrates. An accumulation of the PEDOT:PSS in the valleys of the texturing was observed. Co-solvents decreased the sheet resistance of the films, both DMSO and EG having comparable effects. The reflectance of the devices under test confirmed the anti-reflective properties of PEDOT:PSS films as well as the irregularity of the PEDOT:PSS films. The reflectivity measurements further suggest that EG as a co-solvent is more prone to accumulation and irregular films. The contact resistance of the Ag/PEDOT:PSS interface for this device design was characterized by finding a much lower value than originally assumed. Finally, photovoltaic devices were

fabricated with the PEDOT:PSS recipes and characterized and a significant improvement in device performance was found. This improvement can be attributed to the anti-reflective properties of the PEDOT:PSS films, the reduced series resistance induced by the co-solvents, and the optimization of the front metal contact design. EG (7%) appeared to have a better reproducibility and fundamental performance

Chapter 4. UPCYCLED POLYSTYRENE SULFONATE FOR TRULY RENEWABLE PV ENERGY

4.1. Introduction

The development and adoption of sustainable and renewable energy sources is increasingly becoming one of the most important challenges of our time due to the alarming rate and effects of global warming. Solar PV has emerged as the fastest growing sustainable energy technology platform. Nevertheless, the current approaches to module fabrication remain expensive and energy intensive which has hindered the growth of the field. Furthermore, the development of PV technologies in recent years has failed to address the sustainability of the fabrication approaches, a matter that is worsening to the growing challenge of waste management and pollution.

Hybrid heterojunction PV technology (hybrid HJT) that combine silicon with semiconducting polymers has emerged in recent years as a promising approach to reduce the energy requirements of PV fabrication while providing an efficient pathway for end-of-life recycling strategies [44]. The increasingly high efficiency requirements of PV solutions have motivated the development of complex novel chemistry and fabrication strategies that have pushed the performance of this hybrid technology to competitive efficiency levels.

Nevertheless, the increasing complexity of the chemistry and fabrication approaches demand the use of costly materials and processes with little consideration for the use of recycled feedstocks. The use and optimization of PEDOT:PSS as a hole transport layer (HTL) has emerged as one of the most popular approaches to hybrid PV fabrication. Within this context, the Clevios PH1000 blend by Heraeus has established itself as the material platform of choice due to its superior electrical properties and versatility in accommodating post-deposition treatments. Using the PH1000 blend Yoon et al. [34] achieved the highest reported device efficiency of 17.3% in a front-PEDOT:PSS architecture in 2018. Despite its high performance and wide adoption, the Clevios PH1000 blend is a costly feedstock which has complicated the value proposition of hybrid PV technology and hindered its commercialization potential.

In this chapter, we fabricated hybrid solar cells from upgraded plastic waste. A novel sulfonation method for upgrading post-consumer aromatic plastic waste was used to access PSS and use it as a scaffold for the preparation of PEDOT:PSS. This novel sulfonation technique employs a recyclable sulfonation reagent based on sulfonated imidazolium salts and mild reaction conditions compatible with a wide range of waste aromatic polymer streams. Prior efforts to develop new sulfonation techniques have relied on high reagent concentrations and the use of catalysts but still suffer from several drawbacks including incomplete sulfonation, defects in the polymer chain, and low isolated yields [45], [46]. This novel sulfonation method results in a high degree of

sulfonation (DS) and higher isolated yields than previous techniques, with low defects and precise control over the degree of sulfonation.

Furthermore, the performance of PEDOT:PSS synthesized from the upgraded sulfonated aromatic plastics is comparable to that of the Clevios PH1000 blend in silicon-based hybrid solar cells within the first degree of basic optimization. These initial results show the potential to further decrease the cost and increase the environmental sustainability of hybrid PV technology and hybrid electronics more broadly.

4.2.Experimental

N-type silicon (100)-textured substrates (doped with phosphorous, CZ) with back surface field (BSF) were fabricated. These wafers are 145 micron thick with 1–5 Ω-cm resistivity. Random texturization was performed on both sides using potassium hydroxide (2% KOH yielding pyramid sizes of about 3–5 μm base size) alkaline etching. To create BSF n + layer on the *N*-type wafers, phosphorous oxychloride diffusion was performed at 820 °C, 15 min with $POCl_3$ carrier gas flow rate of 1500 sccm (standard cubic centimeters per minute) for phosphosilicate glass (PSG) growth and dopant drive-in. Finally, a 10-min buffered oxide etch is used to remove the PSG. The sheet resistance value of the BSF side is 55 Ω/square.

Ethylene glycol (EG) was purchased from Fischer Chemical in certified ACS grade. Surfactant Capstone FS-30 (non-ionic fluorosurfactant) was purchased from Chemours. Clevios PH1000 PEDOT:PSS blend was purchased from Heraeus, (Ohio, USA). In this

work, we used 7 wt% ethylene glycol as the co-solvent and 0.25 wt% Capstone FS-30 as the surfactant added to PEDOT:PSS.

All wafers were cleaned using a Piranha etch (H_2SO_4:H_2O_2 = 4:1) for five minutes, followed by a 5-min DI water rise and a two-minute immersion in hydrofluoric acid (HF, 2 wt%), as described in [21]. After cleaning, the substrates were quickly blown dry with nitrogen and spin coated. PEDOT:PSS dispersions were prepared in advance of the spin coating procedure by adding 7 wt% Ethylene Glycol and 0.25 wt% Capstone FS-30 non-ionic surfactant. Appropriate PEDOT:PSS dispersions were then spin coated on the front of the wafers on a Headway Research spin coater. All spin coated samples were baked on a hot plate at 135 °C for 15 min immediately following the PEDOT:PSS deposition. For complete solar cell devices, metal contacts were deposited using electron beam physical vapor deposition. Aluminum (2μm) was used as the back contact and deposited on the BSF-treated side of the wafer, while silver (500nm) was used as the front contact and was deposited with the help of a finger patterned shadow mask directly on the PEDOT:PSS films.

1cm × 1cm textured *n*-type silicon wafers were used as substrates for the devices. PEDOT:PSS blends were spin cast at 2250 rpm for 300 s. The devices were tested using illuminated current density–voltage measurements (JV). JV response was measured by means of a DC source meter (Keithley 2400 Sourcemeter, USA) both in the dark and light, under air mass 1.5G standard illumination.

4.3.Upcycling of Aromatic Plastic Waste Into PEDOT:PSS

Poly(styrene sulfonate) (PSS) was synthesized by the sulfonation of a polystyrene (PS) feedstock through an electrophilic substitution mechanism using recyclable imidazolium salts as the sulfonation agent. PEDOT was then polymerized in the presence of the upcycled PSS via aromatic electrophilic substitution mechanism (SEAr). This process is shown in Figure 17.

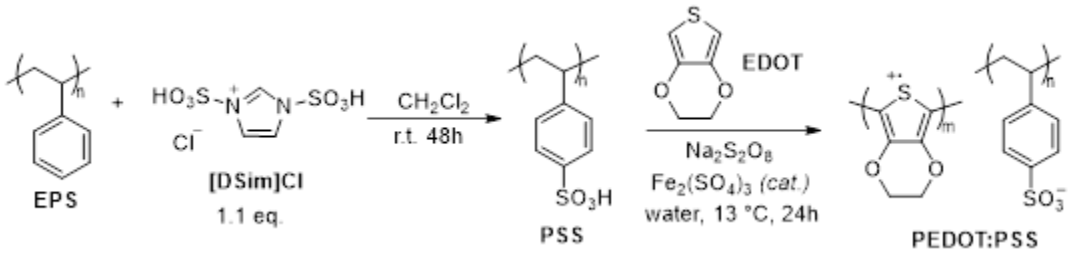

Figure 17. Synthesis of PEDOT:PSS from upcycled PS.

Two different blends of upgraded PEDOT:PSS, labeled PSS-S and PSS-F herein, were prepared by utilizing two different streams of expanded polystyrene- (EPS) waste. The sulfonation of EPS-S and EPS-F led to a 92% and 89% degree of sulfonation, respectively, measured by UV-Vis titration [47] and a 74% and 60% isolated yields.

4.4. Hybrid PV Device Results

Three Hybrid PV devices were fabricated in the manner outlined previously using different PEDOT:PSS blends: PSS-S, PSS-F, and Clevios PH1000. The cell architecture of these devices is shown in Figure 8.

The JV performance of the fabricated devices was measured under standard AM 1.5G standard illumination. The JV response was then used to derive the most important cell parameters for ease of comparison across the samples. The JV results are shown in Figure 18 while the derived cell parameters are shown in Table 4.

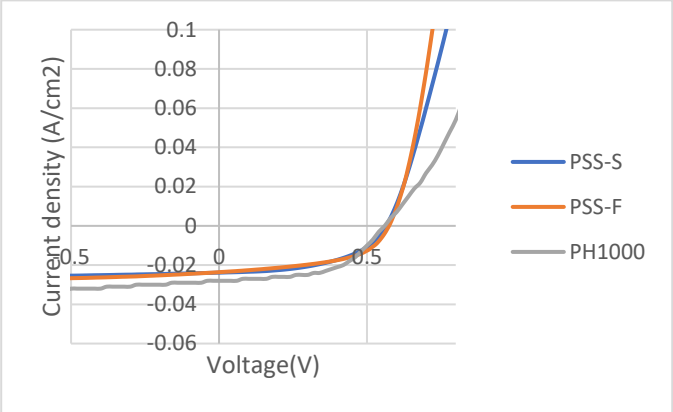

Figure 18. JV performance of hybrid PV devices.

Table 4. Cell parameter results.

	Cell Parameters			
	Voc (V)	***Jsc (mA/cm^2)***	***FF (%)***	***Eff (%)***
PSS-S	0.56	23.9	51.5	6.9
PSS-F	0.57	23.6	52.5	7.1
PH1000	0.56	28	54.9	8.4

4.5. Conclusion

In this work we have demonstrated the superior performance of a novel technique for the sulfonation of aromatic plastic waste feedstocks that utilizes a recyclable sulfonation agent for the synthesis of PSS with high degree of sulfonation. PEDOT:PSS polymerized from the upgraded PSS scaffold was shown to perform at a level comparable to the state-of-the-art commercial Clevios PH1000 blend in hybrid PV devices within a first degree of optimization. These results highlight the potential for hybrid PV technology to leverage highly sustainable fabrication practices and provides an avenue to address the problems associated with pollution of post-consumer plastic waste.

4.6. Acknowledgments

The reaction development for the sulfonation and the synthesis of the upcycled PEDOT:PSS solutions was performed by Chun-Yuan Lo, a graduate student in the group of Prof. Laure Kayser at the University of Delaware. An article on this work was submitted for peer review. Work at the ASU Solar Power Lab by Som Dahal, Rameshwari Ghimire and Stuart Bowden was supported by the Nanotechnology Collaborative Infrastructure Southwest (NCI-SW) with funding from NSF- ECCS1542160. JV measurements were measured at the Institute of Energy Conversion. Electron beam deposition was done at UD Nanofabrication facility.

Chapter 5. DEGRADATION STUDIES AND S-SHAPED JV BEHAVIOR

5.1. Buried Interface Between the Silicon Substrate and PEDOT:PSS

The following is an adapted excerpt, reproduced with permission, of our most recent publication [48] that best summarizes our experimental results regarding the degradation mechanisms and formation of s-shaped JV behavior:

Despite showing much promise and achieving remarkable efficiencies these hybrid devices suffer from poor reliability and rapid performance degradation. The degradation of these devices is very particular, often developing “s-shape” JV characteristics as the devices age. The s-shape is characterized by a kink of the JV curve between the first and the fourth quadrant that dramatically reduces the fill factor (FF) of the device. Similar phenomena have been observed in other photovoltaic technologies and are attributed to a variety of different causes [49], [50]; however, due to the unique nature of this hybrid technology the analogies are limited. Although the degradation of these devices has garnered some attention in recent years, the degradation mechanisms and the source of the s-shaped JV characteristics remain poorly understood. Several factors have been suggested to contribute to the degradation of these devices: The degradation of PEDOT:PSS and its electrical properties, deterioration of the PEDOT:PSS-silicon interface, and deterioration of the PEDOT:PSS-metal contacts.

Despite being praised in the field of organic electronics for its superior chemical stability, the conductivity of PEDOT:PSS films is known to degrade over time [6]. The details of this degradation are not completely understood but it is thought that a combination of morphological changes onset by moisture absorption as well as ultraviolet-activated chemical oxidation are the mechanisms behind the observed loss in conductivity [7], [20], [22]. However, the individual contributions to changes in carrier concentration and mobility have not been established yet. Due to the active role the PEDOT:PSS film plays in the junction formation of these devices it is no surprise that the properties of this film and its interfaces will have drastic effects on the overall device performance.

Due to the theoretical similarity between PEDOT:PSS and a-Si:H, the properties of PEDOT:PSS alone are not likely to result in the observed s-shape characteristics of the degraded hybrid devices. The interface between the PEDOT:PSS film and the silicon substrate plays a key role in the performance of these solar cells. The impressive efficiencies achieved by the HJT technology are often attributed to the quality of the silicon surface passivation provided by the intrinsic a-Si:H layer, which minimizes surface defect driven recombination. This has motivated the investigation of this interface by different groups in order to improve the passivation quality of the silicon surface [28]. For hybrid devices the growth of a thin interfacial oxide layer on the silicon surface after hydrofluoric acid (HF) etching is regarded as a necessary step to ensure high performance devices. However, the current understanding of the interfacial oxide layer is limited and often disregarded, and there are competing theories on its importance and effects on

device performance. The hydrophobic hydrogen terminated silicon surface that develops after the HF etching step may hinder the spin coating of PEDOT:PSS. Many sources in the literature suggest that interfacial oxide grown under ambient conditions for 5 minutes provides wettability for proper PEDOT:PSS spin coating and effective silicon surface passivation. However, it has also been suggested that longer exposure times that result in thicker oxides are detrimental to device performance, as the thick oxide blocks carrier transport [30].

In this work we aim to develop a comprehensive model of the degradation mechanism of these hybrid devices. To the best of our knowledge this is the first attempt at developing such a model. First, we constructed a numerical simulation model of the hybrid devices and simulated the JV performance of cells under different material and interface properties. Second, we conducted a device degradation study to characterize the loss of electrical performance over time under three different environments and fit the data to our model. Third, we confirmed the quality of the front metal contact between the silver and PEDOT:PSS using transmission line measurement (TLM). Fourth, we investigated and quantified the growth of the interfacial silicon oxide in solar cell specimens over time using X-Ray Photoelectron Spectroscopy (XPS) and Synchrotron-based Hard X-Ray Photoelectron Spectroscopy (HAXPES). Finally, we reconcile our simulation model with the experimental data to propose a comprehensive model of the degradation mechanisms in these devices finding that:

1. The interfacial silicon oxide develops rapidly after fabrication and its thickness and composition approaches native oxide characteristics as the

devices age and is the primary factor in the development of s-shaped JV curves.

2. The doping concentration of PEDOT:PSS decreases as the devices age which enhances the s-shape character of the JV response but does not directly cause it.
3. Storage conditions affect the degree and rate of degradation which is driven by the exposure to moisture, oxygen, and light.
4. The interface between PEDOT:PSS and silver remains ohmic over a five-week period and does not significantly degrade over a 10 day period.
5. The relative band alignment between the PEDOT:PSS and the silicon substrate does not change measurably as the devices age and the interface shows no apparent charging issues.

5.2. Experimental

5.2.1. Materials

N-type silicon (100) textured substrates (doped with phosphorous, CZ) with back surface field (BSF) were fabricated. These wafers are 145 micron thick with 1-5 ohm-cm resistivity. Random texturization was performed on both sides using potassium hydroxide (2% KOH yielding pyramid sizes of about 3-5 μm base size) alkaline etching. To create BSF n+ layer on the N-type wafers, phosphorous oxychloride diffusion was performed at 820˚ C, 15 minutes with $POCl_3$ carrier gas flow rate of 1500 sccm (standard cubic centimeters per minute) for phosphosilicate glass (PSG) growth and dopant drive-in.

Finally, a 10-minute buffered oxide etch is used to remove the PSG. The sheet resistance value of the BSF side is 55 ohm/square.

Single-side polished planar n-type silicon (100) and double-side polished intrinsic silicon (100) substrates were purchased from Virginia Semiconductors (Fredericksburg, Virginia, USA). These wafers are 300 microns thick. The n-type substrates have a resistivity of 1-5 ohm-cm while the intrinsic substrates have a resistivity > 5000 ohm-cm.

PEDOT:PSS PH1000 (Heraeus Clevios, USA) was used as the stock polymer dispersion. Solvent ethylene glycol (EG) and surfactant Triton X-100 (non-ionic surfactant) were purchased from Fischer Chemical in certified ACS grade. In this work, we used 7 wt% ethylene glycol as the co-solvent and 0.25 wt% Triton X-100 as the surfactant added to PEDOT:PSS.

5.2.2. Methods

All wafers were cleaned using a Piranha etch (H_2SO_4:H_2O_2= 4:1) for five minutes, followed by a five-minute DI water rise and a two-minute immersion in hydrofluoric acid (HF, 2wt%). After cleaning, the substrates were quickly blown dry with nitrogen and spin coated. PEDOT:PSS dispersions were prepared in advance of the spin coating procedure by adding 7wt% Ethylene Glycol and 0.25 wt% Triton X-100. Appropriate PEDOT:PSS dispersions were then spin coated on the front of the wafers through a 0.22micron filter on a Headway Research spin coater. All spin coated samples were baked on a hot plate at 135°C for 15 minutes immediately following the PEDOT:PSS deposition.

For complete solar cell devices metal contacts were deposited using electron beam physical vapor deposition. Aluminum was used as the back contact and deposited on the BSF-treated side of the wafer, while silver was used as the front contact and was deposited with the help of a shadow mask directly on the PEDOT:PSS films.

$1cm \times 1cm$ textured n-type silicon wafers were used as substrates for the device degradation study. PEDOT:PSS was spin cast at 2250 rpm for 300 seconds. The samples were stored under three different environments: a nitrogen cabinet with constant flow of nitrogen (5 liters per minute), ambient conditions in a dark room with minimum light exposure, and ambient conditions with room lighting. These specimens were tested using illuminated current density-voltage measurements (JV). JV response was measured by means of a DC source meter (Keithley 2400 Sourcemeter, USA) both in the dark and light, under air mass 1.5G standard illumination.

$1cm \times 1cm$ double side polished intrinsic silicon wafers were used as substrates for the transmission line measurements (TLM). PEDOT:PSS was spin cast at 4000 rpm for 120 seconds. 500nm thick Ag contact pads were deposited using electron beam physical vapor deposition with length 0.5mm and width 10mm at spacings of 0.1 mm, 0.2 mm, 0.4 mm, 0.8 mm, 1.6 mm and 3.2 mm. The resistance was measured between adjacent sets of contact pads with a Keithley 2400 Sourcemeter.

$1cm \times 1cm$ single side polished n-type silicon wafers were used as substrates for the XPS and HAXPES study. For the XPS study PEDOT:PSS was spin cast at 4000 rpm for 120 seconds. For the HAXPES study PEDOT:PSS was spin cast at 10000 rpm for 120

seconds. No metal contacts were deposited on the specimens after PEDOT:PSS deposition. The XPS studies were carried out in a Thermo Scientific K-Alpha XPS. The incident X-rays were monochromatic Al Kα (1486.7 eV) with a power of 72 W (12 kV, 6 mA) at a takeoff angle normal to the surface and a base pressure lower than $1 * 10^{-8}$mBar. The X-Ray spot size was elliptical in shape with a semi-major axis of 400 µm. The intense C 1s peak at 284.8 eV was used to calibrate the spectra. The HAXPES studies were carried out at the National Institute of Standard's beamline X24A at the National Synchrotron Light Source at Brookhaven National Lab. Three X-ray beam energies were used throughout the experiment (3311.3 eV, 4659.8 eV, 6008.2 eV) which were calibrated with the Ag 3d peak at 368.2 eV. For this experiment a constant-offset double-crystal Si (220) was used. Additionally, a plane mirror was used upstream of the monochromator to achieve a broader and more diffuse X-ray spot at the sample. The XPS analysis was performed using a 200 mm radius Scienta HR4000 hemispherical electron analyzer with a 200 pass energy and an angular lens mode. XPS spectra quantification and analysis was performed on the Thermo Advantage v5.9911 package by Thermo Fisher Scientific.

A model of PEDOT:PSS-Silicon solar cell was constructed in the numerical simulation tool AFORS-HET (Automat FOR Simulation of HETero structures) [25]. A 65 nm thick PEDOT:PSS layer was modeled on top of a 150 micron n-type silicon substrate. The silicon had a shallow dopant density of $5*10^{15}$ cm^{-3} and was modeled with a mid-gap trap density of 10^{9} cm^{-3}, giving a high bulk minority carrier lifetime of 10 ms. Dangling bonds at the front c-Si interface were modeled using a 1 nm thick layer with a

trap density of $1*10^{20}$ cm^{-3}. These traps are modeled as two Gaussian distributions of acceptor and donor states centered at 0.635eV and 0.485eV, with width 0.18eV.

PEDOT:PSS was modeled as a p-type semiconductor with variable acceptor doping concentration (maximum value of $3*10^{20}$ cm^{-3}), representing the effective doping level of mobile positive charge in the material. Hole mobility was set to 10 cm^2/Vs. This gives a hole conductivity of 480 S/cm, in line with experimentally measured sheet resistance values [21]. Modeled material properties were selected to match with the band energy positions reported by Jäckle et al. [8], [9] The PEDOT:PSS bandgap was given an electron affinity of 3.6 eV and a bandgap of 1.3eV[11]. The PEDOT:PSS was modeled as degenerately doped, with the Fermi level 80 meV below the valence band [8]. In order to achieve the appropriate Fermi level position, the effective density of states (DOS) of the conduction and valence bands were each adjusted to $1.35*10^{19}$ cm^{-3}. It is assumed that photon absorption in the PEDOT:PSS layer is parasitic, modeled by adding a midgap trap state with a density of $1*10^{16}$ cm^{-3} to reduce the carrier lifetime in the PEDOT:PSS layer to 1 ns. The low frequency permittivity of PEDOT:PSS has not been well established, and is known to be sensitive to free carrier concentration. An approximate relative permittivity of 10 is used for this simulation, in accordance with typical values from the Drude-Smith model shown by Reynolds et al. for localization parameter values $c_1 < -0.5$ [26]. Data from Hoppe et al. was used for modeling the refractive index at optical frequencies [23].

The oxide layer was modeled using an interfacial tunneling layer with an electron affinity of 0.9 eV, bandgap of 8.9 eV, and dielectric constant of 3.9. For the rear contact,

a back surface field was modeled with shallow n-type dopant density increasing linearly from the bulk density to 10^{19} cm^{-3} over 10 nm. Flatband metal contacts were assumed for the front and rear.

5.3. Results and discussion

5.3.1. Numerical Simulation Model of the PEDOT:PSS-Oxide-Silicon Interface

Based on our experience with these hybrid devices and our best understanding on the matter of their degradation we hypothesize that the interfacial oxide layer and the degradation of the PEDOT:PSS film are the two culprits of the observed s-shape JV characteristics; specifically, the continual degradation of these aspects is responsible for the dramatic loss of performance as hybrid devices age.

In order to test our hypothesis, a model of the PEDOT:PSS-silicon solar cell was constructed in the numerical simulation tool AFORS-HET (Automat for Simulation of Heterostructures) [25]. The exact details of the properties and parameters used in this simulation are outlined in the experimental section. For the purposes of this analysis only two parameters were varied in the model: the thickness of the interfacial silicon oxide layer (d_{ox}) and the effective doping concentration of the PEDOT:PSS film (N_A). Changes in the effective doping concentration of PEDOT:PSS affect both the work function and conductivity of the film. Two sets of initial simulations were conducted in order to investigate the effect of each parameter on the JV characteristics of the model devices. For the first set of simulations the doping concentration of PEDOT:PSS was fixed at $3*10^{20}$ cm^{-3}, which is the maximum carrier concentration calculated from geometric

considerations by Kirchmeyer et al. [6], while the interfacial oxide thickness was varied between 0.6 and 2nm. For the second set of simulations the interfacial oxide thickness was fixed at 0.6 and 1nm, representative magnitudes for the length scale of the oxide thickness, while the PEDOT:PSS doping concentration was varied between $3*10^{20}$ and $9*10^{18}$ cm^{-3}. The results of these simulations can be seen in Figures 19 and 20.

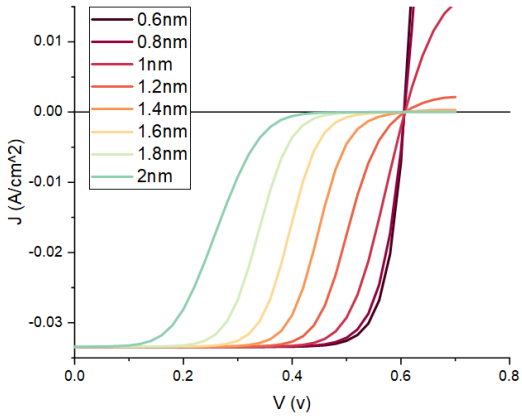

Figure 19. Simulated JV performance of hybrid PEDOT:PSS-silicon model devices with PEDOT:PSS effective doping concentration fixed at $3*10^{20}$ cm^{-3} and oxide thickness varied from 0.6nm to 2nm.

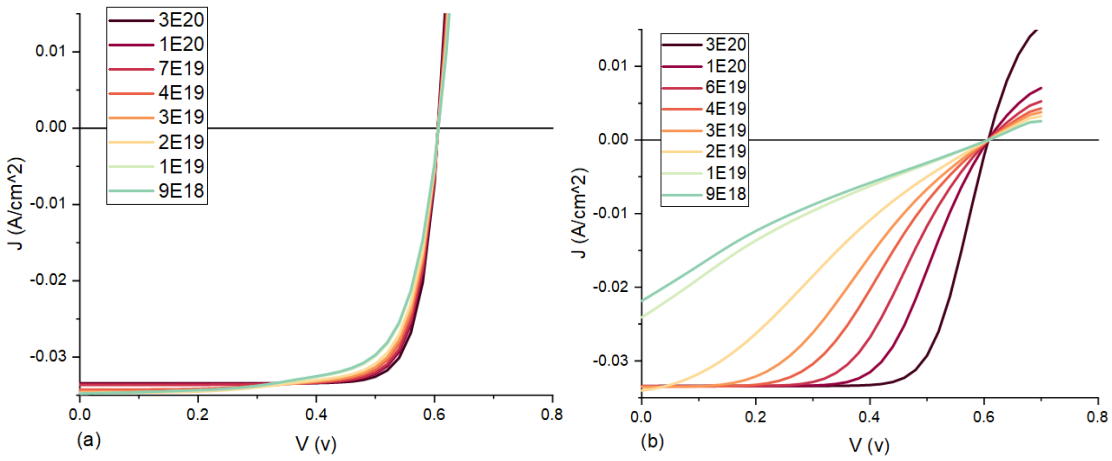

Figure 20. Simulated JV performance of hybrid PEDOT:PSS-silicon model devices with PEDOT:PSS effective doping concentration varied from $3*10^{20}$ cm^{-3} to $9*10^{18}$ cm^{-3} and oxide thickness fixed at (a) 0.6nm and (b) 1 nm.

The results of these initial simulations shown in Figures 19 and 20 exhibit very interesting characteristics. Figure 19 shows that the oxide thickness has a pronounced effect on the s-shape character of the JV curves. The JV performance goes from being near ideal for a 0.6nm oxide, to a highly non-ideal s-shape which appear for oxides as thin as 1.2nm and progressively worsen for higher thicknesses. In quadrant IV of the JV curves, increases in oxide thickness appear to monotonically shift the JV curves to lower voltages decreasing the FF and apparent V_{oc}. Figure 20 shows a very different effect of changes on the effective doping concentration of PEDOT:PSS on the JV performance and degradation of the model devices. For thin oxides such as the 0.6nm modeled in Figure 20a the JV developments as the effective doping concentration of PEDOT:PSS is decreased remains relatively stable with a minor decrease in FF seen by a slight shift inward of the maximum power point. However, for even relatively thin oxides such as the

1nm modeled in Figure 20b the loss of PEDOT:PSS doping concentration results in the development of much stronger s-shaped characteristics. This degradation appears to be symmetric about the $V_{oc,}$ primarily decreasing the FF of the devices but also significantly lowering the J_{sc} at the lowest doping concentrations. It could be said that the loss of effective doping concentration in the PEDOT:PSS greatly enhances the s-shaped character of a device, but on its own is not enough to produce the experimentally observed s-shaped JV characteristics of these hybrid devices.

It is important to acknowledge this model is limited with respect to real devices. In particular PEDOT:PSS was modeled as homogeneous pristine film and the interfacial oxide and corresponding carrier lifetime was modeled as fully saturated SiO_2. Furthermore, the model assumes all changes in PEDOT:PSS film conductivity and work function are due to changes in doping concentration. Nevertheless, the assumptions made on the properties of the materials stand as the best-known upper limits. Therefore, the simulated JV characteristics are the upper limit of real device performance and the trends observed would translate to real devices. The exact way in which changes in the two variable parameters would manifest in real devices will vary slightly from the model, but they are expected to have the same effect on the JV characteristics; specifically the PEDOT:PSS film is expected to show degradation of hole mobility related to morphological changes of the film along with the decrease of doping concentration as well as a potentially inhomogeneous structure, and the interfacial oxide may not be saturated and homogeneous (particularly during the early degradation stages) which may lead to lower surface carrier lifetime but improved charge mobility. In summary, the

chosen variable parameters of this model stand as representative of changes in real device parameters and constitute property limits as a predictive tool.

Based on these initial simulations we further hypothesize that the development of s-shape JV characteristics and loss of performance is primarily driven by a combination of the growth of the interfacial oxide and the de-doping of the PEDOT:PSS film as hybrid devices age. Although other properties may be changing as the devices age and a more refined hypothesis would include them, these two primary factors describe the aging mechanism well and thus any further refinement of the model is outside the scope of this work.

In order to test this hypothesis, we fit the model to the experimentally obtained JV data for all experiments conducted in this work. The statistical R^2 model was used in an iterative process in order to find the best fit for oxide thickness (d_{ox}) and PEDOT:PSS doping concentration (N_A) for the experimental data. For a more complete device fit the shunt resistance of each device was calculated and included in the device simulation as a parallel resistance and the illumination intensity was varied slightly (± 0.3) between measurements to match the J_{sc} as the light source of the JV measurement tool tends to drift slightly between measurements owing to small temperature and calibration variance. For all JV graphs presented in this work solid lines represent the simulated model while the scatter data points represent the measured data. The scatter data points differ in color and shape between measured data sets and the color of the solid lines is set to match the data set being modeled. The tables included within the figures show the best fit parameters d_{ox} and N_A as well as the R^2 value for each model set.

5.3.2. Interfacial Silicon Oxide

In order to establish the effect of the interfacial oxide on the performance of these devices, complete solar cells were fabricated with ambient exposure time varied between 10 minutes and 2 hours after the HF etching but before spin coating the PEDOT:PSS. After fabrication, the devices were characterized by JV measurements, the results of which are shown in Figure 21.

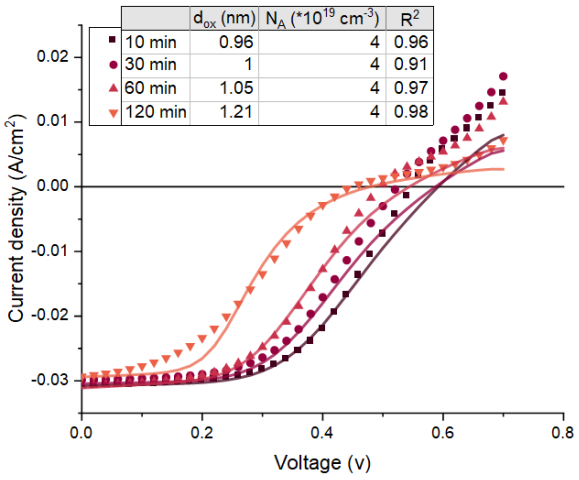

Figure 21. JV characteristics of devices with different interfacial oxide growth times.

As shown in Figure 21, longer exposures to ambient conditions before PEDOT:PSS spin coating yielded devices with lower performance and stronger s-shaped character. These results resemble the simulated performance of increasing oxide thickness and constant PEDOT:PSS doping concentration shown in Figure 19. The fit of the model to the experimental data confirms that the difference in JV performance between the devices can be explained by an increase in oxide thickness as the devices are exposed to ambient conditions for a longer time and that the PEDOT:PSS doping

concentration remains constant across the devices, which is to be expected as the PEDOT was freshly prepared for every device.

5.3.3. Device Degradation Study

Complete solar cells were fabricated and stored under three different environments: ambient conditions with room lighting, ambient conditions in the dark, and a nitrogen purged box. JV characterization was conducted on the devices over a period of six weeks. The results of these measurements are shown in Figure 22.

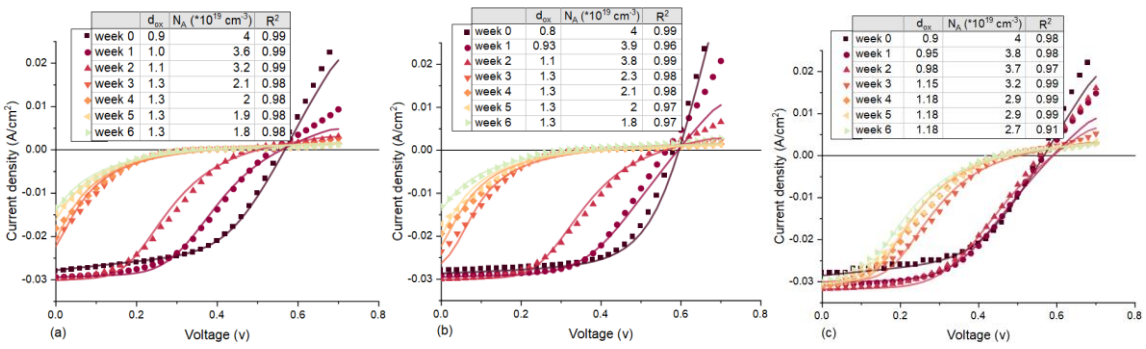

Figure 22. JV characteristics of devices stored in (a) ambient conditions (b) ambient dark conditions (c) nitrogen cabinet.

As shown in Figure 22, the JV performance of all the fabricated devices degraded and developed s-shape characteristics over the period of six weeks during which the experiment took place. Of note is the sharp shift in JV characteristics between week 2 and week 3 for all storage conditions. During the initial degradation period (week 0-week 2) the loss of performance is gradual week to week and is primarily driven by a loss in FF

while the V_{oc} remains relatively constant. Starting on week 3 the devices exhibit a decrease in effective V_{oc} and J_{sc} along with the decrease in FF which translates into significant performance degradation of the devices. It appears as if there was an abrupt change to the cells in the time between week 2 and week 3 that was binary in nature. The best fit parameters obtained from our simulation model reveal two important phenomena: First, for all storage conditions the oxide thickness reaches a stable thickness at the 3-week mark and remains constant through the 6-week mark. Second, the PEDOT:PSS doping concentration decreases more between week 2 and week 3 than any other time period for all storage conditions. Both phenomena are unique and warrant further inspection.

As mentioned previously, the issue of the interfacial silicon oxide, its growth, and its effects on these hybrid devices has so far been a controversial topic, in cases completely disregarded and in others made to bear all the blame for poor device performance. The details of the interfacial oxide growth on silicon are not completely understood but it has been suggested that for short time exposures to ambient conditions of HF etched silicon the oxide layer that develops is thin enough to be considered a tunneling barrier. And as the time of exposure is increased the oxide layer thickens to become blocking and detrimental to device performance [30], [37], [51]–[53]. Recently Jäckle et al. [19] demonstrated the continued growth of the oxide layer on the these hybrid devices. The results of the simulations, however, suggest that the oxide does not grow indefinitely in these devices but instead reaches a saturation thickness between the second and third week of aging. Furthermore, it seems that even at the shortest time

scales of oxide growth the oxide may not be dismissed as a tunneling barrier. As shown in Figure 20, the degradation of the PEDOT:PSS film greatly enhances the JV s-shape character onset by thin oxides such that their effect is not readily apparent in controlled experiments.

In terms of the relevance of the oxide thickness predicted by the model to the actual oxide layer present in real devices, the value predicted by the model corresponds to an effective oxide thickness and stands as a lower bound estimate to the real thickness of the oxide. The presence and quality of suboxide defects (unsaturated SiO_x) within the SiO_2 layer result in films with lower densities, poorer dielectric characteristics, and an increase of up to ten-fold in tunneling currents [54],[55]. A thicker but more defective oxide film may be thought to effectively behave as a thinner saturated homogeneous SiO_2 film. We hypothesize that the predicted effective oxide thickness is a value lower but representative of the magnitude of the real oxide thickness and the saturation thickness reached between the second and third week is a reflection of the chemical saturation and consequent decrease in suboxide defects in the interfacial oxide. Furthermore, the higher V_{oc} predicted by the model compared to the experimentally obtained value for the thinner oxide devices (Figure 21, Figure 22a-c weeks 0 and 1) may be explained by the superior surface passivation qualities of SiO_2 used in the model compared to the actual imperfect surface passivation quality of the oxide in the real devices.

The phenomenon of the predicted loss of PEDOT:PSS doping concentration is a more complicated issue. It is well known that the properties of PEDOT:PSS films vary between samples due to differences in synthesis, processing, and co-solvent treatments

[56]–[59]. Furthermore, it has been reported that upon water absorption PEDOT:PSS films exhibit lower conductivities and work functions attributed to changes in the microstructure of the film which affect the doping concentration and the carrier mobility [60]–[63]. Additionally, the chemical oxidation of PEDOT:PSS is known to de-dope the film, an aspect which has been intentionally exploited for the fabrication of complimentary organic electrochemical transistors [64]. The exact details of the PEDOT:PSS properties are outside the scope of this work, however the modeling results shown in Figures 21 and 22 confirm that the quality of the PEDOT:PSS film upon initial deposition is constant for all samples, as expected for a standard source, co-solvent treatment, and spin coating procedure. Relative changes to the initial doping concentration predicted by the model are meaningful but their absolute value is only a lower estimate, real devices would likely have a carrier mobility lower than the value corresponding to pristine PEDOT:PSS used in the model which means the true value of doping concentration could only be higher than the predictions of the model. The apparent large decrease in N_A between weeks 2 and 3 may be indicative of a moisture saturation point for the PEDOT:PSS film while the chemical oxidation of the film occurs throughout all six weeks, a hypothesis that could be tested in future work.

Despite the limitations of this model, the good fit to experimental data and the standard quality of initially cast PEDOT:PSS films allows for the analysis of the effects of the different storage conditions on device performance degradation. As expected, the devices stored under illuminated ambient conditions show the largest and fastest increase in d_{ox} and decrease in N_A compared to the dark and nitrogen conditions. Furthermore, the

predicted saturation oxide thickness of both samples stored under ambient conditions (Fig 22a and 22b) is the same (1.3nm) whereas the saturation thickness of the sample stored in nitrogen conditions is lower (1.16nm). This indicates that the nitrogen environment is effective at limiting oxide growth in these devices, but not capable of completely stopping its development. Additionally, the degradation of the PEDOT:PSS film seems to be distinct across the storage conditions. Compared to the illuminated ambient conditions the dark ambient and nitrogen environments show a slower degradation rate. The improvement of the dark ambient conditions seems to be marginal, suggesting the chemical oxidation is light-induced but the moisture absorption degradation remains a strong factor. The improvement seen for the nitrogen environment however is significant, particularly in regard to a reduced loss of Jsc; suggesting that both chemical oxidation and moisture absorption are greatly hindered but not completely eliminated in this environment. It is possible, however, that the degradation observed was induced by the removal of the samples from the nitrogen box for testing. The demonstrated ability to slow degradation is promising in indicating potential effectiveness of encapsulation techniques for commercial deployment of this technology.

5.3.4. Transmission Line Measurements

In order to investigate the degradation of PEDOT:PSS and the potential complications that could arise from the degradation of its interface with silver, a TLM degradation study was conducted. The TLM method allows for the separation of the contact resistance effects from the resistance of the conductive substrate. TLM samples were fabricated on polished intrinsic (100) silicon substrates. The samples were separated

into two groups, one group in which the silver TLM pattern was deposited immediately following the PEDOT:PSS deposition and another group where the silver was deposited 10 days after the PEDOT:PSS deposition. All samples were stored in ambient conditions during this study.

All samples tested showed electrical behavior consistent with what was expected during the first 10 days of testing, with the sheet resistance of PEDOT:PSS increasing slightly and the contact resistance remaining relatively constant. The contact resistance of the Ag-PEDOT interface was determined to be $< 0.1\ ohm * cm^2$ for all the samples during this time interval, a magnitude which is small in comparison to other resistances in the system. This was consistent with the samples where the Ag was deposited 10 days after the PEDOT deposition, which indicates that within 10 days the interface between PEDOT:PSS and Ag had not undergone any degradation. The TLM measurements taken after 2 weeks however, started displaying a non-linear relationship between pad spacing and resistance, invalidating the standard TLM analysis. Despite being unable to calculate a sheet resistance and contact resistance value for the remaining five weeks during which IV characterization was performed on the aging devices, it is important to note that every measurement taken displayed a linear IV relationship, confirming the contacts were non-rectifying throughout the duration of the experiment. Due to the small magnitude of the contact resistance, the observed non-degradation of the contact resistance over the 10 day period, and the observed ohmic IV characteristics it is unlikely that the Ag-PEDOT interface plays a major role in the development of the s-shape JV characteristics of degraded hybrid devices.

5.3.5. XPS and HAXPES

In order to characterize and quantify the degradation of the interfacial silicon oxide in these hybrid devices a time evolution study of this interface was carried out using Angle Resolved X-ray Photoemission Spectroscopy (ARXPS). The substrates used for this study were polished (100) n-type silicon. Specimens were prepared following the fabrication procedure of hybrid solar cell devices, but no metal contacts were deposited after PEDOT:PSS deposition. The samples were aged for a period of up to five weeks under ambient conditions. Prior to the XPS measurements the samples were stripped of the PEDOT films by an ethanol rinse and wipe, as the probing depth of conventional XPS makes it impossible to probe the silicon surface through the PEDOT film. XPS spectra were collected for the Si 2p, O 1s, and C 1s peaks at 11 different beam angles ranging from 0 to 60 degrees. Two measurements were taken of each sample at different locations. In addition to the aged specimens a freshly HF etched and a natively oxidized (as received) silicon substrates were measured.

Due to the expected thickness of the interfacial oxide layer predicted by the simulation model of around 1.3nm, ARXPS was chosen over ellipsometry for the estimation of the oxide thickness. ARXPS allows for a more accurate thickness estimation of thin films due to the measurement being independent of any contamination layer adsorbed to the surface which interferes with the ellipsometry measurements. Furthermore, ARXPS allows for the quantification of the relative amounts of different valence states present; the signal from each suboxide species (Si^{+3}, Si^{+2}, Si^{+1}) is distinct from that of saturated SiO_2 (Si^{+4}) which is itself distinct from the silicon substrate (Si0)

and their relative intensities are related to their depth-concentration profile. In order to quantify the Si 2p spectra and estimate the oxide thickness we follow the framework described by Iwata et al. [65]. For the sake of brevity, the method will not be described at length here. The oxide thickness may be calculated from the relationship:

$$\ln\left(\frac{\frac{I_{Si^{+4}}+I_{Si^{+3}}+I_{Si^{+2}}+I_{Si^{+1}}}{I_{Si^{0}}}}{R^{\infty}}+1\right)=\frac{d}{\lambda_{Si,SiO_2}}*\frac{1}{\cos(\theta)} \quad (7)$$

Where I_x is the measured intensity of species x. λ_{Si,SiO_2} is the attenuation length of photoelectrons generated in the Si substrate traveling through the oxide layer (3.5nm[65]), which is related to the Inelastic Mean Free Path (IMPF) but is often determined experimentally. θ is the collection angle of the detector (0 when normal to the surface). And $R^{\infty}$is given by:

$$R^{\infty}=\frac{\rho_{SiO_2}F_{Si}\lambda_{Si,SiO_2}}{\rho_{Si}F_{SiO_2}\lambda_{Si,Si}} \quad (8)$$

where ρ_x is the density of x which for Si and SiO_2 is 2.33 and 2.27 g/cm^3 [54] respectively and F_x is the formula weight of x which for Si and SiO_2 is 28 and 60 respectively. Finally, $\lambda_{Si,Si}$ is the attenuation length of the silicon substrate (2.3nm [65]).

The thickness of the oxide layer may be estimated by fitting a straight line to the relationship between the left-hand side of equation 7 and $\frac{1}{\cos(\theta)}$; the slope of this line times $\lambda_{Si,SiO_2}$is the thickness of the oxide. The results of the oxide thickness estimated for the aged specimens is shown in figure 23.

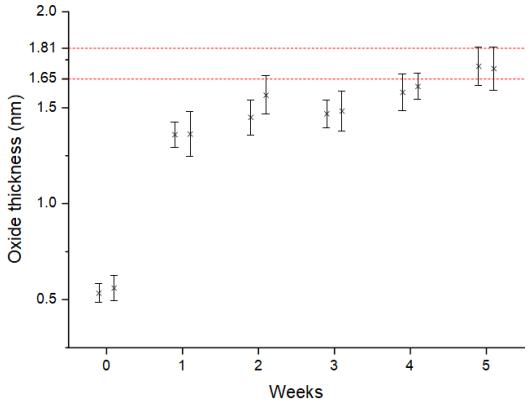

Figure 23. Oxide thickness calculated for aged specimens over a 5-week degradation period. The red horizontal dashed lines represent the thickness found for a native oxide.

The results of the calculated oxide thickness shown in figure 23 suggests the oxide layer in these hybrid devices grows rapidly after fabrication and approaches the native oxide thickness as the devices age. The overall magnitude of the oxide thickness calculated here is in good agreement with the native oxide thickness reported by Iwatta et al. of 1.5nm [65]. The saturation thickness of the native oxide depends on the environmental conditions under which the substrate is stored and slight variations of this value have been reported elsewhere [66]. We further find that by the fifth week of aging the sample has reached the native oxide thickness, but it does not exceed this value at any point during this period.

In addition to the estimation of the oxide thickness, we estimate the relative amounts of the 3 different suboxide valence states with respect to the saturated SiO_2 by calculating the ratio between the corresponding peak intensities. All peaks were fit to the

same Gaussian-Lorentzian convolution function with Shirley background subtraction. The different silicon oxide valence states were referenced to the O1s peak in order to account for possible charging across the oxide ($\Delta BE_{Si^{+4}-O} \cong 429.5eV$). The shape of the Si^0 peak was determined from the spectra from the HF etched substrate while the oxide and suboxide peak shapes were determined from the best fit to the natively oxidized substrate such that the FWHM and chemical shifts to the O1s of each peak remained constant over all angles. The chemical shifts assumed for the Si^{+3}, Si^{+2}, and Si^{+1} peak with respect to the Si^{+4} peak were 1.37, 2.07, and 2.87eV respectively. These values were based on the chemical shifts reported by Iwatta et al. [65] assuming a 3.87eV neutral chemical shift between Si and SiO_2. The peak shapes were assumed to be constant for all samples such that the only change between samples was due to changes of the relative concentration profile of each species, ensuring the validity of the comparisons and conclusions drawn from the quantification of the spectra. Figure 24 shows the evolution of this ratio over the 5 weeks of testing.

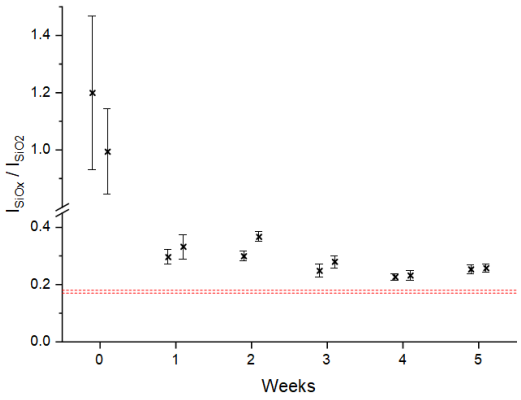

Figure 24. Ratio of suboxide valence states (Si^{+1}, Si^{+2}, and Si^{+3}) to Si^{+4} peak area over a 5-week degradation period. The horizontal dashed lines represent the ratio calculated for the native oxide.

Figure 24 shows a decreasing trend in the presence of suboxide species, suggesting that initially the interfacial oxide contains large amounts of suboxide defects that decrease over time as the film chemically saturates over time. Despite the observed saturation of the oxide films, the relative composition of the films does not reach the saturated composition of the native oxide. As mentioned previously, the effective properties of a defective SiO_2 film are different than those of a fully saturated one; in particular for the calculation of the oxide thickness the attenuation length and the density of the film are expected to vary from the values used in the calculations such that the actual oxide thickness is lower than the calculated value for the defective films. Within a margin of error, we may conclude that the oxide films saturate over time to a stable thickness and composition close to the value of a native oxide film. This confirms the results obtained by the simulated model of the saturation of the effective oxide thickness.

Although this study confirms the growth of the interfacial oxide layer, the degradation mechanism is more complex than previously suggested. An increase in thickness alone is not the only factor that contributes to the degraded electrical properties of the junction. Furthermore, we observed the development of an oxide film immediately after the PEDOT:PSS deposition, suggesting this processing step contributes to the initial stages of oxide growth in agreement with the results reported by Jäckle et al. [19]. It appears that the residual oxygen and moisture trapped in the PEDOT:PSS film, the acidic nature of PSS, and the high temperature curing step enhance the growth of the oxide.

As pointed out by Iwata et al. [65] the quantitative XPS study of this interface is not a straightforward endeavor. There are several factors that complicate this analysis which affect any attempts at quantification. Namely the chosen peak decomposition and respective chemical shifts [67], the choice of background subtraction [68], charging effects [65], elastic and inelastic scattering effects [69], and angle-dependent crystalline electron diffraction [70] all affect the quantification of the XPS spectra. In order to maintain consistency across measurements such that the results are comparable to each other we take care in maintaining the analytical and experimental parameters for the XPS measurement and quantification constant across all the samples measured. Furthermore, the ethanol rinse and wipe procedure to remove the PEDOT:PSS layer from the specimens was carried out in a methodical fashion such that the exposure to environmental conditions of the clean silicon surface was less than a minute between the clean and loading to the vacuum chamber of the XPS instrument to minimize additional contributions of oxide growth.

In order to confirm the results from the ARXPS study and to further investigate the buried PEDOT:PSS/SiOx-$_2$/Si interface a similar aging study was conducted using synchrotron-based Hard X-ray Photoelectron Spectroscopy (HAXPES). HAXPES allows for devices to be probed without removing the PEDOT layer by using much higher energy X-rays which in turn generate higher energy photoelectrons with correspondingly larger escape depths. Probing this buried interface through the PEDOT film is beneficial for a few reasons: First, we guarantee the silicon surface is not being compromised with the stripping of the PEDOT layer. Second, by probing the buried interface we can determine if the band alignment of the devices is changing over time. Finally, the PEDOT:PSS spectra may be quantified in order to study chemical changes in the film. This technique has been utilized previously by Jäckle et al. [19] for similar studies including the estimation of the interfacial oxide thickness.

For the HAXPES aging study, the specimens were fabricated on single side polished (100) n-type silicon substrates. The PEDOT:PSS films were made thinner than those typically used in solar cell devices in order to ensure the films would not completely suppress the signal from the buried silicon. The PEDOT:PSS films were spin coated at 10000 rpm for 120 seconds, the resulting films were determined to be around 51±2 nm thick via ellipsometry. The specimens were fabricated over a period of eight weeks and were kept under ambient conditions. The specimens were probed at three different incident x-ray energies (3311.3, 4659.8, and 6008.2 eV) and spectra of six different relevant peaks was collected: C1s, Si 1s, Si 2s, Si 2p, S 1s, S 2p. Attempts at quantifying the interfacial oxide thickness in an analogous fashion to the ARXPS

procedure on these samples were unsuccessful and yielded unreasonably high oxide thickness estimates.

We investigated the S 1s spectra of the PEDOT:PSS film in order to determine if changes of structure or composition were evident as the samples aged. As reported by Jäckle et al. [19] the S 1s spectra of PEDOT:PSS displays 3 peaks corresponding to the 3 different chemical states of sulfur present in the film; namely from the PEDOT backbone, the ionized PSS^- counter polyanion, and the neutral PSSH, see Figure 25. The reported chemical shift between PSS^- and PSSH components is 0.57eV. Furthermore, the signal of the sulfur peak corresponding to PEDOT exhibits an asymmetric tail which has been attributed to the doping state of the PEDOT backbone as reported by Greczynski et al. [71]. In order to characterize and quantify the contribution of the tail component, related to the doping concentration, the PEDOT sulfur peak was fit to a Gaussian-Lorentzian convolution function blended to an asymmetric exponential Voight-type function as described by equation 9.

Let GL be the Gaussian-Lorentzian convolution function, H the peak height, and x the energy difference to the peak center ($x = E - E_0$) such that x=0 corresponds to the binding energy of the peak. Then the peak shape of the asymmetric exponential Voight-type function is given by:

$$H(GL - (1 - GL)T) for\ x < 0 \tag{9}$$

$$HGL\ for\ x > 0 \tag{10}$$

Where:

$$T = TM * CT + (1 - TM) * EXP(x * ET) \quad (11)$$

Where:

TM =tail mixing ratio (0=exponential tail only, 1=constant tail only)

CT = constant tail height (1=tail height same as peak height, 0=no constant tail)

ET = exponential tail (0=infinite tail, 1=no tail)

The contribution to the peak area for x<0 from the tail component with respect to the total area (Eq 9-Eq 10) may then be interpreted as the contribution from the doping state of PEDOT that causes the asymmetry. Fresh PEDOT:PSS/Silicon specimens were prepared immediately prior to the HAXPES measurements in order to determine the shape of a fresh PEDOT sulfur peak. The PSS^- and PSSH components were fit to the same Gaussian-Lorentzian convolution function with equal FWHM and the previously reported chemical shift. The results of this fit for the fresh specimens were in good agreement with the results obtained by Jäckle et al. [19]. As the fresh PEDOT spectra was only collected for the lowest x-ray excitation energy the analysis is limited to this energy through all the samples. Figure 25 shows the S 1s spectra decomposition for a fresh PEDOT:PSS and a degraded specimen. Figure 26 shows the percentage contribution of the asymmetric exponential Voight-type function to the total peak area for x<0 determined for the aged specimens.

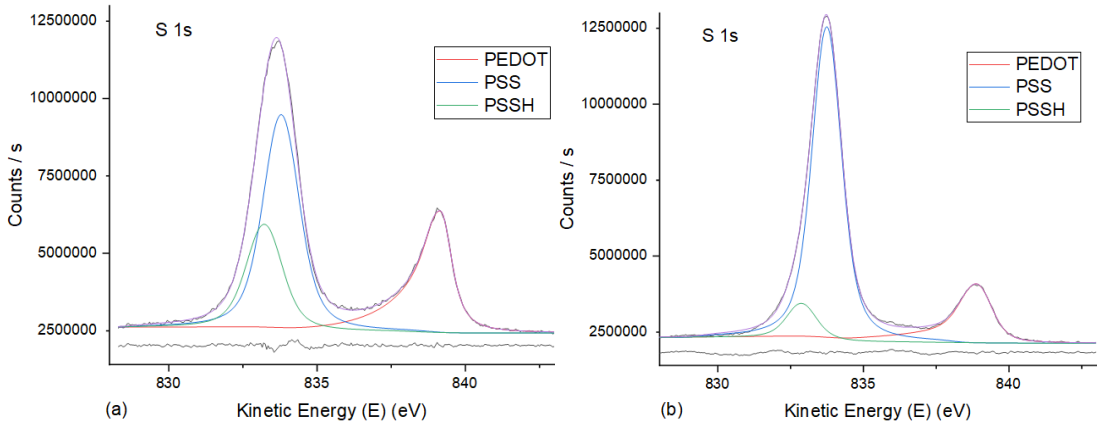

Figure 25. S 1s peak decomposition for (a) a fresh PEDOT:PSS specimen and (b) a specimen that has aged for 8 weeks.

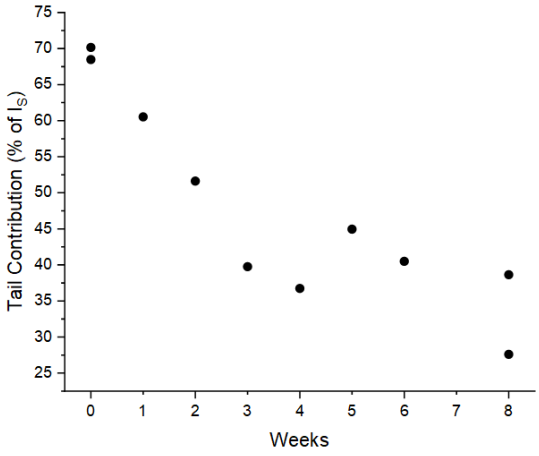

Figure 26. Contribution of asymmetric exponential tail function to peak area as a function of aging time.

The results shown in Figure 26 shows the contribution of the tail function to the total peak area decreases as the devices age. This may be interpreted as a loss in doping concentration in the PEDOT backbone. These results confirm the predictions from the simulated model that the effective doping concentration in PEDOT:PSS is decreasing as

the devices age. It is important to acknowledge the limitations of this analysis. The assumption of only three S species with well-defined chemical shifts provides a good fit for fresh PEDOT:PSS, however as the devices age this approach is an incomplete description of the chemical states of S in the film. The overall structure and composition of the film is expected to change as the samples degrade, potentially causing different sulfur species to be present in the film. Notably this approach to peak decomposition yielded a decrease in the relative intensity of the assumed PSSH to PSS^- peak as the samples aged. If the PSS^- species is related to the doping of the PEDOT backbone then this result would be in disagreement with the observed loss in doping concentration of the PEDOT:PSS backbone. Rather we believe this simple two component model of the PSS sulfur species is an incomplete description of the chemical state of the film as the devices age, however any further analysis of this peak and its composition is beyond the scope of this work. Nevertheless, by maintaining a consistent peak decomposition model across all specimens, the comparison of the contribution of the asymmetric Voight-type function to the area of the PEDOT sulfur peak remains valid.

Finally, we investigated the possibility of the band alignment of the devices changing as they age and whether there was significant charging occurring across the interface. A buildup of fixed charges across this interface would greatly disturb the band alignment of the PEDOT:PSS and the Si and have a detrimental effect on solar cell performance. It is possible, for example, that residual free protons in the PEDOT:PSS film may have migrated towards the oxide as the devices aged causing an overall charge imbalance across the interface, thereby inducing a voltage across the interface opposite to

the photovoltage. In order to evaluate this, the energy difference between the silicon substrate 1s peak and the PEDOT sulfur 1s peak were calculated for each specimen. We found the energy difference between the two peaks across all the aged specimens remained relatively constant ($\Delta E = 632.50 \pm 0.15eV$) across all measurements with the variance showing no apparent trends. These results suggest that the band alignment between PEDOT:PSS and the silicon substrate does not change significantly as the devices age and it also confirms there is no apparent charging effects across the interface. It is possible that instead of no charging occurring across the interface all samples showed the same degree of charging induced by the x-ray irradiation, i.e. that the charging reaches equilibrium soon after the x-ray dose is started. In either case this result further confirms the validity of the PEDOT asymmetric exponential tail analysis as the peak position corresponds to the same chemical species of sulfur in the PEDOT chain. Furthermore, these results also suggest the PEDOT:PSS film is not undergoing any significant chemical changes that would alter its apparent band structure (HOMO-LUMO positions). If for instance the PEDOT backbone conjugation was broken at some point while the devices aged this would be reflected in a change in the binding energy difference between the silicon substrate and the sulfur in the PEDOT backbone.

It is important to note that polished (100) substrates were used for both the XPS and HAXPES studies in contrast with the KOH textured substrates used for solar cells. In the textured substrates the (111) surface is in contact with the PEDOT instead of the (100), this surface is known to be much more thermodynamically stable and thus exhibits slower oxidation kinetics. This might explain to some degree the increased performance

seen with textured substrates over planar ones. Furthermore, the results of the simulation fit to degraded device performance suggests the effective oxide saturation thickness is reached between weeks 2 and 3 whereas the oxide thickness calculated from ARXPS appears to reach the saturation point by the second week.

The TLM, ARXPS and HAXPES studies were limited to specimens that had degraded under ambient conditions which limits our ability to consider the difference an inert nitrogen environment would make in the measured properties of the devices. The fit of the simulation model to the experimental JV response of devices stored in a nitrogen cabinet suggest that the inert nitrogen environment reduces the rate of degradation of the devices hindering both the growth of the interfacial oxide layer and the de-doping of the PEDOT:PSS film, however in the present work we have not investigated these claims in the same way as for the air-degraded specimens. Nevertheless, it is reasonable to expect an analogous study of nitrogen stored specimens would yield results consistent with the simulated model fit.

5.4. Conclusion

In this study we present the first comprehensive model of the degradation mechanism and the development of s-shaped JV characteristics of the PEDOT:PSS/Silicon hybrid heterojunction photovoltaic devices. We developed a numerical simulation model of these photovoltaic devices based on the latest understanding of the hybrid material system and showed that the thickness of the interfacial silicon oxide and the doping concentration of PEDOT:PSS are responsible for

the observed s-shaped JV responses of these devices. The simulated model provided exceptionally good fits to experimental JV data, which along with the physical parameters of solar cell-like specimens characterized via TLM, ARXPS, and HAXPES suggested that with respect to the degradation mechanisms:

1. The interfacial silicon oxide develops rapidly after fabrication and its thickness and composition approaches native oxide characteristics as the devices age and is the primary factor in the development of s-shaped JV curves.
2. The doping concentration of PEDOT:PSS decreases as the devices age which enhances the s-shape character of the JV response but does not directly cause it.
3. Storage conditions affect the degree and rate of degradation which is driven by the exposure to moisture, oxygen, and light.
4. The interface between PEDOT:PSS and silver remains ohmic over a five-week period and does not significantly degrade over a 10 day period.
5. The relative band alignment between the PEDOT:PSS and the silicon substrate does not change measurably as the devices age and the interface shows no apparent charging issues.

The silicon-organic hybrid electronic technology shows great promise of delivering high performing inexpensive devices with versatile form factors. So far, the greatest challenge this technology faces is the unreliability and fast degradation of practical devices. In this work we show that any further efforts to develop this technology

should be centered at the silicon-organic interface. Although there are further details to unveil with regards to the degradation mechanisms of these devices, the most important aspect for further studies must be the development of a chemically protective silicon surface passivation treatment that hinders the growth of the interfacial silicon oxide layer and does not hinder carrier extraction.

5.5. Acknowledgments

Work at the ASU Solar Power Lab by Som Dahal, Rameshwari Ghimire and Stuart Bowden was supported by the Nanotechnology collaborative Infrastructure Southwest (NCI-SW) with funding from NSF- ECCS1542160. Electron beam deposition was done at UD Nanofabrication facility under guidance of Scott McCracken. TLM measurements were done under the guidance of Prof. Yuping Zeng and Peng Cui. XPS characterization was performed at The Surface Analysis Facility in the University of Delaware supported by the National Science Foundation grant number 1428149 and under the guidance of Wenbo Wu and with the help of Miyu Mudalamane. This research used resources of the National Synchrotron Light Source II, a U.S. Department of Energy (DOE) Office of Science User Facility operated for the DOE Office of Science by Brookhaven National Laboratory under Contract No. DE-SC0012704. HAXPES measurements were performed at NIST beamline SST-2, located at NSLS-II under the guidance of Dr. Conan Weiland. This material is based upon work primarily supported by the Engineering Research Center Program of the National Science Foundation and the Office of Energy Efficiency and Renewable Energy of the Department of Energy under NSF Cooperative Agreement No. EEC-1041895. Any opinions, findings and conclusions

or recommendations expressed in this material are those of the author(s) and do not necessarily reflect those of the National Science Foundation or Department of Energy.[2]

[2] Reproduced with permission. [48]

Chapter 6. ORGANIC SURFACE PASSIVATION TREATMENTS COMPATIBLE WITH HIGH PERFORMANCE HYBRID HJT PV CELLS

6.1.Introduction

The quality of the passivation of the silicon surface is one of the most important factors for the performance of the solar cells. Proper surface passivation contributes to minimizing the surface defect density, minimizing charge recombination, and greatly improving open circuit voltages. The high performance of the amorphous silicon HIT cells is attributed to exceptional passivation quality of the amorphous Si:H deposited on the surfaces of the crystalline silicon substrate. In the case of hybrid solar cells, in order to maintain a lower cost advantage a different passivation technique must be used. The quality of the p-benzoquinone (BQ) passivation has been studied and validated previously. EDOT-acid has been studied for its effect on improving the adhesion of electrodeposited PEDOT to inorganic substrates due to its chemical bonding to the surface [72]. Due to this chemical bond to the surface of silicon EDOT-acid could in principle also exhibit passivating qualities due to its occupation of dangling surface bonds. The easiest way to study the passivating properties of EDOT-acid is via Photoconductance Decay, which is the same method used previously for studying BQ. In this technique, a light is shined on the semiconductor sample and the excess minority carriers are determined by measuring the change in conductivity of the sample.

The most common way of performing this technique is in a contactless fashion where an inductance coil beneath the sample is used to measure the conductivity. The tests are run either in a steady state or in a quasi-steady state fashion where the analysis of the data becomes much simpler. This technique is particularly useful for assessing the quality of surface passivation due to its sensitivity to surface defects.

Prior work investigated the passivation mechanism of different solution-based organic treatments as an alternative silicon surface passivation treatment that could be compatible with our hybrid HJT cell architecture. Although the use of organic treatments for the passivation of silicon surfaces has been the subject of numerous investigations, so far none of the proposed strategies have proven reliable for the fabrication of high performance PV cells. Among the most promising organic treatments is the use of a benzoquinone (BQ) and methanol (MeOH) solution in which the silicon substrates are immersed for one hour. Chen et al. demonstrated the superior passivation qualities of this treatment and found the mechanism to be radical-assisted, an important consideration for the work done in this dissertation. Furthermore, this treatment was successfully employed to fabricated a hybrid HJT solar cell with 9.1% efficiency [28], which is comparable to the average in the field. Given the expected effect of the improved surface passivation, devices fabricated with this treatment should perform at much higher efficiencies.

In this chapter we will investigate the use of functionalized EDOT molecules, such as EDOT-acid, as alternative silicon surface treatments in terms of the passivation quality offered while in later chapters we will investigate the complementary effects in facilitating in-situ PEDOT deposition techniques.

In the case of surface passivation strategies, there are two main passivation mechanisms that must complement each other for the passivation properties to translate into prototype devices: chemical and electrical passivation. Chemical passivation refers to the passivation of the silicon surface dangling bonds by means of chemical bonding with a different material. By creating stable chemical bonds, the density of mid-gap trap states from the dangling surface bond states is minimized. However, in the case of organic molecules, the bond between the silicon and the small molecule may be compromised by the presence of an oxidative environment where it is more favorable (thermodynamically and kinetically) for the silicon surface to oxidize rather than maintain the organic passivation structure. Electrical passivation refers to the formation of an electric field across the silicon interface that causes band bending in the substrate such that the interface acts as a carrier selective contact. This electric field must be complementary to the electric field caused by the junction formation with the emitter material. In the case of small organic molecules, the field arises from the dipole formed upon bonding the molecule with the silicon surface due to the difference in electronegativity between the materials. This induced electric field can be measured as the change in work function of the material and the direction of work function change indicates the direction of the induced band bending (upwards or downwards).

In the case of our hybrid HJT cell architecture where the substrate is n-Si and the emitter is PEDOT:PSS, the band bending at the front surface of the device is upwards corresponding to the formation of an inversion layer where the minority carrier concentration surpasses the bulk majority carrier concentration. As long as this inversion

persists the device can be expected to show high PV performance. However, due to the instability of organic materials and treatments under ambient conditions, the performance of these devices is easily compromised, and the exact source of the degradation mechanism has not been identified successfully so far.

6.2. Passivation Quality Metrics

One of the most important metrics in determining the quality of a given passivation strategy is the minority or effective carrier lifetime (τ). Quasi-steady state photoconductance decay allows for the measurement of effective carrier lifetime by utilizing an inductive coil that measures the conductance of a substrate while being illuminated by a slowly decaying flash of light. The effective lifetime can be extracted as a function of injected excess minority carrier density. The effective carrier recombination lifetime combines the effects of both bulk and surface recombination (with respective lifetimes τ_b and τ_s).

$$\frac{1}{\tau} = \frac{1}{\tau_b} + \frac{1}{\tau_s} \tag{12}$$

Another important metric in measuring the effective carrier recombination at the surface of material is the surface recombination velocity (S). This metric is independent of substrate thickness (d), which allows for easy comparisons across the literature and samples. Effective carrier lifetime (τ) can then be expressed in terms of S, d, and minority carrier diffusion constant D.

$$\frac{1}{\tau} = \frac{1}{\tau_b} + \left(\frac{d}{2S} + \frac{d^2}{\pi^2 D}\right)^{-1} \tag{13}$$

A precise measure of surface recombination velocity from the measured effective carrier lifetime requires knowledge of the bulk recombination velocity (τ_b). τ_b can either be determined from taking measurements of substrates of different thicknesses or an upper limit of S can be determined by assuming an infinite bulk carrier lifetime. This approximation is only valid if the test substrate is both very high quality and purity. Effective passivation of silicon surfaces can yield minority carrier lifetimes of several milliseconds and reduce the surface recombination velocity to values less than 10cm/s.

6.3. Silicon Passivation Strategies Background

As has been discussed up to this point, the passivation of the silicon surface is perhaps one of the most important challenges in the field of silicon PV. The large number of surface defects states from the silicon dangling bonds has a greatly detrimental effect on the band dispersion of devices and promote the rapid recombination of carriers. The state-of-the-art high performance silicon PV technologies include: Heterojunction with Intrinsic Thin Layer (HIT) [33], Tunnel Oxide Passivated Contact (TOPCon) [73], and Interdigitated Back Contact (IBC) [74] solar cells. These solar cells all rely on excellent surface (and interfacial) passivation, either through oxides, nitrides or amorphous silicon layers.

The most commonly used passivation techniques rely on expensive fabrication techniques for the growth of high-quality oxides or nitrides. Architectures using hydrogenated amorphous Si (a-Si:H) [33] and microcrystalline Si [73] have also been able to produce well-passivated interfaces. These strategies involve the use of techniques

such as: ALD (atomic layer deposition), PECVD (plasma-enhanced chemical vapor deposition), and thermal oxidation [75].

The aforementioned silicon passivation techniques are both energy intensive and costly and have not been shown to be compatible with a hybrid PV cell architecture. Alternative organic solution-based passivation treatments are gaining interest due to the facile room temperature processing techniques. Among these alternative techniques, the use of methanol [76], iodine-methanol [77], and BQ-methanol [28] have shown promise in delivering high quality silicon surface passivation [78].

The work performed previously by Hack [79] and Chen [80] on the passivation quality of the BQ/MeOH passivation strategy is the basis for the work presented in this dissertation with respect to the passivation quality of functionalized EDOT-molecules.

In addition to the potential passivation quality of these treatments, the functionalized EDOT-molecules serve to provide a pathway for covalent adhesion between the silicon substrate and the PEDOT films. However, given the lack of success in prior attempts to incorporate organic passivation treatments to spin coated devices, the proper utilization of these treatments requires a shift in processing and fabrication technique for the direct polymerization of PEDOT on the treated silicon surface. In this dissertation we evaluate the potential of three different EDOT-molecules to serve as the interfacial silicon surface treatment for use in in-situ deposition techniques, namely electrodeposition and oxidative chemical vapor deposition (oCVD). Due to the rarity of

the materials used, the results presented in this dissertation are aimed to be a preliminary screening of candidate materials to help guide future and ongoing R&D work.

6.4. BQ/MeOH Treatment Background

With regard to the chemical bonding mechanism of organic molecules and the silicon surface there are two main factors at play: the kinetics of the expected reaction and the thermodynamic favorability of the resulting silicon surface re-arrangement. It is well known that the silicon-methanol bond is stable and provides high quality passivation [76], however the kinetics of the reaction are very slow.

Chen et al. [28] investigated the passivation mechanism of BQ and HQ molecules in methanol solution, the structure of which can be seen in Figure 27 below. It is known that BQ/HQ couple in methanol solution to for the direct formation of HQ from BQ without the appearance of semiquinone radicals.

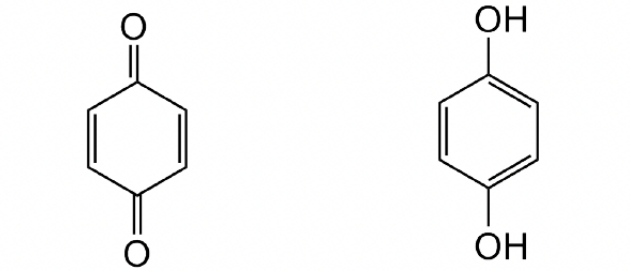

Figure 27. Chemical structure of BQ and HQ molecules studied as passivation treatments.

Chen et al. demonstrated that the radical-assisted bonding mechanism is present in the BQ/MeOH treatment provides much faster kinetics and allows for easy incorporation into a fabrication process flow. The proposed radical initiation mechanism can be seen in

figure 28 and the results of the passivation quality kinetics for the BQ/MeOH treatment can be seen in Figure 29 below.

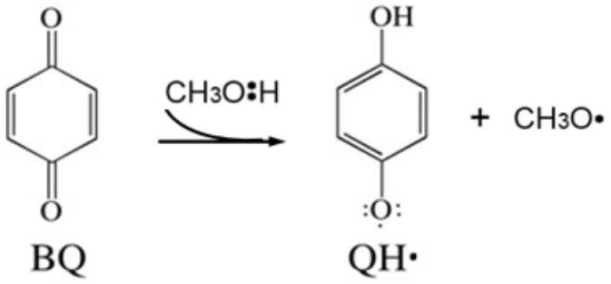

Figure 28. BQ can extract H* from ME and become HQ*. Both QH* and the resulting methanol radical CH_3O* can bond to the silicon surface to provide passivation effects.

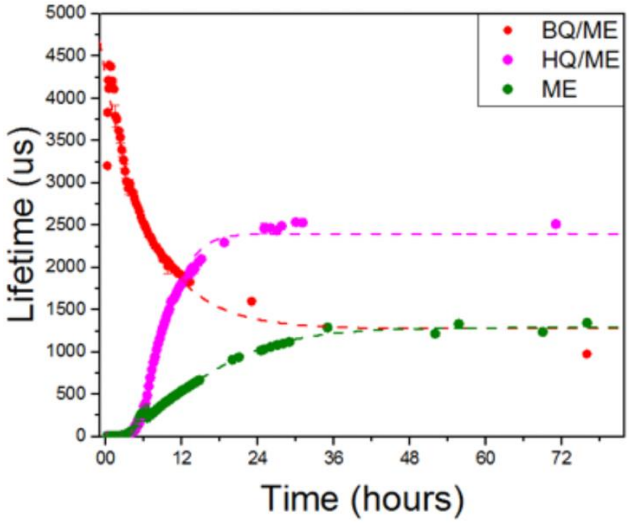

Figure 29. Time resolved measured effective lifetime of BQ/MeOH (0.01M) and HQ/MeOH (0.01M) silicon surface treatments [28].

It can be seen in Figure 29 that the BQ/MeOH passivation treatment provides near instantaneous improvement in effective lifetime reaching its highest (4500μs) around 30 minutes of treatment and then decreasing gradually to the level of the methanol control treatment. Both the methanol and the HQ/MeOH treatment show much gradual increases

in effective lifetime reaching plateaus around 1300μs and 2500μs respectively measured at minority carrier density (MCD=10^{15} cm^{-3}).

6.5. Passivation Quality of EDOT-Functionalized Molecules

One of the most important technical goals of this work is to identify and develop a silicon surface treatment to address three major concerns: provide high surface carrier lifetimes, facilitate the in-situ deposition of the PEDOT film, via electrodeposition or oxidative chemical vapor deposition (oCVD), and improve the adhesion of the PEDOT film to the silicon substrate. During the in-situ polymerization process, the PEDOT chains are formed directly on the surface of the substrate via a cation-radical oxidative polymerization of the EDOT monomers. Despite evidence of homogeneous and conformal coatings even in irregular surfaces, the polymerization mechanism does not guarantee strong covalent adhesion to the substrate. One of the main objectives of the new passivation treatment will be to promote the chemical adhesion of the film to the silicon substrate by providing a pathway for the covalent attachment of the polymer chains to the silicon substrate in addition to the passivation qualities. We expect that such treatment will also limit the oxidation of the silicon surface by providing a sterically and kinetically limited pathway for the oxidation of the silicon surface.

The three of the molecules studied are: EDOT-acid, Chloromethyl-EDOT, and Hydroxymethyl-EDOT as can be seen in Figure 30. These EDOT molecules are soluble in polar solvents and the chemical functionalization allows them to react directly with the Si-H bond at the silicon surface that results from hydrofluoric acid etching. Figure 31 shows the proposed mechanism by which EDOT-acid reacts with the H-terminated

silicon and participates in the polymerization reaction. Other EDOT functionalities may also behave in a similar manner with varying kinetics, surface coverage, and resulting passivation quality.

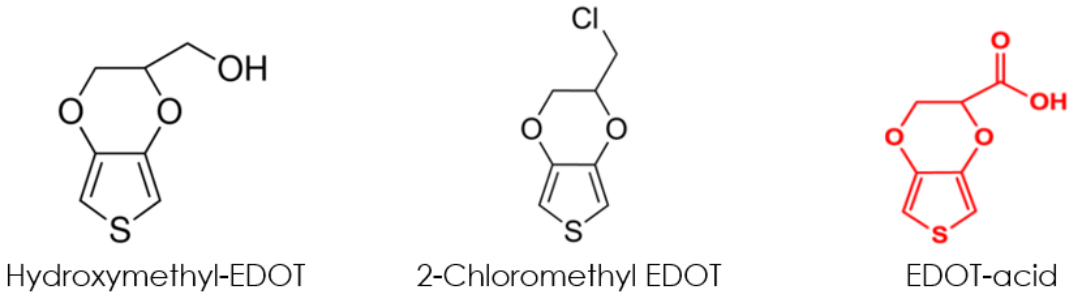

Figure 30. Structure of functionalized EDOT-molecules tested as part of this work.

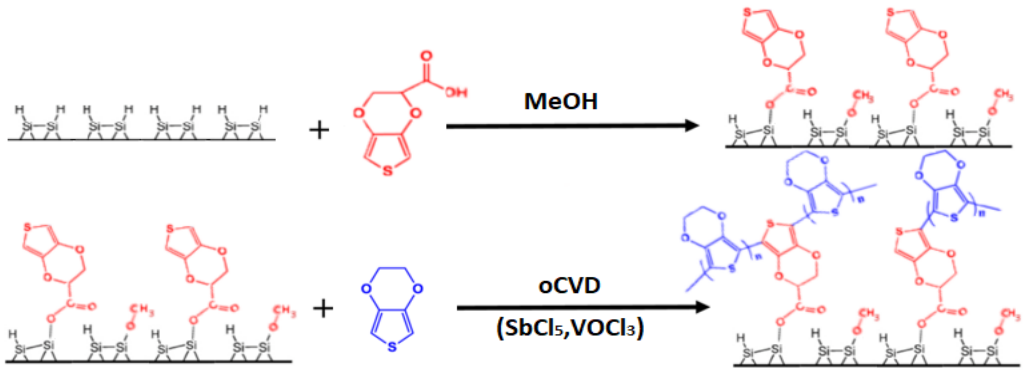

Figure 31. Mechanism for EDOT-acid/MeOH passivation treatment of H-terminated Si and in-situ PEDOT polymerization.

6.6. Results and Discussion

Following the procedure outlined by Chen [28], three different functionalized EDOT molecules were tested in the Sinton WCT-120 Lifetime tester. Double side

polished n-type (1-5 ohm.cm) FZ silicon wafers with certified bulk lifetime were used as the substrates for effective carrier lifetime testing. The silicon wafers underwent piranha cleaning for five minutes followed by five-minute immersion in DI water and finally a two-minute immersion in hydrofluoric acid (HF) to etch the interfacial oxide. Immediately post cleaning, the substrates were immersed in a 0.005M methanol solution of the molecule being tested and sealed in a thin acid resistant plastic bag. The samples were then placed on the measuring stage of the Sinton WCT-120 and the lifetime tested as a function of time every 15 minutes. An optical constant of 0.7 was used for all experiments based on previous studies [28]. The substrates remained in solution over the duration of the experiment. The results presented here were taken based on the quasi-steady state photoconductance (QSSPC) mode at minority carrier density (MCD)=$1*10^{15}$ cm^{-3} and are thus intended for easy comparison across the candidate molecules. Due to the length of the experiments and the inaccuracies in using the QSSPC mode at lifetimes higher than 200µs, the absolute value of the quality of the resulting silicon surface passivation cannot be established until further experiments are performed. All molecules were tested with substrates cut from the same stock wafer to minimize the variation of substrates.

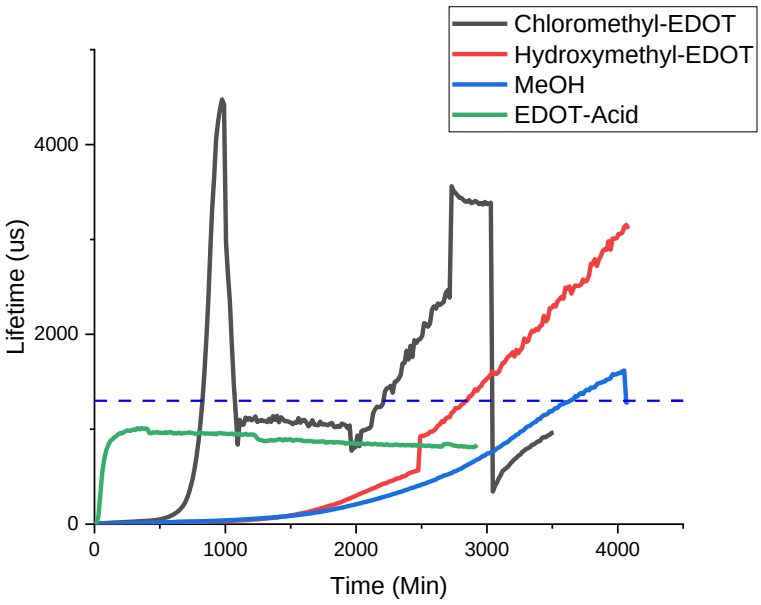

Figure 32. Time resolved measured effective lifetime of candidate molecules and methanol control. Dashed line represents the plateau of the methanol control treatment (1300µs).

As can be seen in Figure 32, the reaction kinetics of all treatments tested are very slow, but the EDOT-molecules appear to provide significant additional passivation to the silicon surface compared to the methanol control treatment. Among all the molecules tested EDOT-acid appears to provide a significant level of passivation much more rapidly than any other treatment, peaking around 1000µs after 2 hours of treatment. Furthermore, the reaction appears to be stable with a gradual decrease in apparent lifetime beyond the 2-hour mark, which could be due to the growth of the interfacial oxide under the experimental conditions that degrades the overall quality of the passivation treatment.

In the case of Chloromethyl-EDOT (black line), it appears that the reactions between the EDOT molecule and the methanol with the silicon surface are competing in quite a dramatic fashion. It is clear however that the Chloromethyl-EDOT, despite

considerably slow kinetics (1000 minutes) provides a high degree of passivation. It is important to note that all experiments were carried out with ambient light throughout the duration of the experiment, which has been noted to assist in radical-assisted reaction mechanisms such as the BQ/MeOH treatment. Nevertheless, as the reactions took place over several days, the change in the intensity of ambient light may have had an effect in the reaction of the molecules, particularly in the case of Chloromethyl-EDOT.

This work also confirms previous studies on the steady state quality of the methanol control treatment, measured as the effective carrier lifetime reported in transient photoconductance decay (PCD) mode at MCD=$1*10^{15}$ cm^{-3}, was found to plateau around 1300μs, in agreement with the work by Chen et al. Furthermore H-terminated Si was found to have an effective carrier lifetime less than 40μs [28].

6.7. Conclusions and outlook for future work

It cannot be understated that the future commercial viability of hybrid HJT PV technology is heavily dependent on the development of a compatible organic surface treatment that can provide superior passivation qualities, enable high efficiency devices, while remaining cost competitive with the inorganic alternative strategies.

Our previous efforts in developing organic inexpensive surface passivation treatments for the silicon substrate were undermined by the growth of the interfacial silicon oxide layer and the PEDOT:PSS spin coating process and never properly translated to the performance of PV devices. We have demonstrated the superior passivation quality of the BQ/MeOH treatment (surface recombination velocity of 6cm/s) [28] and have preliminarily demonstrated the passivation quality of different

functionalized EDOT molecule treatments. Nevertheless, the reaction kinetics of these treatments are not yet fully understood and present an important challenge for future work. In order to take full advantage of the passivation qualities offered by these treatments within an adapted fabrication processing scheme, the reaction kinetics must allow for the coverage of the silicon surface within a much reasonable frame of time.

The adapted fabrication process will limit the growth of the interfacial silicon oxide which will allow the cells to retain the quality of the surface passivation treatments translating into higher V_{oc} and PCE figures. The interaction of the passivation treatments with the in-situ deposition of PEDOT presents a new consideration in addition to the improvement of carrier lifetimes. The use of EDOT-acid was shown by Wei and colleagues at the University of Delaware to improve the adhesion of electropolymerized PEDOT to inorganic substrates by providing covalent attachment between the substrate and the polymer chains [72]. The use of functionalized EDOT molecules in the context of the proposed processing scheme will similarly allow the PEDOT chains to polymerize from the covalently attached EDOT and improve the adhesion to the silicon and the homogeneity of the film. The full benefits of each surface treatment will only be apparent upon fabrication of sample devices.

Chapter 7. IN SITU ELECTRODEPOSITION OF PEDOT TOWARDS HIGHER CONDUCTIVITIES, ENHANCED MECHANICAL PROPERTIES, AND DEGRADATION RESILIENCE

7.1. Introduction

Extensive research has been conducted on optimizing PEDOT:PSS to overcome the aforementioned problems of these hybrid devices. One of the best performing hybrid devices with PEDOT in the front achieved a PCE of 16.3% by using a moisture resistant capping layer on top of the PEDOT film and in this way ensure tight conformal contact between with the silicon and prevent moisture-driven degradation of the microstructure [81]. Whereas the back-PEDOT cell (20.6%) achieved the same effect by having PEDOT effectively encapsulated by the silicon despite the claim of the authors that this increased performance was solely due to the lack of parasitic absorption by the PEDOT [35]. Despite these considerable advancements in the performance of hybrid cells, the goal of fabricating the devices at low temperature and decreased cost has been overlooked.

Alternative processing methods and materials could inherently overcome the shortcomings of spin coated PEDOT:PSS and maintain the low cost of fabrication. Electrochemical deposition stands out as a processing technique that would open many opportunities in this field.

The main challenge in using materials other than PEDOT:PSS is the difficulty in processing other conjugated polymers due to their insolubility and high melting point. Electrochemical deposition allows for the direct polymerization of the material of interest on the substrate from a solution of its monomer and oxidant. In this way other chemistries can be investigated, and the polymer would have improved conformal and in some cases even chemical adhesion to the substrate avoiding the formation of voids and optimizing the contact between the materials. Furthermore, electrodeposition is even more cost-effective processing method due to the efficient utilization of the monomer and the minimal waste of raw material.

PEDOT itself can be doped with a wide range of alternative counter ions forming different complexes that exhibit similar properties to PEDOT:PSS. Some of the most common counter ions studied to dope PEDOT are perchlorate, hexafluorophosphate, and nitrate. Exploring these alternative counterions is made possible by the use of electrochemistry due to the fact that salts of these ions can be introduced to the solution along with the monomers. Charge transport occurs along the PEDOT backbone and the different chemical dopants may induce a similar carrier concentration along the PEDOT chains, resulting from one hole for every 3 EDOT units, if the polymerization process is optimized. [6, p. 87] This means that, in principle, these alternative materials would maintain a similar band dispersion of PEDOT:PSS which would in turn induce the required inversion in silicon and would also act as a HTL by repelling electrons and selectively collecting holes.

Electrochemical deposition of conjugated polymers has been investigated for different applications, most notably in the field of bio-electronic interfacing [82], however there has not been abundant research in its use for hybrid solid state devices. There have been studies that have focused on using electrodeposition for use as HTL in all organic cells [83], [84]. In this chapter we evaluate the viability of this processing method as a way to overcome the challenges identified with the spin coated PEDOT:PSS PV devices currently under investigation. This endeavor requires careful consideration of the process and its potential implications on device performance within the framework previously built by analysis of hybrid devices. Of particular interest is the system of electrodeposited PEDOT perchlorate with the use of EDOT-acid as a surface treatment for silicon. EDOT-acid is a small PEDOT monomer that has been modified with a carboxylic group which can be made to react chemically with the surface of an inorganic substrate. This chemical treatment has been investigated previously as an effective method to improve the mechanical adhesion of the film to an ITO substrate [72]. The chemical bond resulting from the interaction of the carboxylic group with the surface of silicon is similar to the chemical bonds of previously validated passivating methods [28], which raises the question of its potential to provide a similar field effect passivation of the silicon surface.

Electrochemical polymerization of conjugated polymers is a process analogous to the electrodeposition commonly used for metals. In this deposition method a dilute solution of monomer and supporting electrolyte (dopant) is placed in a three-electrode cell where the working electrode is the conductive substrate where the film is to be

deposited, the reference electrode is a known standard, and the counter electrode is a precious metal. An external electrical potential is applied between the working and the counter electrode; this electrical potential induces the oxidation of the monomers in the solution near the working electrode forming radical cations. The electrical potential applied can be potentiostatic (constant voltage), galvanostatic (constant current), and cyclic voltammetry (control both current and voltage in some predetermined pattern). The radical cations formed can then react with each other to form the polymer chains. These polymer chains then precipitate onto the substrate, however certain surface treatments of the substrate and polymerization conditions can promote direct reaction with the surface of the substrate which then leads to the formation of polymer chains directly on the working electrode [72].

There are many variable factors in electrochemical deposition, namely: the current-voltage conditions applied, the solvent and electrolyte chosen, and the area and surface treatment of the substrate. These factors have profound implications in the properties of the resulting polymer films as they impact almost every aspect of interest to us: thickness, morphology, conductivity, and transparency. It is clear that controlling the electrochemical deposition conditions will have a significant impact on the performance of the hybrid cells fabricated in this manner. The spin coating process has undergone significant study and optimization that has allowed cell performance to be improved from 3% in some early studies [32] to the current champion efficiencies that have emerged in the past two years. Keeping this in mind, it is most important to identify the fundamental potential for electrodeposition to meet the required criteria for a functioning PV device.

7.2. Results and Discussion

First and most importantly is to establish the viability of using silicon as the deposition substrate, as to the best of our knowledge there is no available literature on this particular system. It is known that the deposition substrate must be conductive and due to the relatively low doping concentration of our substrates (about 1-5ohm.cm) it was uncertain whether this would be a viable deposition substrate. We conducted preliminary studies and found that the EDOT-perchlorate system produced PEDOT films that covered the entire surface of the silicon. This was achieved with two different perchlorate salts: lithium perchlorate and tetrabutylammonium perchlorate (TBAP). Lithium diffusion into silicon and its surface oxide is known to be an issue for the performance of solid-state devices such that TBAP was chosen as the supporting electrolyte going forward.

The thickness and homogeneity of the film is crucial not only for the anti-reflectivity properties but also for proper device performance, as incomplete or otherwise faulty coatings will cause shunts that will drastically hinder the efficiency of the device. Furthermore, the film must be thin enough to minimize the parasitic absorption and resistance losses of the polymer. Therefore, for the fabrication of efficient hybrid devices, it is critical to accurately control the deposition procedure to achieve homogeneity and a proper thickness of the film. There has been little work done on the control of the electrodeposition parameters to achieve film thickness on the scale of what is needed for implementation in hybrid devices, to be more specific, none using silicon as the substrate. Del-Oso et al. [83] found that the thickness-time relationship for the potentiostatic deposition of PEDOT-perchlorate on ITO substrates followed a linear trend which

indicates this system follows the Faraday law of electrolysis. The authors however report thickness of 20-40nm with 100-200s of reaction whereas Vlamidis et al. [84] reports thickness of 200nm for a potentiostatic deposition of 10 seconds. It is clear that the electrodeposition procedure must be optimized on a case-by-case basis, but a linear relationship is expected for homogenous deposition due to the system following Faraday's law. Accurate thickness control is one of the reasons why the homogeneity of the film is particularly important in this case, but beyond this reason inhomogeneity would greatly difficult the systematic study and optimization of the devices. This problem is further complicated when using textured silicon substrates as their irregularity might have considerable effects on the spatial distribution of the material's deposition, particularly due to charge concentration on sharp edges such as the peaks of the pyramids. Despite the additional complications of working with textured substrates, the added benefit provided by the silicon's texturing paired with the improved contact of the polymer film to the silicon surface makes this an issue worth investigating further.

The homogeneity of the electrodeposited films has been shown to strongly depend on the monomer and electrolyte concentration as well as the solvent used during the deposition. It has been reported that lower monomer concentration of 0.3M paired with a mixture of toluene/acetonitrile (4:1 v/v) as the solvent yields the most homogeneous films, which is attributed to decreased polymerization kinetics [83]. Del Valle et al. reported that homogeneity of the film is improved by using cyclic voltammetry and smaller counter ions [85]. We have conducted studies with the goal of identifying the parameters that would yield most homogeneous deposition and get a sense of the time-

thickness relationship for the system using textured silicon substrates. Besides testing different solvent and electric potential conditions, we also investigated the influence of using EDOT-acid as a surface treatment for silicon. We used Scanning Electron Microscopy (SEM) to assess the homogeneity of the deposited films and provide an estimate of the film's thickness by imaging the cross-section. We determined that although using toluene did improve the homogeneity of the film, treating the silicon surface with EDOT-acid had the most significant impact in improving film homogeneity. It should also be noted that the quality of the resolution of the SEM images confirms the high conductivity of the electrodeposited films. Figure 33 below shows an SEM image of the most optimal conditions tested.

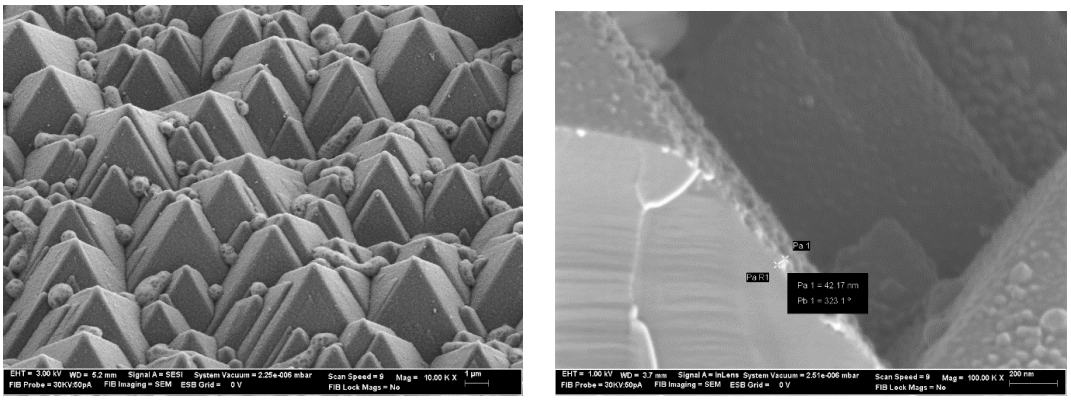

Figure 33. Electrodeposited film with EDOT-acid surface treatment and toluene/acetonitrile solvent. 0.9V constant potential applied for 10s. Estimated thickness was 42nm (right).

7.3. Compatibility of Electrodeposition Technique and PV Cell Fabrication

Despite the promising prospects of direct electrodeposition of PEDOT on the silicon surface via electrodeposition, no functioning solar cells were fabricated. There are two main concerns that were observed early into the investigation that discouraged further studies into this technique: (1) The growth of the interfacial oxide could not be controlled by simple nitrogen purging and the resulting samples had all developed oxides that hindered any attempt at fabricating a functioning solar cell device. (2) Attempts at using a single-sided electrochemical cell for the PEDOT deposition to avoid the shunting of the cell from the deposition on the back side of the device were unsuccessful as the thin silicon substrates proved too brittle to process in this manner as significant pressure must be applied between the silicon substrate and the sealing ring of the cell, see figure 34.

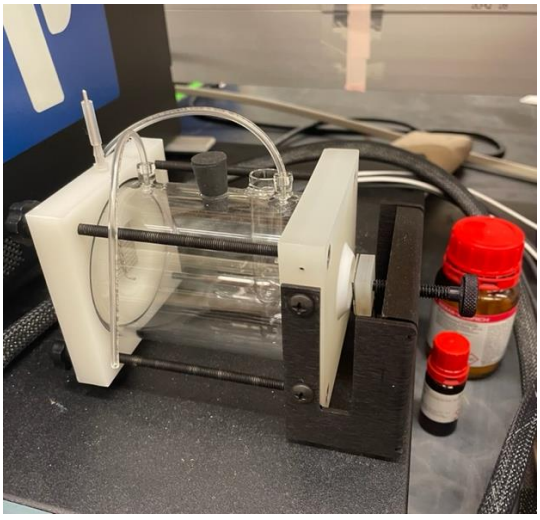

Figure 34. Single-side electrochemical cell used in electrodeposition experiments.

7.4. Conclusion and Takeaway Lessons

Although at this stage electrodeposition was found to not be an appropriate processing technique, it remains highly promising for future R&D projects. It is possible that further studies may reveal strategies to avoid or overcome the two main concerns presented by this technique. However, the remainder of this dissertation is focused on applying the learnings from the use of this in-situ deposition technique to a different more appropriate processing method: oxidative chemical vapor deposition (oCVD).

Chapter 8. FUTURE AND ONGOING WORK

8.1. oCVD Polymerization of PEDOT Doped with $SbCl_5$ or $VOCl_3$ for Record Breaking Conductivities.

We have performed extensive work on the device architecture, the chemical and physical properties of the PEDOT:PSS film, and the passivation of the silicon surface. These devices have employed spin coating for the deposition of PEDOT:PSS, ethylene glycol and Triton X as secondary dopant and surfactant of the PEDOT:PSS, and a Benzoquinone/Methanol (BQ/MeOH) treatment for the passivation of the silicon surface. Furthermore, we have spent a considerable effort in optimizing our processing technique to handle thin silicon substrates (180-75μm) with the aim of developing cells for applications requiring lightweight and conformable form factors, with the additional benefit of having a lower fabrication cost. Silicon wafers with a thickness less than 75 μm exhibit mechanical properties that allow for conformable form factors, and at sufficiently low thickness the wafers can be considered to be flexible. Our hybrid technology platform is a prime candidate to develop conformable and flexible cells as the organic materials will contribute to the mechanical resilience of the device and the processing avoids high temperatures that damage thin substrates.

The operation of this hybrid PV technology is comparable to that of the a-Si:H HIT architecture. In both technologies, the photoactive junction is induced by the carrier selective materials deposited on the surface of the crystalline Si substrate as opposed to the diffused PN junctions of traditional PV technologies. The a-Si:H HIT technology has demonstrated exceptionally high performance which is enabled by two key factors: (i) The high quality of the passivation of the silicon surface provided by the intrinsic a-Si:H layer. In these devices the surface of the semiconductor substrate contains electronic defects that enhance carrier recombination of the photogenerated excitons degrading the photovoltage. Passivation refers to the process of chemically treating the surface defects to reduce the rate of recombination and improve the resulting photovoltage. The quality of passivation treatments is measured by the resulting carrier lifetime or related surface recombination velocity; a higher lifetime-lower surface recombination velocity-implies a lower rate of carrier recombination and higher device performance. (ii) The relative band alignment between the silicon substrate and the carrier selective materials (doped a-Si:H) is ideal to maximize either electron or hole carrier capture and minimize resistive losses. The relative band alignment is related to the alignment of the tops of the valence bands, the bottoms of the conduction bands, and the doping concentration of the materials.

The work in this chapter aims to address these technical challenges by employing solvent-free oxidative chemical vapor deposition (oCVD) for the deposition of the PEDOT layer. More specifically our goal is to apply the oCVD deposition of PEDOT doped with $SbCl_5$ or $VOCl_3$ on thin textured silicon substrates achieving homogenous films of 65 nm in thickness and conductivity >7500 S/cm.

oCVD is a novel technique for the deposition of conductive polymer films where the film is polymerized directly on the substrate surface from a vapor-phase mixture of monomer and oxidant in a mild vacuum environment (0.1-10 Torr), see Figure 35. Both EDOT monomer and the oxidant molecule, either antimony pentachloride ($SbCl_5$) or vanadium oxytrichloride ($VOCl_3$), are liquid solutions at room temperature. These solutions are vaporized via mild heating (<100^oC) and introduced to the reactor chamber by a stream of inert N_2 carrier gas. The oxidant enables the chemical conversion of EDOT monomer into PEDOT polymer via oxidative polymerization and simultaneously the PEDOT polymer physically grows as a thin film on a supporting substrate surface. The resulting film is then rinsed with either methanol or tetrahydrofuran (THF) to remove any residual oxidant, such that there are no heavy metals present in the resulting PEDOT film.

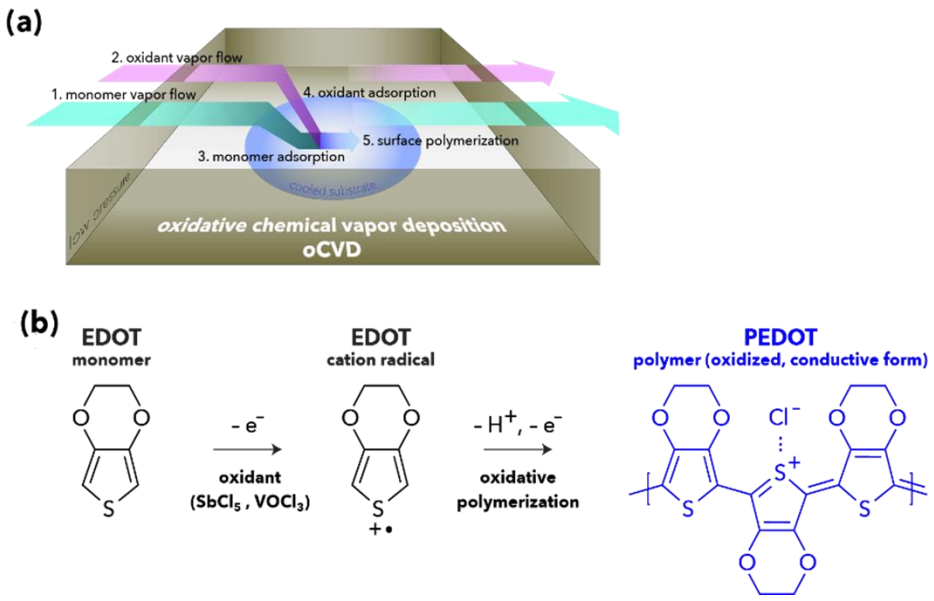

Figure 35. Oxidative chemical vapor deposition (oCVD) of PEDOT. **(a)** oCVD reactor setup, showing vapor flow of monomer and oxidant into a vacuum chamber, where the monomer polymerizes into PEDOT polymer thin film on a substrate. **(b)** oCVD reaction mechanism, illustrating the oxidation by the oxidant of the EDOT monomer into cation radicals, which then undergo oxidative polymerization to produce the oxidized, conductive form of PEDOT polymer.

There are two main advantages of employing oCVD for the deposition of PEDOT as opposed to spin coating PEDOT:PSS:

1. In PEDOT:PSS the PEDOT backbone is primarily responsible for the transport of electrical charges while the PSS provides both doping and induces the water solubility of the complex. Without PSS, PEDOT based materials are not soluble and thus cannot be easily processed. This induced solubility, however, has been shown to have significant disadvantages. Moisture content in PEDOT:PSS has

been shown to be detrimental to the electronic properties of films [7]. The two mechanisms by which moisture absorption degrade the quality of these films are: (i) the decrease in the concentration of free carriers in the PEDOT backbone and (ii) the decrease of the free carrier mobility. oCVD overcomes the moisture-related challenges of PEDOT:PSS by directly depositing a moisture-independent film. Recently published work shows films with extraordinary conductivities (>7500 S/cm [27]) compared to the maximum reported conductivity of PEDOT:PSS optimized with co-solvents (1000 S/cm). In addition, oCVD PEDOT as a hole transport layer in an inverted perovskite solar cell was shown to yield a higher power conversion efficiency compared to an equivalent cell with PEDOT:PSS due to higher film quality with the greater in-plane π-π stacking and shorter stacking distance that enhance charge transport [86]. The observed improvement in conductivity results from both an increase in concentration of free carriers and higher free carrier mobility.

2. The oCVD deposition takes place in a mild vacuum environment which has additionally been flushed with an inert gas such as nitrogen or argon. This coupled with the relatively low deposition temperature (the substrate is temperature controlled to 25-150 °C) means that the interfacial silicon oxide growth is limited during the deposition process.

The deposition of highly conductive PEDOT films doped with alternative oxidants has been well documented but remains a challenging endeavor. For this reason we have

partnered with Professor Kenneth Lau at Rowan University, an expert in the field, to conduct the experiments outlined in this section.

8.1.2. Experimental

N-type silicon (100)-textured substrates (doped with phosphorous, CZ) with back surface field (BSF) were fabricated. These wafers are 145 micron thick with 1–5 Ω-cm resistivity. Random texturization was performed on both sides using potassium hydroxide (2% KOH yielding pyramid sizes of about 3–5 μm base size) alkaline etching. To create BSF n + layer on the N-type wafers, phosphorous oxychloride diffusion was performed at 820 °C, 15 min with POCl3 carrier gas flow rate of 1500 sccm (standard cubic centimeters per minute) for phosphosilicate glass (PSG) growth and dopant drive-in. Finally, a 10-min buffered oxide etch is used to remove the PSG. The sheet resistance value of the BSF side is 55 Ω/square.

EDOT was purchased from Fischer Chemical in certified ACS grade. Vanadium Oxytrichloride ($VOCl_3$) was purchased from Sigma Aldrich.

All wafers were cleaned using a Piranha etch (H2SO4:H2O2 = 4:1) for five minutes, followed by a 5-min DI water rise and a two-minute immersion in hydrofluoric acid (HF, 2 wt%), as described in [3]. After cleaning, the substrates were quickly blown dry with nitrogen and introduced into the oCVD reaction chamber. The oCVD reaction conditions were varied across the samples. For complete solar cell devices, metal contacts were deposited using electron beam physical vapor deposition. Aluminum (2μm) was used as the back contact and deposited on the BSF-treated side of the wafer, while silver (500nm)

was used as the front contact and was deposited with the help of a finger patterned shadow mask directly on the PEDOT:PSS films.

1.5cm × 1.5cm textured n-type silicon wafers were used as substrates for the devices. The devices were tested using illuminated current density–voltage measurements (JV). JV response was measured by means of a DC source meter (Keithley 2400 Sourcemeter, USA) both in the dark and light, under air mass 1.5G standard illumination.

8.1.3. Results and Discussion

The most important factor in achieving the superior properties of oCVD PEDOT (higher free carrier concentration and mobility compared to PEDOT:PSS) and translating these to a higher performing hybrid PV device is the optimization of the reaction conditions. These include: the choice of oxidant doping molecule, the kinetics of the reaction (dictated by the temperature and pressure of the reactor), and the deposition time. These parameters have to be adjusted to ensure maximum conductivity, conformal coating of the textured silicon substrate, and a smooth homogeneous film with no pinholes. $VOCl_3$ was chosen as the oxidant molecule over $SbCl_5$ because it was expected to result in a more homogeneous coating on textured substrates due to a lower sticking coefficient as a lighter, lower vapor pressure molecule while providing a similar degree of oxidative doping. Hybrid PV devices were fabricated in the manner outlined previously using different reaction conditions. The cell architecture of these devices is shown in Figure 36.

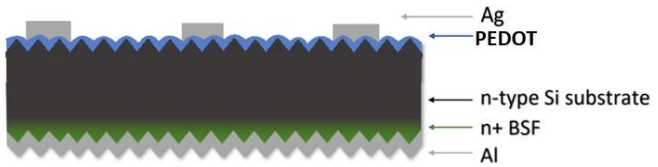

Figure 36. Schematic of hybrid PV device architecture.

The JV performance of the fabricated devices was measured under standard 1.5G standard illumination. Table 5 outlines the reaction conditions tested across five different samples. The JV results of the resulting devices are shown in Figure 37.

Table 5. oCVD reaction conditions and device results.

	Reactor pressure (mTorr)	Substrate Temperature (°C)	Reaction Time (min)	Efficiency (%)
A	1000	95	30	2.8
B	300	100	15	7.5
C	300	100	7	2.6
D	300	100	10	3.8
E	1000	110	20	8.2

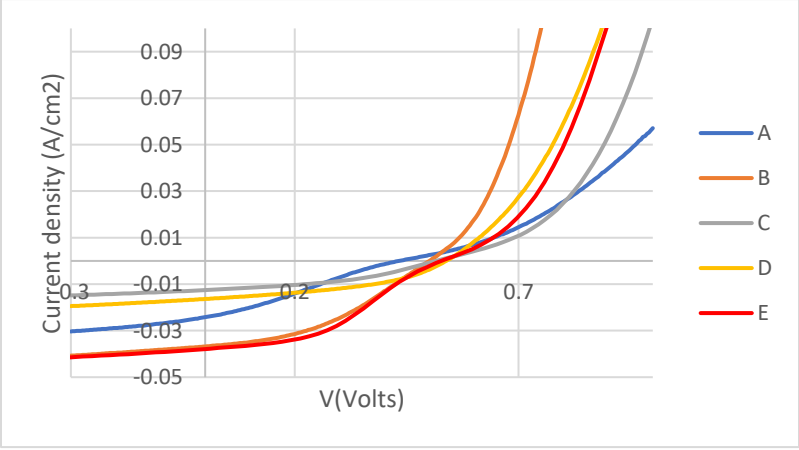

Figure 37. JV performance of hybrid PV devices fabricated via oCVD.

As can be seen from the resulting device efficiencies in Table 5, the highest performances were achieved with a reaction time of 15 and 20 minutes while maintaining the reactor pressure at 300 and 1000 mTorr and the substrate temperature at 100 and 110^{o}C respectively. These results suggest relatively slow reaction kinetics such that 15-20 minutes of reaction results in a thickness that maximizes the antireflective properties of the PEDOT film. It can also be seen that these high efficiency devices were fabricated at temperatures higher than the glass transition temperature of PEDOT (>100^{o}C) which results in films with superior conductivity as discussed by Heydari and colleagues [27]. It is also apparent from the results of the low efficiency devices that the optimization of the reaction conditions has to be a priority for future work.

8.2. Enhancement in Mechanical Resilience of Thin Silicon Substrates for Low Weight Flexible PV Modules

Our hybrid PV technology is an ideal platform to develop conformable and flexible solar cells. We have conducted preliminary studies showing the use of PEDOT:PSS significantly enhances the mechanical resilience of the silicon substrates. In these experiments 2x1 in^{2}-180 μm thick silicon substrates that had been previously HF-treated to produce a hydrophobic H-terminated surface were coated with different PEDOT:PSS formulations and subjected to a destructive 3-point bend test in a custom-made frame where the maximum load at failure was recorded. We tested 3 different surfactants which provide different levels of adhesion between the hydrophobic silicon surface and the PEDOT:PSS film. Figure 38 shows the results of this study along with still-frame images of uncoated and coated samples just before failure. The results of this preliminary mechanical test

suggest a significant improvement in the mechanical robustness of thin silicon substrates upon the addition of the PEDOT:PSS film. Furthermore, the quality of the adhesion between the film and the substrate is an important factor in the mechanical support provided by the film. These results have not been published and are considered proprietary. Going forward with this project we plan to test the mechanical resilience of our hybrid cells fabricated with oCVD deposition of PEDOT with different surface treatments and the protective coatings by testing the tensile strength of the samples via a 3-point bend test with a more advanced frame capable of controlling the load rate.

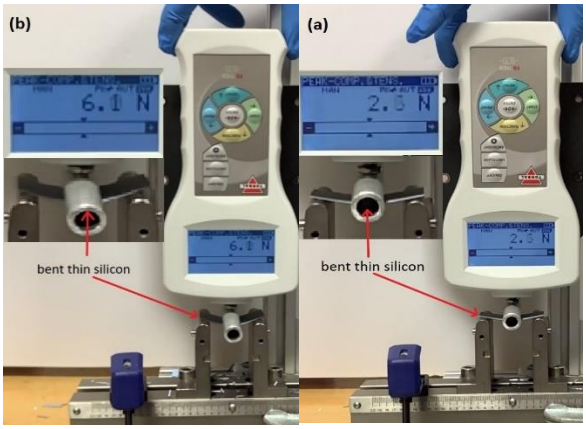

Figure 38. Still frame image of (a) uncoated silicon substrate (b) silicon substrate coated with 65nm PEDOT:PSS+0.25%Triton X moments before failure of the device.

Table 6. Maximum loads recorded at failure of different PEDOT:PSS and surfactant formulation.

(c)	Maximum load at failure (N)
uncoated	3.2-3.4-3.5
Triton X (high adhesion)	6.6-7.1
FS-34 (medium adhesion)	4.6-5.4
FS-30 (low adhesion)	4.1-4.6

8.3. Design of Flexible, Reliable, and 50% Lower Weight PV Modules Compatible With Floating Photovoltaic Deployment.

To capitalize on the opportunities presented by our thin-silicon hybrid HJT PV technology related to mechanically flexible and lower weight PV solutions, an appropriate module architecture consisting of a cell interconnection scheme and a protective packaging strategy must be employed. Our proposed module design builds on current commercially available silicon-based flexible modules. Despite the availability of these solutions, they remain an expensive specialized product due to the reliance on a thick solid copper back-contact for their mechanical resilience. The two key goals of the protective packaging in the context of our hybrid HJT technology are: (1) to prevent mechanical damage to the solar cells and (2) to prevent corrosion of the electrical contacts and organic materials. Figure 39 shows a schematic of our proposed module architecture and cell interconnection scheme.

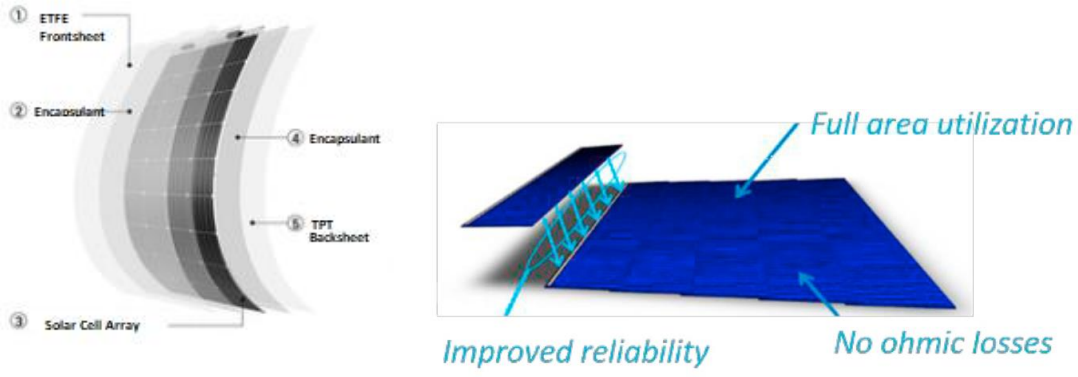

Figure 39. Schematic of the proposed protective packaging strategy (left) and cell interconnection scheme [87] (right).

The proposed protective packaging is composed of an ethylene tetrafluoroethylene (ETFE) transparent front sheet, a Tedlar-PET-Tedlar (TPT) white back sheet, the solar cell array, and the encapsulant material which will be tested as part of this project. The cells will be interconnected via a shingled module scheme, where cells are assembled in strings by connecting the front of a cell to the back of the next by means of an Electrically Conductive Adhesive (ECA). The strings are then connected in a series and parallel arrangement to match the typical I-V curve for the given size module. This cell interconnection approach has distinct advantages compared to traditional ribbon-connected strings including lower ohmic losses, better area utilization, lower processing temperature, lower operating temperature, and improved aesthetics. Furthermore, in the context of flexible modules the thin interconnecting ribbons are prone to fatigue failure which may result in complete module failure. Nevertheless, the mechanical performance of the ECA must be validated to minimize the risk of detachment, however due to the distribution of the contact along the cell width, the risk of complete detachment and module failure is reduced.

The third and final goal of this project is to apply a protective polymer encapsulation coating to ensure the durability of the devices under 85RH/85^{o}C accelerated aging environments. Although the use of the oCVD technique overcomes the two primary degradation mechanisms of these hybrid cells, the ingress of moisture and oxygen will result in the corrosive degradation of the devices. The encapsulation coating will prevent the ingress moisture and oxygen protecting the device from corrosion. Furthermore, the encapsulation coating will provide additional mechanical support and

scratch protection to the silicon substrate. Finally, the encapsulation coating will be environmentally friendly for use in FPV applications.

The protective encapsulation material must be tested and selected based on several properties:

1. the protective qualities of the film, measured by the ability to hinder the ingress of moisture and oxygen that would result in the corrosion of the PV device.
2. The mechanical structural support provided by the film to the device.
3. The optical properties of the film measured by the complex index of refraction to minimize parasitic absorption and optimize any antireflective effects.
4. The overall processing cost.

We will leverage the experience and technology of GVD Corporation to adapt their protective coating solutions to our hybrid solar cells. Notably, their proprietary SignalSeal coating has shown remarkable anti-corrosion potential under 1000 h of 85RH/85^{o}C accelerated aging on RF circuits, see Figure 40 provided by GVD.

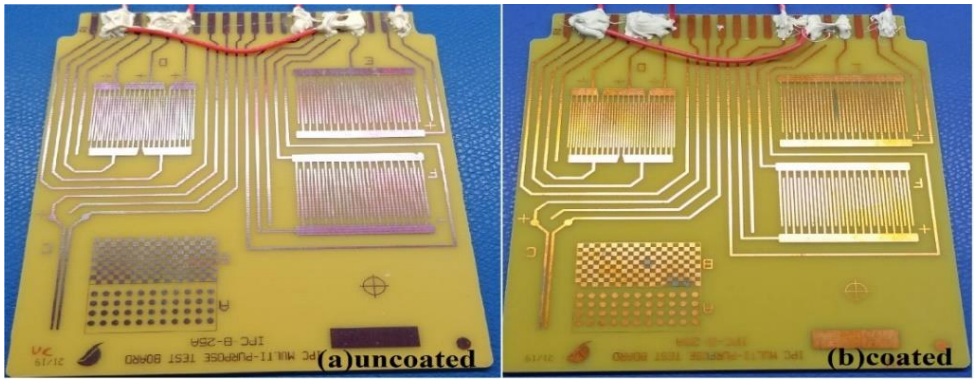

Figure 40. Results of 85RH/85ºC accelerated aging tests for 1000 h on RF circuits (a) with no protective coating (b) with GVD's proprietary SignalSeal protective coating treatment.

It is visually evident from the development of the opaque-maroon oxide on the corroded uncoated sample in Fig 40(a) vs the metallic reflective state of the coated circuitry in Fig 40(b) that the SignalSeal coating limited the corrosion of the printed circuits, which is also corroborated by their IV response. Furthermore, the coating is thin, transparent, and environmentally friendly. During this project we will assess the use of this, and other coatings provided by GVD in addition to commercially available alternatives for the encapsulation of our hybrid cells.

8.4. Design of FPV Solution Based on Hybrid Modules with Aerodynamic Mounting Schemes

In order to translate the lower weight and flexibility of our proposed module technology into a disruptive floating photovoltaic solution, a lower cost floating support structure with an aerodynamic mounting scheme must be optimized and fabricated in

accordance with the characteristics of the modules. To this end we have established a collaborative R&D relationship with Sun Edge, a Delaware based FPV designer and installer. Working in parallel to our R&D efforts, Sun Edge will design and fabricate an FPV structure that takes full advantage of the lighter weight and flexibility of our modules. A schematic cross-section of the proposed FPV concept structure to be optimized can be seen in Figure 41.

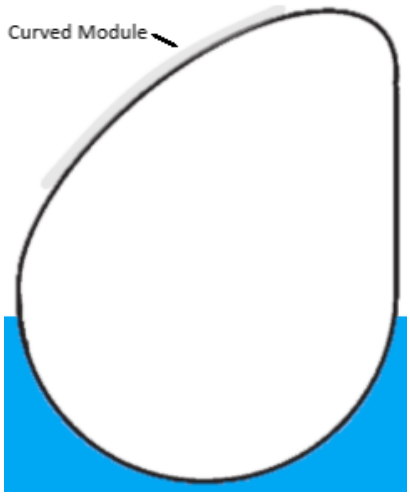

Figure 41. Cross-section of the proposed FPV structure concept.

The cross-section diagram in Figure 41 is shown as a simple illustration of the proposed integrated float-module structure. The base of the structure is a semi-circle with the waterline expected to lie just below where the base joins the rest of the structure. The front face where the module is mounted is an ellipse, inclined to 40º, which corresponds roughly to the latitude angle of the area where the system is expected to be deployed near Newark, DE. Elliptical cross-sections are very aerodynamically efficient, with a low drag coefficient which translates to lower wind loading. The ellipse joins a vertical line at its

tangent point, so that wind-driven air will flow over the top and start to flow smoothly downward behind the module. Although turbulence is expected behind the module, it will be less than for an inclined flat plate. The design work will be carried out by computational fluid dynamics and materials optimization methods, with the resulting structure being optimized for minimization of material costs, which will tend towards the aerodynamically optimal design.

Although currently we cannot make an accurate assessment of the costs savings related to the overall floating structure and installation, we estimate >50% savings on the float costs of the structure compared to the requirements for conventional mono-PERC modules. These savings consist of ~35% savings on raw materials and an additional >10% savings on labor, due to increased assembly automation being possible with lightweight thin-film modules. These savings are exclusive to the aerodynamic benefits and the lower weight of the proposed curved module structure, which permit lighter weight floating structures that will not need to bear as much wind or snow loads.

Chapter 9. ENTREPRENEURIAL JOURNEY AND TECHNO-ECONOMIC CONSIDERATIONS

SHIO LLC was founded with the goal of bridging the gap between the fundamental research conducted at the university and the commercialization of our hybrid HJT technology. In addition to continuous customer and market development we are actively working on the fabrication and commercialization strategies. At SHIO, we believe evolution rather than revolution as the path forward to commercializing this technology. Our business model focusses on disrupting this industry by de-risking the technology, establishing proof-of-concept, and building strategic partnerships and collaborations. Throughout the course of an eventual Phase II SBIR project we will address the challenges related to the fabrication facility design and the establishment of the pilot production plant. Our current focus is to deliver a high-value hybrid PV solution for FPV applications and leverage our industrial partner Sun Edge to help commercialize the technology in this market by providing a lower cost floating structure and installation services.

Table 7. CAPEX cost estimates for 10-year plant operation

	Fabrication Cost/W	
Process	Ref a-Si:H HIT	SHIO
Diffusion	0.02	
PECVD	0.02	
PECVD		
oCVD		0.02
TCO		
Metals	0.03	0.03
Module	0.01	0.01
Module	0.01	0.01
Module	0.01	0.01
Module		
Module	0.01	0.01
Diffusion	0.02	
PECVD	0.02	
oCVD		0.02
TCO		
Metals	0.03	0.01
Module	0.04	0.04
$/W	0.024	0.015
	% CAPEX savings	36.95

An important aspect of the value proposition of our hybrid HJT PV technology is the lower cost of fabrication compared to the commercial PV technologies. We have conducted preliminary techno-economic analysis of our hybrid technology that has suggested our process will have 37% lower capital expenditure costs (CAPEX) than comparable silicon heterojunction technologies (a-Si:H HIT). Conventional solar cells rely on high temperature and high vacuum-based processing. At SHIO, we are disrupting the PV cell manufacturing environment by eliminating the requirement for CAPEX intensive, high-vacuum based equipment like diffusion furnaces and PECVD chambers and replacing them with an oCVD tool with low-temperature and low-vacuum requirements. Based on our customer discovery and reports from Louwen and colleagues [88], for a 3600 wafer/hour production line, the tools our process would replace when compared to traditional diffused junction cells are: diffusion furnaces ($3 million) and PECVD tools for silicon nitride ($3 million). When compared with SHJ, our process would replace even

more PECVD tools which are needed for the amorphous silicon deposition that amount to an estimated cost of about $11 million. This is nearly the cost of a whole diffuse junction line (~$12.5 million) whereas the cost of a whole SHJ line is estimated to be about $28 million [88]. A fully-functional oCVD tool capable of coating ~6" substrates has an estimated cost between $275,000 and $325,000, as quoted by GVD. These oCVD tools have a lifetime of at least 10 years with > 90% uptime and very low operational costs (<$100K over lifetime). Translating costs incurred by the oCVD process to a cell fabrication facility for its entire lifetime assuming a throughput of 3600 wafers/hour, cleanroom cost of 200$/$m^2$/yr, industry standard labor costs and economic input parameters (with straight line depreciation rate of 8% and average tool uptime over 90%), we predict CAPEX savings of 37% compared to a standard a-Si:H HIT line as seen in Table 1. We are currently in the process of completing more thorough models for the levelized cost of energy (LCOE) and balance of systems cost (BOS) of our hybrid technology for FPV applications under the advisement of the national renewable energy laboratory (NREL), an effort that will continue for the duration of this project and that will be updated regularly based on our ongoing technological accomplishments. Nevertheless, it is worth mentioning that silicon is the largest single cost-component of a module and over half of total module cost [89].

Along with technological development, our vision is for all-American PV manufacturing with job creation. There are more stories of bankruptcies in the field of solar in the USA than success stories. From 2012 to 2016, nearly 30 US based manufacturers were forced to shut their doors, casting off hundreds of technicians, process engineers and

R&D scientists. Considering that the U.S. solar market is booming, there is a serious and urgent need for domestic manufacturing. The USA has always been a leader in the PV industry but has not been successful in maintaining manufacturing jobs domestically which has jeopardized the overall competitiveness and energy security of the nation. The scalability of the oCVD process, its compatibility with continuous production lines, the expertise of the American tool manufacturers in this area, and the flexibility provided by the lower upfront investment makes the development of an American fabrication facility a reasonable aspiration. We believe we have the necessary team, experience, and technology to help return to an all-American manufacturing PV economy.

Over the next five years SHIO will bring its novel FPV solution to market and generate revenue. To do this the company must complete research and development on the product. With proof of concept the company will raise the capital necessary to begin production of the module for. Beyond our immediate focus on the FPV market, we aim to address other emerging markets such as agrivoltaics, building integrated PV, UAVs, wearables, and remote IOT devices in the future.

9.1. Entrepreneurial Efforts

During our customer development work in the various I-Corps programs and independently, we have identified several market opportunities that would benefit from the versatile form factor, low weight, and lower cost of our hybrid PV technology. Of particular interest at this stage of the project is the market for floating photovoltaic installations (FPV). With nearly 3 quarters of our planet covered with water, it is

astonishing that leveraging the space of water masses has not historically been a focus for photovoltaics.

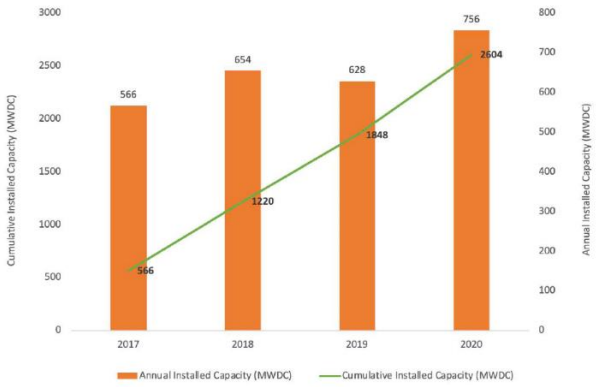

Figure 42. Annual global FPV capacity, 2017-2020 [90].

PV generation has grown rapidly over the past decade and is expected to continue this trend over the next couple of decades. This rapid growth will, and is already, putting pressure on land use, particularly in locations where land is relatively scarce and expensive. FPV has gained popularity very recently as an attractive solution to the competing land use problem of solar PV generation, growing worldwide from less than 1MW in 2007 to approximately 2.6 GW of installed power in 2020. Figure 42 shows the growth trend of FPV installations within the last four years. In the US FPV deployment has lagged compared to the Asian markets (which hold 90% of the global installed capacity) with only two FPV installations before 2016 to more than 20 by the end of 2020 [91]. A recent study published by the National Renewable Energy Laboratory (NREL) showed that if only 27% of the surface area of the suitable 24,419 water bodies in the US were to be covered in FPV systems, they would generate approximately 10% of the nation's energy need. This translates to a potential of roughly 11,090 MW of solar power [92]. Given the relative

newness of this approach to PV and the conservative nature of this market all the current FPV installations are using conventional utility-grade panels (Chinese PERC mono crystalline panels being the most popular choice) with innovations occurring on the floating support structure design and installation. Given the current state of FPV, there is tremendous opportunity for innovation and disruption.

More broadly, FPV installations have a symbiotic relationship with water management and electricity generation. Solar modules operate more efficiently at lower temperatures produce. The proximity of the modules to the water in FPV structures has a cooling effect increasing the amount of electricity the modules produce. At the same time, the installation shades the body of water, which reduces evaporation and slows the growth of algae. As noted by WaterWorld Magazine, "shading can reduce the evaporation rate by up to 70%. Therefore, a 3-acre pond covered with FPV could save over 4 million gallons of water each year. The shading effect can also improve water quality. As water bodies are exposed to the sun, photosynthesis promotes growth of organic matter, including algae. By shading the water, algae growth is reduced, minimizing the associated treatment and labor costs." [93] The shade from the solar modules also improves the habitat for fish and birds.

Our hybrid PV technology offers a competitive value proposition for FPV applications by replacing the heavy glass-protected conventional modules whose high weight is currently a pain point for this industry. By employing thin silicon substrates, an organic carrier selective contact, and a polymer protective coating our modules will be 67% lighter than traditional technologies. This decrease in module weight translates

directly into cost savings related to the requirements of the floating structure and its installation. Furthermore, traditional commercial solar modules are rigid and prone to cracking from mechanical stress. Although many bodies of water are calm, the constant and unpredictable stresses coupled with occasional bad weather significantly reduce the lifetime of the modules and negatively impact the energy yields in the long term as different components of the module fail and degrade. The robust mechanical properties of our hybrid cells provided by the polymer films will reduce the risk of mechanical failure. Additionally, all the materials employed in our cells are environmentally friendly, which enables their deployment on potable water reservoirs. This market remains mostly untapped despite the pressing need to shade the reservoirs to prevent evaporation, particularly in the American southwest where droughts are becoming an increasingly urgent problem. FPV represent a valuable strategy to address this issue, however, concerns with the contamination of the water supply have hindered the growth of this market.

Our technology will also enable us to fabricate cost-competitive flexible solar cells for a wide array of applications. The global flexible solar panel market is valued at 483.8 million USD in 2020 and is expected to reach 884.4 million USD by the end of 2026, growing at a compound annual rate of +8.9% during 2020-2028 [94]. Due to the growth of the Internet of Things (IOT) and Flexible Hybrid Electronics (FHE) industries, novel PV technologies such as all-organic cells, previously deemed unsuitable for other applications due to their low efficiencies (8-16%), have found niche applications where their value proposition is competitive [95]. Technically, the work on this proposal

provides a pathway for conformal silicon technology, beyond photovoltaic. The FHE industry represent the next generation of electronics and is expected to continue to grow significantly in the coming years.

On a broader scale, the fabrication of current commercial PV solutions remains a capital and carbon intensive non-renewable process. Our hybrid PV technology addresses these concerns in three ways: First, the organic material feedstock is abundant and of low cost. Second, the processing required for fabrication occurs at much lower temperatures and milder vacuums, reducing the overall energy requirements and associated cost. Lastly, a circular economy may be established for these hybrid solar cells. After reaching the end of its life a hybrid cell may be easily stripped of the organic coatings, the metal contacts salvaged, and the silicon substrate re-processed with fresh polymer coatings for the fabrication of new cells. Being able to recycle the hybrid cells will further reduce the cost of the material feedstock and contribute to the overall sustainability of solar PV. Furthermore, the chosen processing techniques are highly scalable and compatible with continuous processing lines

9.2. Intellectual Property (IP) Landscape

In terms of the IP landscape relevant to our commercial ambitions there are four major components: (i) the oCVD deposition of highly conductive PEDOT, (ii) the encapsulation and protection strategy, (iii) the silicon surface passivation, (iv) and the panel assembly. With regards to each of them:

i. The US patent 9,793,479 “methods for fabricating devices including photovoltaic devices” expiring in 2035 and held by the Massachusetts Institute of Technology is relevant to our technology as it claims the process of utilizing oCVD for the fabrication of PV devices. Fortunately, the MIT Technology Licensing Office is very experienced with and open to licensing IP to early-stage startup companies, with licensing terms that reflect the substantial investment of time and money on product development. Nevertheless, the licensing negotiations would be more successful at a later stage of development once we can demonstrate the commercial feasibility of our technology as a result of this PFI project.

ii. Our proposed encapsulation strategy is based on the proprietary technology of GVD corporation, an MIT spin-off out of the same lab that filed the aforementioned patent. We have developed a good working relationship with GVD throughout the course of the year and they have expressed their interest in the success of this project. Upon successful completion of this PFI project we plan to engage in negotiations regarding exclusivity of use of their encapsulation solution for PV applications.

iii. The US patent 8,114,785 “electrical passivation of silicon-containing surfaces using organic layers” which expired in 2019 is relevant to our technology as it relates to the patentability of our proposed passivation treatment. We have advanced talks with the UD Office of Economic Innovation and Partnerships (OEIP) to decide the best path forward for the

IP protection of this aspect of our technology. In the meantime, all the details of this process are being treated as proprietary trade secrets with the use of appropriate NDA agreements for any disclosure events.

iv. As per our discussions with OEIP the panel assembly and/or some of the details regarding the method of fabrication could be candidates for patent protection at a later stage of development.

9.3. Competing Technology Assessment

In terms of PV technology alternatives that may be relevant for comparison it is important to consider the larger landscape that dictates decision-making for deployment of FPV projects, particularly in regard to the environmental-health/safety-economic considerations. For the purposes of identifying relevant competing PV technologies for use in FPV it is important to consider two groups: commercially established and emerging. Among the commercially established technologies are: (i) traditional crystalline silicon (earlier assessment), (ii) high performance crystalline silicon cells (such as Sunpower's IBC technology and Panasonic's a-Si:H HIT), and (iii) thin films (CdTe, CIGS, and GaAs). Among the emerging technologies are: (iv) all-organic PV, and (v) perovskites. With respect to each of these:

i. It is very challenging to adapt traditional crystalline silicon PV technologies to lightweight flexible module packages. The most recent effort we were able to identify was of modules being designed for vehicle integrated PV in Korea [96]. In this work the glass layer is being replaced

with a polymer film (acrylic, PMMA, and polycarbonate) and additional lightweight composite load bearing structures which is claimed to result in weight reductions of approximately 50% compared to the traditional glass protected modules. However, the authors acknowledge that so far, the module designs have insufficient mechanical properties and have not passed the relevant industry standard (IEC61215). Nevertheless, our proposed module design is competitive, or slightly lighter than the approaches described in this paper due to their need to include additional load-bearing material in their module design.

ii. High performance crystalline silicon technologies have advanced significantly in recent years, with a record cell performance of 26.7%. Nevertheless, given the fragility of silicon the mechanical resilience of the device continues to be an issue for development of lightweight flexible modules. A notable product comparable to our proposed technology already available in the market is the flexible module offered by SunPower. The technology employed by SunPower employs an integrated back contact (IBC) scheme with a “thick solid copper foundation” that provides “massive strength” to thin silicon cells which allowed them to develop this product. Recent work performed in Poland utilized this technology to evaluate its use in residential applications on aged buildings with lower roof load bearing standards [97]. Given the proprietary nature of their technology we cannot make an accurate assessment of the weight

savings our proposed strategy would provide, however the omission of a thick solid copper foundation will certainly result in significant weight savings at a module level. Furthermore, their IBC technology is notably expensive which makes the value proposition case for FPV applications harder to make. Additionally, there would be concerns of copper leeching into the body of water.

iii. Although recent advancements in the field of thin films have resulted in a significant growth of this industry, there is a major drawback of their use in FPV applications: the constituent materials of these cells pose a significant risk of contaminating the body of water. Some of the materials such as cadmium and gallium are carcinogenic and toxic while metals such as copper can cause long-term exposure disease. Our proposed modules will be completely non-toxic and environmentally friendly, therefore while thin film technologies might be light-weight and in some cases flexible they are not competitive in the FPV field.

iv. All-organic PV technologies have improved significantly in recent years and could represent the biggest risk to our technology in the long-term. Nevertheless, this technology remains at a stage where the commercially available products are not competitive from a conversion efficiency standpoint.

v. As is the case for thin-film technologies, the risk of contaminating the body of water with toxic substances would likely make this technology not competitive in the FPV market.

9.4. Techno-Economic Analysis and Value Proposition in Floating PV applications

According to the latest NREL report on the economics of FPV installations "Floating Photovoltaic System Cost Benchmark: Q1 2021 Installations on Artificial Water Bodies," [90] the floating structure is the single highest cost component of the structural balance of system (SBOS) costs of an FPV project (accounting for 75%-85% of the SBOS) and the primary driver behind a $0.26/W cost premium compared to ground-mounted installations ($1.29/W vs $1.03/W). The reports states that the cost of floats in the US varies between $0.2/W and $0.9/W depending on the manufacturer and the size of the project for Mono PERC modules (19% efficiency). Furthermore, a sensitivity analysis performed on the cost model shows that the float cost, wind load, and snow load are the three most influential factors. The two latter factors directly influencing the number of floats and anchoring lines required. The figure below shows the results of the sensitivity analysis.

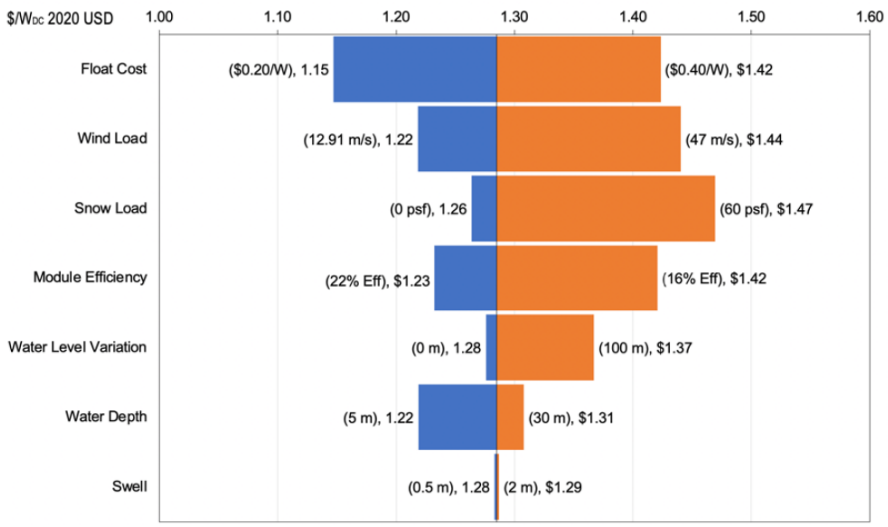

Figure 43. Sensitivity of FPV installed system cost to varying input assumptions [90].

As can be seen in the figure, a 50% reduction in float costs results in $0.27/W reduction in total costs. Going beyond the savings in float cost directly related to the lighter weight of our proposed technology, the flexibility of the modules will allow for innovative aerodynamic mounting schemes to reduce the wind and snow loads on the structure further decreasing the buoyancy requirements of the structure and therefore the number of additional floats needed. We acknowledge the significance of the business opportunity related to savings on the floating support structure cost as it relates directly to our proposed value proposition which is why we have established a collaborative relationship with our commercialization partner Sun Edge (a Delaware based FPV installer) so that they may design the floating and mounting schemes to take full advantage of our proposed module technology in parallel to our R&D activities. As mentioned earlier, we are actively working with the support of NREL to develop a direct cost as well as an LCOE and BOS costs models for the use of our technology in FPV

applications. Although currently we cannot make an accurate assessment of the costs savings related to the overall floating structure and installation, we estimate >50% savings on the float costs of the structure compared to the requirements for conventional mono PERC modules.

Having outlined our proposed module strategy it is important to clearly highlight the value proposition of the hybrid HJT modules for FPV applications: **Solar modules based on our hybrid HJT technology are at least 50% lower in weight than the currently used glass-covered high efficiency silicon modules and are mechanically flexible which allows for aerodynamic mounting on FPV structures. This translates to significant cost savings related to the float requirements and associated cost of the floating structure.** Furthermore, these modules will be fabricated at a much lower cost than modules based on traditional HJT cells and will deliver high efficiency (>20% conversion efficiency) at long lifetime (>95% of the initial power rating after 1000 hours of 85RH/85^{o}C accelerated aging).

PERMISSIONS

Effects of Co-Solvents on the Performance of PEDOT:PSS Films and Hybrid Photovoltaic Devices

Role of oxide at interface between organic layer and silicon substrate in hybrid solar cells

Licensee:	Mr. David Angel Trujillo
Order Date:	Jul 19, 2022
Order Number:	5352621230099
Publication:	Journal of Materials Research
Title:	Role of oxide at interface between organic layer and silicon substrate in hybrid solar cells
Type of Use:	Thesis/Dissertation

SPRINGER NATURE LICENSE
TERMS AND CONDITIONS

Feb 26, 2024

This Agreement between Mr. David Angel Trujillo ("You") and Springer Nature ("Springer Nature") consists of your license details and the terms and conditions provided by Springer Nature and Copyright Clearance Center.

License Number	5352621230099
License date	Jul 19, 2022
Licensed Content Publisher	Springer Nature
Licensed Content Publication	Journal of Materials Research
Licensed Content Title	Role of oxide at interface between organic layer and silicon substrate in hybrid solar cells
Licensed Content Author	David A. Angel Trujillo et al
Licensed Content Date	Jan 19, 2021
Type of Use	Thesis/Dissertation
Requestor type	academic/university or research institute
Format	electronic
Portion	full article/chapter
Will you be translating?	no

Circulation/distribution	1 - 29
Author of this Springer Nature content	yes
Title	Interfacial Engineering of Hybrid Heterojunction PV Devices for the Next Generation Lightweight, Flexible, and Low-Cost Solar Modules.
Institution name	University of Delaware
Expected presentation date	Oct 2022
Requestor Location	Mr. David Angel Trujillo 153 Courtney st NEWARK, DE 19711 United States Attn: University of Delaware
Total	0.00 USD

REFERENCES

[1] U. Nations, “United Nations Meetings Coverage and Press Releases,” 2015. .

[2] G. Meller and T. Grasser, *Organic Electronics*, vol. 91, no. 5. Springer Berlin Heidelberg, 2010.

[3] “New Design Strategy Pushes Organic Photovoltaics Past 18% Efficiency.” [Online]. Available: https://www.nrel.gov/news/program/2021/new-design-strategy-increases-organic-pv-efficiency.html?fbclid=IwAR1GsNzMjO1_W_f8geoAL5P2OvHaHpx6TWp_SCS6Ma3hWmOQTfGSPUc8-DA.

[4] A. Elschner, F. Jonas, S. Kirchmeyer, and W. Lövenich, “29.2: Invited Paper: PEDOT-Based Layers for TCO-Substitution and Hole-Injection,” *SID Symposium Digest of Technical Papers*, vol. 39, no. 1, p. 407, 2008, doi: 10.1889/1.3069683.

[5] B. Gil, A. J. Yun, Y. Lee, J. Kim, B. Lee, and B. Park, “Recent Progress in Inorganic Hole Transport Materials for Efficient and Stable Perovskite Solar Cells,” *Electronic Materials Letters*, vol. 15, no. 5, pp. 505–524, 2019, doi: 10.1007/s13391-019-00163-6.

[6] S. Kirchmeyer, A. Elschner, and and K. Reuter, *Pedot:Principles and Applications of an Intrinsically Conductive Polymer*. 2010.

[7] J. Rivnay, S. Inal, B. A. Collins, M. Sessolo, E. Stavrinidou, X. Strakosas, C. Tassone, D. M. Delongchamp, and G. G. Malliaras, “Structural control of mixed ionic and electronic transport in conducting polymers,” *Nature Communications*, vol. 7, pp. 1–9, 2016, doi: 10.1038/ncomms11287.

[8] S. Jäckle, M. Mattiza, M. Liebhaber, G. Brönstrup, M. Rommel, K. Lips, and S. Christiansen, “Junction formation and current transport mechanisms in hybrid n-Si/PEDOT:PSS solar cells,” *Scientific Reports*, vol. 5, pp. 1–12, 2015, doi: 10.1038/srep13008.

[9] S. Jäckle, M. Liebhaber, C. Gersmann, M. Mews, K. Jäger, S. Christiansen, and K. Lips, “Potential of PEDOT:PSS as a hole selective front contact for silicon heterojunction solar cells,” *Scientific Reports*, vol. 7, no. 1, pp. 1–8, 2017, doi: 10.1038/s41598-017-01946-3.

[10] A. Iyer, “UNDERSTANDING AND OPTIMIZING THE PERFORMANCES OF PEDOT:PSS BASED HETEROJUNCTION SOLAR CELLS,” University of Delaware, 2021.

[11] D. H. Macdonald, A. Cuevas, M. J. Kerr, C. Samundsett, D. Ruby, S. Winderbaum, and A. Leo, “Texturing industrial multicrystalline silicon solar cells,” *Solar Energy*, vol. 76, no. 1–3, pp. 277–283, 2004, doi: 10.1016/j.solener.2003.08.019.

[12] H. Seidel, L. Csepregi, A. Heuberger, and H. Baumgärtel, “Anisotropic Etching of Crystalline Silicon in Alkaline Solutions: II . Influence of Dopants,” *Journal of The Electrochemical Society*, vol. 137, no. 11, pp. 3626–3632, 1990, doi: 10.1149/1.2086278.

[13] “p-n junctions.” [Online]. Available: https://en.wikipedia.org/wiki/P–n_junction.

[14] S. Shen, J. Zhang, S. Zhou, Y. Han, P. Gao, B. Sun, N. Zhao, and C. P. Wong, “Nanostructured Silicon-Based Heterojunction Solar Cells with Double Hole-Transporting Layers,” *Advanced Electronic Materials*, vol. 5, no. 2, pp. 1–6, 2019, doi: 10.1002/aelm.201800070.

[15] J. P. Thomas and K. T. Leung, “Defect-minimized PEDOT:PSS/planar-si solar cell with very high efficiency,” *Advanced Functional Materials*, vol. 24, no. 31, pp. 4978–4985, 2014, doi: 10.1002/adfm.201400380.

[16] D. Zielke, A. Pazidis, F. Werner, and J. Schmidt, “Organic-silicon heterojunction solar cells on n-type silicon wafers: The BackPEDOT concept,” *Solar Energy Materials and Solar Cells*, vol. 131, pp. 110–116, 2014, doi: 10.1016/j.solmat.2014.05.022.

[17] J. Y. Kim, J. H. Jung, D. E. Lee, and J. Joo, “Enhancement of electrical conductivity of poly(3, 4-ethylenedioxythiophene)/poly(4-styrenesulfonate) by a change of solvents,” *Synthetic Metals*, vol. 126, no. 2–3, pp. 311–316, 2002, doi: 10.1016/S0379-6779(01)00576-8.

[18] X. Jiang, P. Zhang, J. Zhang, J. Wang, G. Li, X. Fang, L. Yang, and X. Chen, “High Performance of PEDOT:PSS/n-Si Solar Cells Based on Textured Surface with AgNWs Electrodes,” *Nanoscale Research Letters*, vol. 13, 2018, doi: 10.1186/s11671-018-2462-0.

[19] S. Jäckle, M. Liebhaber, J. Niederhausen, M. Büchele, R. Félix, R. G. Wilks, M. Bär, K. Lips, and S. Christiansen, “Unveiling the Hybrid n-Si/PEDOT:PSS Interface,” *ACS Applied Materials and Interfaces*, vol. 8, no. 13, pp. 8841–8848, 2016, doi: 10.1021/acsami.6b01596.

[20] M. Pietsch, M. Y. Bashouti, and S. Christiansen, “The role of hole transport in hybrid inorganic/organic silicon/poly(3,4- ethylenedioxy-thiophene):poly(styrenesulfonate) heterojunction solar cells,” *Journal of Physical Chemistry C*, vol. 117, no. 18, pp. 9049–9055, 2013, doi: 10.1021/jp308349f.

[21] A. Iyer, J. Hack, D. A. A. Trujillo, B. Tew, J. Zide, and R. Opila, “Effects of co-solvents on the performance of PEDOT: PSS Films and hybrid photovoltaic devices,” *Applied Sciences (Switzerland)*, vol. 8, no. 11, pp. 1–12, 2018, doi: 10.3390/app8112052.

[22] J. P. Thomas, L. Zhao, D. McGillivray, and K. T. Leung, “High-efficiency hybrid solar cells by nanostructural modification in PEDOT:PSS with co-solvent

addition," *Journal of Materials Chemistry A*, vol. 2, no. 7, pp. 2383–2389, 2014, doi: 10.1039/c3ta14590e.

[23] H. Hoppe, N. S. Sariciftci, and D. Meissner, "Optical constants of conjugated polymer/fullerene based bulk-heterojunction organic solar cells," *Molecular Crystals and Liquid Crystals*, vol. 385, no. 1, pp. 113–119, 2002, doi: 10.1080/713738799.

[24] "OPAL 2." https://www2.pvlighthouse.com.au/calculators/opal 2/opal 2.aspx.

[25] R. Varache, C. Leendertz, M. E. Gueunier-Farret, J. Haschke, D. Muñoz, and L. Korte, "Investigation of selective junctions using a newly developed tunnel current model for solar cell applications," *Solar Energy Materials and Solar Cells*, vol. 141, pp. 14–23, 2015, doi: 10.1016/j.solmat.2015.05.014.

[26] J. R. Reynolds, B. C. Thompson, T. A. Skotheim, N. Kim, I. Petsagkourakis, S. Chen, M. Berggren, X. Crispin, M. P. Jonsson, and I. Zozoulenko, *Electric Transport Properties in PEDOT Thin Films*. 2019.

[27] M. Heydari Gharahcheshmeh, M. T. Robinson, E. F. Gleason, and K. K. Gleason, "Optimizing the Optoelectronic Properties of Face-On Oriented Poly(3,4-Ethylenedioxythiophene) via Water-Assisted Oxidative Chemical Vapor Deposition," *Advanced Functional Materials*, vol. 2008712, pp. 1–12, 2020, doi: 10.1002/adfm.202008712.

[28] M. Chen, J. H. Hack, A. Iyer, K. J. Jones, and R. L. Opila, "Radical-driven silicon surface passivation by benzoquinone- and hydroquinone-methanol and photoinitiators," *Journal of Physical Chemistry C*, vol. 121, no. 39, pp. 21364–21373, 2017, doi: 10.1021/acs.jpcc.7b05686.

[29] L. He, C. Jiang, H. Wang, H. Lei, D. Lai, and Rusli, "11.3% efficient planar Si-PEDOT: PSS hybrid solar cell with a thin interfacial oxide," *Conference Record of the IEEE Photovoltaic Specialists Conference*, pp. 2785–2787, 2012, doi: 10.1109/PVSC.2012.6318170.

[30] L. He, C. Jiang, H. Wang, D. Lai, and Rusli, "High efficiency planar Si/organic heterojunction hybrid solar cells," *Applied Physics Letters*, vol. 100, no. 7, pp. 1–4, 2012, doi: 10.1063/1.3684872.

[31] S. Avasthi, S. Lee, Y. L. Loo, and J. C. Sturm, "Role of majority and minority carrier barriers silicon/organic hybrid heterojunction solar cells," *Advanced Materials*, vol. 23, no. 48, pp. 5762–5766, 2011, doi: 10.1002/adma.201102712.

[32] N. A. Kotulak, "DEVELOPING NOVEL HYBRID HETEROJUNCTIONS FOR HIGH EFFICIENCY PHOTOVOLTAICS by," 2014.

[33] M. Taguchi, A. Yano, S. Tohoda, K. Matsuyama, Y. Nakamura, T. Nishiwaki, K. Fujita, and E. Maruyama, "24.7% Record efficiency HIT solar cell on thin silicon

wafer," *IEEE Journal of Photovoltaics*, vol. 4, no. 1, pp. 96–99, 2014, doi: 10.1109/JPHOTOV.2013.2282737.

[34] S. S. Yoon and D. Y. Khang, "High Efficiency (>17%) Si-Organic Hybrid Solar Cells by Simultaneous Structural, Electrical, and Interfacial Engineering via Low-Temperature Processes," *Advanced Energy Materials*, vol. 8, no. 9, pp. 1–8, 2018, doi: 10.1002/aenm.201702655.

[35] D. Zielke, C. Niehaves, W. Lövenich, A. Elschner, M. Hörteis, and J. Schmidt, "Organic-silicon Solar Cells Exceeding 20% Efficiency," *Energy Procedia*, vol. 77, pp. 331–339, 2015, doi: 10.1016/j.egypro.2015.07.047.

[36] "PV Lighthouse Online Calculator." https://www2.pvlighthouse.com.au/calculators/Grid calculator/Grid calculator.aspx.

[37] J. Sheng, K. Fan, D. Wang, C. Han, J. Fang, P. Gao, and J. Ye, "Improvement of the SiOx passivation layer for high-efficiency Si/PEDOT: PSS heterojunction solar cells," *ACS Applied Materials and Interfaces*, vol. 6, no. 18, pp. 16027–16034, 2014, doi: 10.1021/am503949g.

[38] R. Shen, Z. Sun, Y. Shi, Y. Zhou, W. Guo, Y. Zhou, H. Yan, and F. Liu, "Solution Processed Organic/Silicon Nanowires Hybrid Heterojunction Solar Cells Using Organosilane Incorporated Poly(3,4-ethylenedioxythiophene):Poly(styrenesulfonate) as Hole Transport Layers," *ACS Nano*, vol. 15, no. 4, pp. 6296–6304, 2021, doi: 10.1021/acsnano.0c10526.

[39] M. U. Halbich, D. Zielke, R. Gogolin, R. Sauer-Stieglitz, W. Lövenich, and J. Schmidt, "Improved surface passivation and reduced parasitic absorption in PEDOT:PSS/c-Si heterojunction solar cells through the admixture of sorbitol," *Scientific Reports*, vol. 9, no. 1, pp. 1–8, 2019, doi: 10.1038/s41598-019-46280-y.

[40] D. Zielke, A. Pazidis, F. Werner, and J. Schmidt, "Organic-silicon heterojunction solar cells on n-type silicon wafers: The BackPEDOT concept," *Solar Energy Materials and Solar Cells*, vol. 131, pp. 110–116, 2014, doi: 10.1016/j.solmat.2014.05.022.

[41] N. Amin, S. Santhiran, N. M. Kassim, A. A. Alkahtani, M. A. Islam, and M. Y. Mohd Yusof, "Impact Analysis of Metallization Design and Recombination Losses on Performance of Crystalline Silicon Solar Cells," *Energies*, vol. 16, no. 18, 2023, doi: 10.3390/en16186505.

[42] S. Mahato, L. G. Gerling, C. Voz, R. Alcubilla, and J. Puigdollers, "PEDOT:PSS as an Alternative Hole Selective Contact for ITO-Free Hybrid Crystalline Silicon Solar Cell," *IEEE Journal of Photovoltaics*, vol. 6, no. 4, pp. 934–939, 2016, doi: 10.1109/JPHOTOV.2016.2557072.

[43] D. K. SCHRODER, *Semiconductor material and device characterization*. 2005.

[44] T. Zhang, S. Iqbal, X. Y. Zhang, W. Wu, D. Su, and H. L. Zhou, “Recent advances in highly efficient organic-silicon hybrid solar cells,” *Solar Energy Materials and Solar Cells*, vol. 204, Jan. 2020, doi: 10.1016/j.solmat.2019.110245.

[45] P. Balding, R. Cueto, P. S. Russo, and W. R. Gutekunst, “Synthesis of perfectly sulfonated sodium polystyrene sulfonate over a wide molar mass range via reversible-deactivation radical polymerization,” *Journal of Polymer Science, Part A: Polymer Chemistry*, vol. 57, no. 14, pp. 1527–1537, 2019, doi: 10.1002/pola.29415.

[46] A. R. Moosavi-Zare, M. A. Zolfigol, and E. Noroozizadeh, “Regioselective Sulfonation of Aromatic Compounds over 1,3-Disulfonic Acid Imidazolium Chloride under Aqueous Media,” *Synlett*, vol. 27, no. 11, pp. 1682–1684, 2016, doi: 10.1055/s-0035-1561938.

[47] M. E. SantosMiranda, C. Marcolla, C. A. Rodriguez, H. M. Wilhelm, M. R. Sierakowski, T. M. BelleBresolin, and R. Alves de Freitas, “I . The role of N-carboxymethylation of chitosan in the thermal stability and dynamic,” *Polym Int*, vol. 55, no. December 2005, pp. 961–969, 2006, doi: 10.1002/pi.

[48] D. A. Angel Trujillo, A. Iyer, J. Hack, and R. L. Opila, “Role of oxide at interface between organic layer and silicon substrate in hybrid solar cells,” *Journal of Materials Research*, 2021, [Online]. Available: https://link.springer.com/article/10.1557/s43578-020-00049-6.

[49] R. Saive, “S-Shaped Current – Voltage Characteristics in Solar Cells : A Review,” no. 2, pp. 1–8.

[50] U. Das, S. Hegedus, L. Zhang, J. Appel, J. Rand, and R. Birkmire, “Investigation of hetero-interface and junction properties in silicon heterojunction solar cells,” *Conference Record of the IEEE Photovoltaic Specialists Conference*, pp. 1358–1362, 2010, doi: 10.1109/PVSC.2010.5614372.

[51] J. P. Thomas, L. Zhao, M. Abd-Ellah, N. F. Heinig, and K. T. Leung, “Interfacial micropore defect formation in PEDOT:PSS-Si hybrid solar cells probed by TOF-SIMS 3D chemical imaging,” *Analytical Chemistry*, vol. 85, no. 14, pp. 6840–6845, 2013, doi: 10.1021/ac401084x.

[52] J. Schmidt, V. Titova, and D. Zielke, “Organic-silicon heterojunction solar cells: Open-circuit voltage potential and stability,” *Applied Physics Letters*, vol. 103, no. 18, pp. 1–5, 2013, doi: 10.1063/1.4827303.

[53] M. Junghanns, J. Plentz, G. Andrä, A. Gawlik, I. Höger, and F. Falk, “PEDOT:PSS emitters on multicrystalline silicon thin-film absorbers for hybrid solar cells,” *Applied Physics Letters*, vol. 106, no. 8, pp. 18–21, 2015, doi: 10.1063/1.4913869.

[54] S. M. A. Durrani, M. F. Al-Kuhaili, and E. E. Khawaja, “Characterization of thin

films of a-SiOx ($1.1 < x < 2.0$) prepared by reactive evaporation of SiO," *Journal of Physics Condensed Matter*, vol. 15, no. 47, pp. 8123–8135, 2003, doi: 10.1088/0953-8984/15/47/015.

[55] H. Niimi, H. Yang, G. Lucovsky, J. W. Keister, and J. E. Rowe, "Barrier layer model determined by XPS data for tunneling current reductions at monolayer nitrided Si-SiO2 interfaces," *Applied Surface Science*, vol. 166, no. 1, pp. 485–491, 2000, doi: 10.1016/S0169-4332(00)00480-3.

[56] N. Koch, A. Vollmer, and A. Elschner, "Influence of water on the work function of conducting poly(3,4- ethylenedioxythiophene)/poly(styrenesulfonate)," *Applied Physics Letters*, vol. 90, no. 4, pp. 10–13, 2007, doi: 10.1063/1.2435350.

[57] J. Huang, P. F. Miller, J. S. Wilson, A. J. De Mello, J. C. De Mello, and D. D. C. Bradley, "Investigation of the effects of doping and post-deposition treatments on the conductivity, morphology, and work function of poly(3,4-ethylenedioxythiophene)/poly(styrene sulfonate) films," *Advanced Functional Materials*, vol. 15, no. 2, pp. 290–296, 2005, doi: 10.1002/adfm.200400073.

[58] O. Bubnova *et al.*, "Semi-metallic polymers," *Nature Materials*, vol. 13, no. 2, pp. 190–194, 2014, doi: 10.1038/nmat3824.

[59] D.-J. Yun, H. Ra, J. Kim, I. Hwang, J. Lee, S.-W. Rhee, and J. Chung, "Characterizing Annealing Effect of Poly (3,4-ethylenedioxythiophene) Polymerized with Poly (4-styrenesulfonate) Conjugated Film on the Molecular Arrangement and Work Function by Core-Level and Valence-Level Band Spectra," *ECS Journal of Solid State Science and Technology*, vol. 1, no. 1, pp. M10–M14, 2012, doi: 10.1149/2.028201jss.

[60] E. S. Muckley, C. B. Jacobs, K. Vidal, J. P. Mahalik, R. Kumar, B. G. Sumpter, and I. N. Ivanov, "New Insights on Electro-Optical Response of Poly(3,4-ethylenedioxythiophene):Poly(styrenesulfonate) Film to Humidity," *ACS Applied Materials and Interfaces*, vol. 9, no. 18, pp. 15880–15886, 2017, doi: 10.1021/acsami.7b03128.

[61] A. M. Nardes, M. Kemerink, M. M. de Kok, E. Vinken, K. Maturova, and R. A. J. Janssen, "Conductivity, work function, and environmental stability of PEDOT:PSS thin films treated with sorbitol," *Organic Electronics*, vol. 9, no. 5, pp. 727–734, 2008, doi: 10.1016/j.orgel.2008.05.006.

[62] S. R. Dupont, F. Novoa, E. Voroshazi, and R. H. Dauskardt, "Decohesion kinetics of PEDOT:PSS conducting polymer films," *Advanced Functional Materials*, vol. 24, no. 9, pp. 1325–1332, 2014, doi: 10.1002/adfm.201302174.

[63] D. Bailo, A. Generosi, V. R. Albertini, R. Caminiti, R. De Bettignies, and B. Paci, "Time-resolved morphological study of 'PEDOT:PSS' hole transporting layer for polymer solar cells," *Synthetic Metals*, vol. 162, no. 9–10, pp. 808–812, 2012, doi: 10.1016/j.synthmet.2012.02.028.

[64] J. Fan, S. S. Rezaie, M. Facchini-Rakovich, D. Gudi, C. Montemagno, and M. Gupta, “Tuning PEDOT:PSS conductivity to obtain complementary organic electrochemical transistor,” *Organic Electronics*, vol. 66, no. October 2018, pp. 148–155, 2019, doi: 10.1016/j.orgel.2018.12.013.

[65] S. Iwata and A. Ishizaka, “Electron spectroscopic analysis of the SiO2 / Si system and correlation with metal – oxide – semiconductor device characteristics Electron spectroscopic analysis of the SiO 2 / Si system and correlation with metal – oxide – semiconductor device characteri,” *Journal of Applied Physics*, no. 79, p. 6653, 1996.

[66] M. Morita, T. Ohmi, E. Hasegawa, M. Kawakami, and M. Ohwada, “Growth of native oxide on a silicon surface,” *Journal of Applied Physics*, vol. 68, no. 3, pp. 1272–1281, 1990, doi: 10.1063/1.347181.

[67] M. M. Banaszak Holl, S. Lee, and F. R. McFeely, “Core-level photoemission and the structure of the Si/SiO2 interface: A reappraisal,” *Applied Physics Letters*, vol. 65, no. 9, pp. 1097–1099, 1994, doi: 10.1063/1.112109.

[68] S. Tougaard, “Universality classes of inelastic electron scattering cross-sections,” *Surface and Interface Analysis*, vol. 25, no. 3, pp. 137–154, 1997, doi: 10.1002/(SICI)1096-9918(199703)25:3<137::AID-SIA230>3.0.CO;2-L.

[69] K. Olejnik and J. Zemek, “Applicability of magic angle for angle-resolved X-ray photoelectron spectroscopy of corrugated SiO2/Si surfaces: Monte Carlo calculations,” *Surface Science*, vol. 602, no. 14, pp. 2581–2586, 2008, doi: 10.1016/j.susc.2008.06.007.

[70] T. Katayama, H. Yamamoto, M. Ikeno, Y. Mashiko, S. Kawazu, and M. Umeno, “Elimination of X-ray photoelectron diffraction effect of Si(100) for accurate determination of SiO2 overlayer thickness,” *Japanese Journal of Applied Physics, Part 2: Letters*, vol. 38, no. 7 A, 1999, doi: 10.1143/jjap.38.l770.

[71] G. Greczynski, T. Kugler, M. Keil, W. Osikowicz, M. Fahlman, and W. R. Salaneck, “Photoelectron spectroscopy of thin films of PEDOT–PSS.pdf,” vol. 121, pp. 1–17, 2001.

[72] B. Wei, J. Liu, L. Ouyang, C. C. Kuo, and D. C. Martin, “Significant Enhancement of PEDOT Thin Film Adhesion to Inorganic Solid Substrates with EDOT-Acid,” *ACS Applied Materials and Interfaces*, vol. 7, no. 28, pp. 15388–15394, 2015, doi: 10.1021/acsami.5b03350.

[73] F. Feldmann, M. Bivour, C. Reichel, M. Hermle, and S. W. Glunz, “Passivated rear contacts for high-efficiency n-type Si solar cells providing high interface passivation quality and excellent transport characteristics,” *Solar Energy Materials and Solar Cells*, vol. 120, pp. 270–274, 2014, doi: 10.1016/j.solmat.2013.09.017.

[74] P. J. Cousins, D. D. Smith, H. C. Luan, J. Manning, T. D. Dennis, A. Waldhauer,

K. E. Wilson, G. Harley, and W. P. Mulligan, “Generation 3: Improved performance at lower cost,” in *2010 35th IEEE Photovoltaic Specialists Conference*, 2010, pp. 275–278, doi: 10.1109/PVSC.2010.5615850.

[75] J. R. Bakke, K. L. Pickrahn, T. P. Brennan, and S. F. Bent, “Nanoengineering and interfacial engineering of photovoltaics by atomic layer deposition,” *Nanoscale*, vol. 3, no. 9, pp. 3482–3508, 2011, doi: 10.1039/c1nr10349k.

[76] D. J. Michalak, S. Rivillon, Y. J. Chabal, A. Estève, and N. S. Lewis, “Infrared spectroscopic investigation of the reaction of hydrogen-terminated, (111)-oriented, silicon surfaces with liquid methanol,” *Journal of Physical Chemistry B*, vol. 110, no. 41, pp. 20426–20434, 2006, doi: 10.1021/jp0624303.

[77] B. Chhabra, C. Weiland, R. L. Opila, and C. B. Honsberg, “Surface characterization of quinhydrone-methanol and iodine-methanol passivated silicon substrates using X-ray photoelectron spectroscopy,” *Physica Status Solidi (a)*, vol. 208, no. 1, pp. 86–90, 2011, doi: 10.1002/pssa.201026101.

[78] H. M’saad, J. Michel, J. J. Lappe, and L. C. Kimerling, “Electronic passivation of silicon surfaces by halogens,” *Journal of Electronic Materials*, vol. 23, no. 5, pp. 487–491, 1994, doi: 10.1007/BF02671234.

[79] J. H. Hack, “Band-Bending and Induced Junctions of Silicon Heterojunction Solar Cells,” *University of Delaware*, 2021.

[80] M. Chen, “RADICAL-DRIVEN SILICON SURFACE PASSIVATION FOR ORGANIC- INORGANIC HYBRID PHOTOVOLTAICS by,” 2017.

[81] J. He, P. Gao, Z. Yang, J. Yu, W. Yu, Y. Zhang, J. Sheng, J. Ye, J. C. Amine, and Y. Cui, “Silicon/Organic Hybrid Solar Cells with 16.2% Efficiency and Improved Stability by Formation of Conformal Heterojunction Coating and Moisture-Resistant Capping Layer,” *Advanced Materials*, vol. 29, no. 15, pp. 1–7, 2017, doi: 10.1002/adma.201606321.

[82] J. Yang and D. C. Martin, “Microporous conducting polymers on neural microelectrode arrays: I electrochemical deposition,” *Sensors and Actuators, B: Chemical*, vol. 101, no. 1–2, pp. 133–142, 2004, doi: 10.1016/j.snb.2004.02.056.

[83] J. A. Del-oso, B. A. Frontana-uribe, J. Maldonado, M. Rivera, M. Tapia-tapia, G. Roa-morales, and B. A. Frontana-uribe, “Electrochemical deposition of poly [ethylene-dioxythiophene] (PEDOT) films on ITO electrodes for organic photovoltaic cells : control of morphology , thickness , and electronic properties,” *Journal of Solid State Electrochemistry*, pp. 2025–2037, 2018, doi: 10.1007/s10008-018-3909-z.

[84] Y. Vlamidis, M. Lanzi, E. Salatelli, I. Gualandi, B. Fraboni, L. Setti, and D. Tonelli, “Electrodeposition of PEDOT perchlorate as an alternative route to PEDOT:PSS for the development of bulk heterojunction solar cells,” *Journal of*

Solid State Electrochemistry, vol. 19, no. 6, pp. 1685–1693, 2015, doi: 10.1007/s10008-015-2802-2.

[85] M. A. del Valle, A. M. Ramírez, L. A. Hernández, F. Armijo, F. R. Díaz, and G. C. Arteaga, "Influence of the supporting electrolyte on the electrochemical polymerization of 3,4-ethylenedioxythiophene. effect on p- and n-Doping/Undoping, Conductivity And Morphology," *International Journal of Electrochemical Science*, vol. 11, no. 8, pp. 7048–7065, 2016, doi: 10.20964/2016.08.46.

[86] M. H. Gharahcheshmeh, M. M. Tavakoli, E. F. Gleason, M. T. Robinson, J. Kong, and K. K. Gleason, "Tuning, optimization, and perovskite solar cell device integration of ultrathin poly(3,4-ethylene dioxythiophene) films via a single-step all-dry process," *Science Advances*, vol. 5, no. 11, pp. 1–13, 2019, doi: 10.1126/sciadv.aay0414.

[87] D. Tonini, G. Cellere, M. Bertazzo, A. Fecchio, L. Cerasti, and M. Galiazzo, "Shingling technology for cell interconnection: Technological aspects and process integration," *Energy Procedia*, vol. 150, no. Snec, pp. 36–43, 2018, doi: 10.1016/j.egypro.2018.09.010.

[88] A. Louwen, W. Van Sark, R. Schropp, and A. Faaij, "A cost roadmap for silicon heterojunction solar cells," *Solar Energy Materials and Solar Cells*, vol. 147, pp. 295–314, 2016, doi: 10.1016/j.solmat.2015.12.026.

[89] D. M. Powell, R. Fu, K. Horowitz, P. A. Basore, M. Woodhouse, and T. Buonassisi, "The capital intensity of photovoltaics manufacturing: Barrier to scale and opportunity for innovation," *Energy and Environmental Science*, vol. 8, no. 12, pp. 3395–3408, 2015, doi: 10.1039/c5ee01509j.

[90] V. Ramasamy, R. Margolis, V. Ramasamy, and R. Margolis, "Floating Photovoltaic System Cost Benchmark : Q1 2021 Installations on Artificial Water Bodies Floating Photovoltaic System Cost Benchmark : Q1 2021 Installations on Artificial Water Bodies," no. October, 2021.

[91] W. B. Group, "Where Sun Meets Water : Floating Solar Market Report," Washington, D.C, 2018. [Online]. Available: https://documents.worldbank.org/en/publication/documents-reports/documentdetail/579941540407455831/floating-solar-market-report-executive-summary.

[92] R. S. Spencer, J. Macknick, A. Aznar, A. Warren, and M. O. Reese, "Floating Photovoltaic Systems: Assessing the Technical Potential of Photovoltaic Systems on Man-Made Water Bodies in the Continental United States," *Environmental Science and Technology*, vol. 53, no. 3, pp. 1680–1689, 2019, doi: 10.1021/acs.est.8b04735.

[93] C. Gilligan, "Asia region to drive floating solar installation growth in the next five

years," *IHS Markit*, 2020.

[94] "Global Flexible Solar Panel Report 2020," *Market Research Inc.*, [Online]. Available: https://www.mccourier.com/flexible-solar-panel-market-report-is-comprehensive-with-covid-19-impact-analysis-top-companies-global-solar-solopower-systems-growth-opportunity-sales-trends-service-demand-applications-for/.

[95] "Organic Solar Cells Market Size, Share and COVID-19 Impact Analysis, By Application, and Regional Forcast 2020-2027," 2020. [Online]. Available: https://www.fortunebusinessinsights.com/industry-reports/organic-solar-cell-market-101555.

[96] S. Kim, M. Holz, S. Park, Y. Yoon, E. Cho, and J. Yi, "Future options for lightweight photovoltaic modules in electrical passenger cars," *Sustainability (Switzerland)*, vol. 13, no. 5, pp. 1–7, 2021, doi: 10.3390/su13052532.

[97] K. Mik, P. Zawadzki, J. Tarłowski, M. Bugaj, P. Grygiel, and S. Bykuć, "Multifaceted analyses of four different prototype lightweight photovoltaic modules of novel structure," *Energies*, vol. 14, no. 8, 2021, doi: 10.3390/en14082239.